The Dissertation Committee for Mahdi Kefayati
certifies that this is the approved version of the following dissertation:

Harnessing Demand Flexibility to Minimize Cost, Facilitate Renewable Integration, and Provide Ancillary Services

Committee:

Ross Baldick, Supervisor

Gustavo de Veciana

Constantine Caramanis

David P. Morton

Parviz Adib

Wei-peng Chen

Harnessing Demand Flexibility to Minimize Cost, Facilitate Renewable Integration, and Provide Ancillary Services

by

Mahdi Kefayati, B.E.; M.E.; M.S.E.

DISSERTATION

Presented to the Faculty of the Graduate School of

The University of Texas at Austin

in Partial Fulfillment

of the Requirements

for the Degree of

DOCTOR OF PHILOSOPHY

THE UNIVERSITY OF TEXAS AT AUSTIN

August 2014

To Him,

who knows everything!

To my wife and daughter,

Razieh and Fatima Grace.

To my mother and father,

whose unconditional love, support and sacrifice have lit my life.

Acknowledgments

First, foremost and solely, I thank God, the most merciful, the all-knowing and the almighty, for everything.

I wish to extend my gratitude to the multitudes of people who helped me throughout my journey as a PhD student. I would like to sincerely thank my supervisor, Dr. Ross Baldick, for his priceless help and support. Dr. Baldick supported me intellectually and financially, challenged me to unleash my potential, gave me the opportunity to present my work and connect to the community, and most importantly gave me the freedom to develop my own research agenda. I would like to extend my appreciation to my committee members, Dr. Gustavo de Veciana, Dr. Constantine Caramanis, Dr. David Morton, Dr. Parviz Adib, and Dr. Wei-peng Chen for their invaluable guidance. In particular, I am grateful to Dr. Caramanis who advised and supported me in the earlier part of my PhD and guided me to develop core technical skills necessary to become an independent researcher.

I would like to express my most sincere gratitude to the love of my life, Razieh Nokhbeh Zaeem, not only for her unconditional love and emotional support, but also for her company as a friend and colleague with whom I have the delightful opportunity to learn and grow technically and as a human. She is the one who have always been by my side and responded to my imperfections

with pure love.

Time would fail me to tell how I am indebted to my parents, Simin and Mohammad Hossein. They are simply the best parents one could dream of. May God endow them with best of rewards, for their patience, endurance, and never ending love. I thank my sister Marzieh and my brothers Mohammad Hadi and Mohammad Sadegh for filling my empty space in the family, and apologize them for not being with them for this long. Lastly, I would like to make special mention of my daughter, Fatima Grace, and thank her for accommodating me and her mom and lighting our life.

I appreciate the time I spent and the discussions I had with my colleges in Energy System Laboratory and Wireless Communication and Networking Group at the University of Texas at Austin: Mansoureh Peydayesh, Mohammad Majidi, Sambuddha Chakrabarti, Dave Tuttle, Mike Legatt, Héctor Chavez, Deepjyoti Deka. I also thank Ms. Melanie Gulick, the graduate coordinator of the Electrical and Computer Engineering department.

Living far from home would be much harder without the company of my dear friends and their families, who treated me, Razieh and Fatima as their family and stood by our side in times of need.

This work was funded in part by the EV-STS, NSF, PSERC, ERCOT, and Pecan Street Inc. under various grants and donations.

Harnessing Demand Flexibility to Minimize Cost, Facilitate Renewable Integration, and Provide Ancillary Services

Publication No. _____

Mahdi Kefayati, Ph.D.
The University of Texas at Austin, 2014

Supervisor: Ross Baldick

Renewable energy is key to a sustainable future. However, the intermittency of most renewable sources and lack of sufficient storage in the current power grid means that reliable integration of significantly more renewables will be a challenging task. Moreover, increased integration of renewables not only increases uncertainty, but also reduces the fraction of traditional controllable generation capacity that is available to cope with supply-demand imbalances and uncertainties. Less traditional generation also means less rotating mass that provides very short term, yet very important, kinetic energy storage to the system and enables mitigation of the frequency drop subsequent to major contingencies but before controllable generation can increase production.

Demand, on the other side, has been largely regarded as non-controllable and inelastic in the current setting. However, there is strong evidence that a

considerable portion of the current and future demand, such as electric vehicle load, is flexible. That is, the instantaneous power delivered to it needs not to be bound to a specific trajectory.

In this thesis, we focus on harnessing demand flexibility as a key to enabling more renewable integration and cost reduction. We start with a data driven analysis of the potential of flexible demands, particularly plug-in electric vehicle (PEV) load. We first show that, if left unmanaged, these loads can jeopardize grid reliability by exacerbating the peaks in the load profile and increasing the negative correlation of demand with wind energy production. Then, we propose a simple local policy with very limited information and minimal coordination that besides avoiding undesired effects, has the positive side-effect of substantially increasing the correlation of flexible demand with wind energy production. Such local policies could be readily implemented as modifications to existing "grid friendly" charging modes of plug-in electric vehicles. We then propose improved localized charging policies that counter balance intermittency by autonomously responding to frequency deviations from the nominal frequency and show that PEV load can offer a substantial amount of such ancillary services.

Next, we consider the case where real-time prices are employed to provide incentives for demand response. We consider a flexible load under such a pricing scheme and obtain the optimal policy for responding to stochastic price signals to minimize the expected cost of energy. We show that this optimal policy follows a multi-threshold form and propose a recursive method to

obtain these thresholds. We then extend our results to obtain optimal policies for simultaneous energy consumption and ancillary service provision by flexible loads as well as optimal policies for operation of storage assets under similar real-time stochastic prices. We prove that the optimal policy in all these cases admits a computationally efficient form. Moreover, we show that while optimal response to prices reduces energy costs, it will result in increased volatility in the aggregate demand which is undesirable.

We then discuss how aggregation of flexible loads can take us a step further by transforming the loads to controllable assets that help maintain grid reliability by counterbalancing the intermittency due to renewables. We explore the value of load flexibility in the context of a restructured electricity market. To this end, we introduce a model that economically incentivizes the load to reveal its flexibility and provides cost-comfort trade-offs to the consumers. We establish the performance of our proposed model through evaluation of the price reductions that can be provided to the users compared to uncontrolled and uncoordinated consumption. We show that a key advantage of aggregation and coordination is provision of "regulation" to the system by load, which can account for a considerable price reduction. The proposed scheme is also capable of preventing distribution network overloads. Finally, we extend our flexible load coordination problem to a multi-settlement market setup and propose a stochastic programming approach in obtaining day-ahead market energy purchases and ancillary service sales.

Our work demonstrates the potential of flexible loads in harnessing re-

newables by affecting the load patterns and providing mechanisms to mitigate the inherent intermittency of renewables in an economically efficient manner.

Table of Contents

List of Tables

List of Figures

Chapter 1

Introduction

1.1 Paradigm Shift in Power Systems

Renewable energy plays a key role for a sustainable future. However, renewable sources, such as wind and solar PV, are usually intermittent and much less controllable than the traditional forms of electricity generation. This intermittency poses serious challenges to the electricity network, where continuously maintaining supply-demand balance is essential for reliable operation. Intermittency increases variability and uncertainty of the electricity generation, which complicates resource planning and scheduling and consequently results in an increased demand for reserves. Moreover, since most of the renewable generators are coupled to the grid through power electronic devices, they usually provide much less inertia to the grid than synchronous generators with a rotating mass. Understanding the fact that the stored kinetic energy has a critical role in stabilizing and smoothing short-term supply demand imbalances, replacing conventional generators with renewables, typically results in a "lighter" system which is potentially less stable. Finally, being less controllable means that renewable generators have much less potential in providing reserves and hence widespread adoption of renewables and particularly wind energy can result in reserve adequacy issues [28].

1.2 Demand Flexibility and Its Potential

In contrast to generation, electric demand has been typically treated as inelastic and uncontrollable. So much so that *uncontrollable*, and usually renewable, generation is often incorporated with demand as "net load." However, a substantial amount of electric demand is flexible in the sense that it is not bound to a specific power trajectory. Electric loads such as HVAC systems, heating and cooling, and PEV charging are major examples which, based on a US Energy Information Administration study [108], comprise more than one third of US residential electric demand. Similar results exist for other sectors, particularly office buildings and data centers. As an abstraction, flexible demand can be modeled in most cases as a definite amount of *energy* that should be delivered to the load subject to a *deadline* and potentially some *rate constraints*.

In order to fully utilize demand flexibility, proper control and communication infrastructure is indispensable. Smart grids are the right step in providing the infrastructure for communication with and control of demand-side resources. Demand flexibility, coupled with proper communication and control infrastructure, as smart grids become mainstream, can enable more control over the demand and basically transform the demand to another (partially) controllable element in the supply-demand equation.

As a result of these two trends, we are departing from a paradigm in which controllable generation matches uncontrollable demand to one in which controllable assets on both supply and demand-sides are utilized to

maintain the delicate balance of the electrical grid. In other words, as the amount of non-dispatchable generation increases, we need more control on the demand-side for reliable operation of the system. Since the contribution of assets to maintaining safe operating conditions is a valuable service which should be paid for, this shift has market implications, particularly regarding how we distribute the cost of reserves necessitated by uncontrollable/uncertain generation. Moreover, distributed and variable nature of demand-side assets pose a challenge in their wide adoption.

The need to enable demand-side participation has been recognized at different levels of policy making and market operation. The Federal Energy Regulatory Commission (FERC) has issued recent orders regarding demand response participation in organized wholesale markets [41] and frequency regulation compensation [42]. Different Independent System Operators (ISO) have also taken steps towards facilitating demand-side participation in the market. For example, the Electric Reliability Council of Texas (ERCOT) which serves as the Texas independent system operator, has programs that enable loads to respond to economic and reliability signals through Voluntary Load Response and Emergency Response Service as well as participating in the Ancillary Services (AS) market [98]. Moreover, ERCOT ran a pilot project for evaluating the effects of Fast Responding Regulation Service (FRRS) potentially provided by non-conventional assets [100] from 2012 to 2013 and decided to keep the pilot as part of the standard market operation. The Midcontinent ISO (MISO) [69] and California ISO (CAISO) [20] have similar programs to enable demand

participation. Such programs are key for incentivizing demand-side resources and particularly flexible resources to participate in the market and justify the overheads associated with their participation.

1.3 Overview of the Dissertation

In this dissertation, we focus on investigating the potential of flexible demands in reducing costs, facilitating integration of renewables, and provision of ancillary services. We start with studying plug-in electric vehicle (PEV) demand as one of the prime examples of flexible loads. PEV demand is particularly interesting not only because transportation electrification is key to a sustainable future, but also because of the flexibility of the resulting electric load. We first propose a simple yet effective measure for demand flexibility and show that, based on empirical vehicle transportation data, PEV demand is substantially flexible. Then, we investigate the effect of different charging policies on the grid and conclude that under current charging practices, there is a high correlation between the PEV demand and the load in the ERCOT system in an average sense. We then propose a simple charging policy, called Average Rate (AR) policy, that uses only local information, namely arrival and departure time of the vehicle as well as its energy requirements, and show that under this policy PEV demand has much less correlation with usual electric demand and better correlation with renewable generation in the ERCOT system. To make the proposed localized policy more robust to uncertainties in driver behavior, we then propose a modified version or AR policy, called

Average Rate with Minimum Range (ARMR), that achieves a minimum desired range in minimal time while maintaining the general properties of AR policy, so that unexpected changes in transportation plans would minimally affect drivers' comfort.

Next, we study alternative behavior models for PEV users and study its impact on load patterns. We conclude this part of the dissertation by quantifying the potential of PEV load in providing autonomous frequency response and show that the frequency responsive capacity provided by PEVs loads under AR policy, even at modest electrification levels, is comparable to the total amount of regulation purchased in ERCOT.

Localized policies can be very effective in an average sense, however, in presence of more information and incentives, more efficient coordination should be possible. To this end, we study the response of flexible loads under real-time stochastic prices and show that the optimal policy follows an extended threshold policy. We further propose a recursive method for obtaining the optimal policy and show that the optimal policy has an efficient parameterization and the parameters can be computed efficiently. We then extend the model and the resulting optimal policy to the case where the flexible loads sell their flexibility as Ancillary Services in conjunction with their energy purchases. We prove that a similar optimal policy can be obtained and its parameters can be obtained in a computationally efficient manner. Next, we show that our model for flexible loads can be extended to storage assets and prove that under some conditions, the optimal policy for operating a storage asset with

ramp rate constraints can be parametrized and computed efficiently.

In order to measure the effectiveness of our proposed optimal policy for energy consumption and AS provision, we test it through simulation and study the collective impact of widespread adoption of our proposed optimal policy by flexible loads. We conclude that while prices provide an effective mechanism to shift consumption to off-peak hours, the collective behavior of price responsive flexible demand would adversely impact the grid and does not incentivize efficient response from the loads. Moreover, each load might not be large enough to participate directly in the AS market. These issues motivates us to consider the benefits of closer coordination.

We therefore move on to a more coordinated setup where an Energy Service Company (ESCo) or Load Aggregator (LA) contracts flexible loads to deliver their requested energy demand by their desired deadline. The ESCo then participates in the wholesale electricity market as a buyer for energy and a seller for ancillary services. Moreover, the ESCo is assumed to only use the spare capacity of the distribution network. While most methods proposed in such a setup assume constant "subscription plan" based contracts between the ESCo and the loads, we propose a pricing mechanism, called "Transaction Pricing," which rewards each load's flexibility in an economically efficient manner and hence provides the right incentives for the loads to expose their flexibility. Our simulation results show that under typical loads at the distribution network level, besides reduced costs of energy delivery and more efficient use of the distribution network infrastructure, the proposed mechanism offers

better prices for the majority of flexible loads, even when they have access to wholesale prices for energy and consume optimally. Furthermore, our results show that the ESCo provides substantial amounts of AS to the market and payments due to AS provision are responsible for the lion's share of the advantage in the energy price offered to the flexible loads.

Many restructured electricity markets in US are organized in a multi-settlement fashion, consisting of at least a day-ahead market (DAM) and a (close to) real-time market (RTM). Moreover, in some jurisdictions like ERCOT, AS can only be offered in DAM. Therefore, to consider a more efficient and realistic setup for coordinating energy delivery to flexible loads, we then consider the decision problem faced by the ESCo for participating in the multi-settlement setup. We particularly focus on DAM participation where decision about AS provision should be made without perfect knowledge of flexible loads' availability and demand. We formulate this problem as a two stage stochastic program and propose a data driven scenario generation technique. Finally, we evaluate the performance of the proposed DAM participation method through simulations and show that total costs can be reduced into half compared to uncontrolled charging of PEVs. We also observe AS sales contributes to roughly a quarter of the cost reduction.

The rest of this dissertation is organized as follows: In Chapter 2 we present our analysis of PEV demand flexibility and the localized policies which utilize it. Chapter 3 is dedicated presentation of our results on optimal response of flexible loads to real-time prices. In Chapter 4 we extend the results

of Chapter 3 to include AS provision by flexible loads. In Chapter 5, we extend our model for flexible loads under stochastic prices to optimal storage operation. In Chapter 6 we move beyond prices for energy consumed period by period to prices for total energy delivery. Considering a more coordinated model, we present our novel method for pricing energy delivery transactions for flexible loads to provide ancillary services in an economically efficient manner. Chapter 7 is dedicated to optimal decision making for participation in a multi-settlement market and in Chapter 8 we conclude this dissertation. Proof of key theorems are moved to the appendices to improve readability.

Chapter 2

Localized Charging Policies for Harnessing PEV Demand Flexibility

2.1 Introduction

Transportation is one of the major consumer of energy in US and around the world. According to the latest Department of Energy (DOE) Transportation Data Book [34], 27.8% of *total* US energy consumption is attributed to transportation. Of this amount, 58.9% is consumed by cars and light duty trucks to make up 16.4% of total energy consumed by Americans. To put this in perspective, according to DOE energy usage estimates [64], which is also depicted in Figure 2.1, 39.2% of energy consumed in US is spent for electricity generation.

With this outlook, reduction in Green House Gas (GHG) emissions alone may provide an argument for transportation electrification. Yet, the synergy between flexible demands from electric vehicles and intermittent generation, mostly due to renewables, provides a more profound argument towards this end. Of course, there are challenges ahead, but given the substantial size of the potential PEV energy demand, it might be one of the major facilitators of renewable integration. Moreover, since the transportation electrification land-

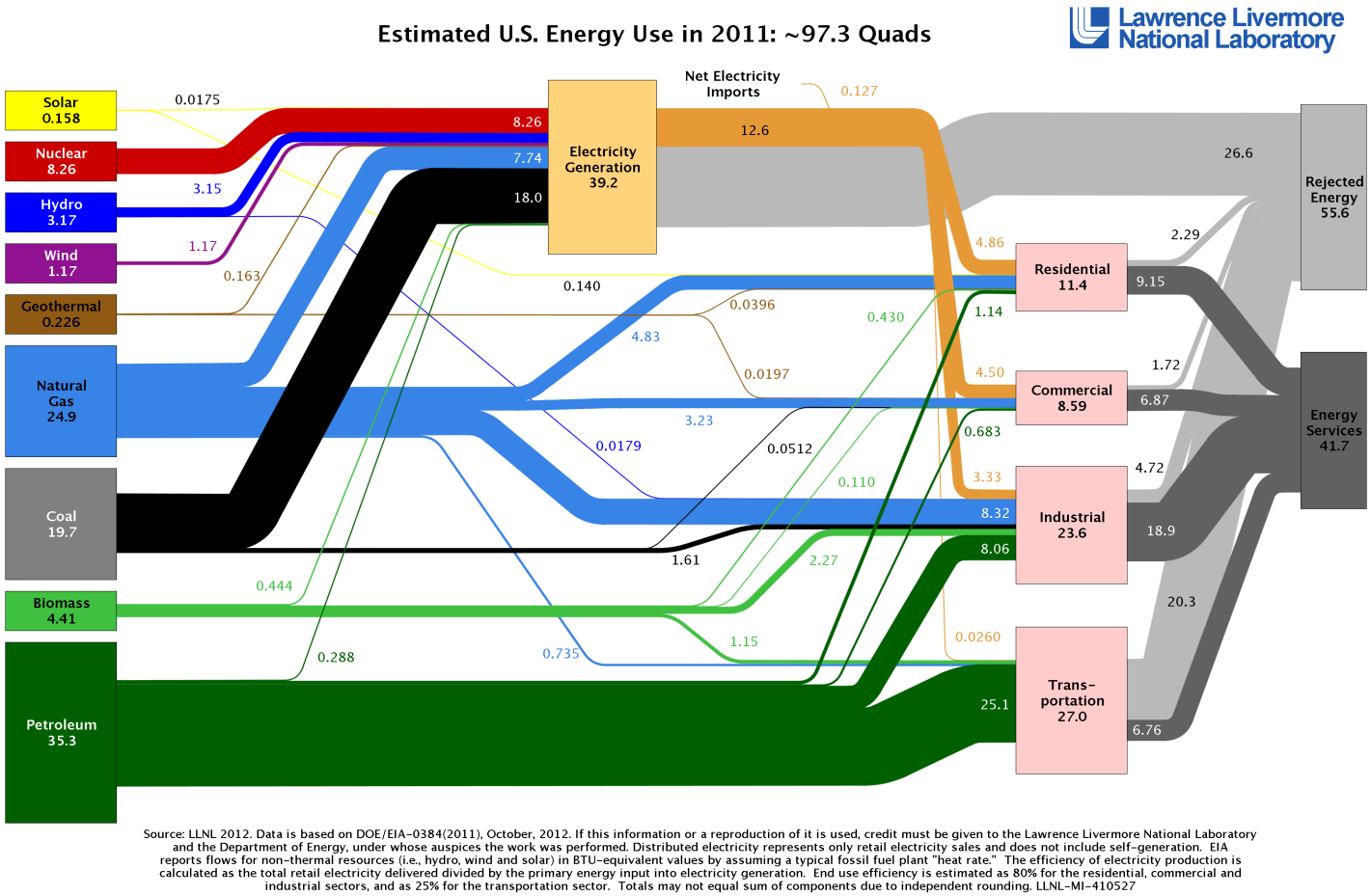

Figure 2.1: Estimated U.S. Energy Use in 2011 [64].

scape is not completely formed yet, there is much more room for pushing for more efficient designs and less worry about legacy systems and compatibility as standards are being developed.

Transformation of energy demand from gasoline to electric demand on the grid can substantially impact the grid as well. Most basically, this new energy demand should be transmitted through the grid, which would potentially need expansion in its capacity and lead to other inefficiencies [88]. However, if managed properly, it can be used to increase the efficiency of infrastructure usage [26, 30, 31, 46, 47, 49, 62]. Therefore, investigating the effects of different charging policies and designing efficient ones with respect to information available at each charging station is an important problem.

In this section, we focus on understanding the potential of PEVs, particularly their energy demand pattern, its flexibility and how it translates into electric demand. Taking a data driven approach, we aim to answer the following key questions:

- How much is the potential?
- How do the current EV charging approaches perform in aligning their load with the renewable, particularly wind, generation?
- Are there simple, yet effective, policies for utilizing PEV demand flexibility based on local information available at the PEV load for matching renewables?

To answer these questions, we first utilize empirical travel data deduced from vehicle locations and map them into the PEV availability and energy demand. We refer to times when the vehicle is not moving as "dwell times." We analyze the electric demand and dwell times of PEVs to measure empirical demand flexibility of PEV load. Then, we map the demand data to electric demand as seen by the grid when PEVs employ various conventional charging policies available on current PEVs like the Chevy Volt and Nissan Leaf. We observe that due to the natural availability patterns of vehicle usage as well as wind generation (in Texas), uncontrolled PEV demand shows negative correlation with wind in average sense. Finally, we propose a novel and simple charging policy which improves this negative correlation. It is worth noting that this policy does not need grid information and can be easily integrated into current PEVs, perhaps though a software update.

The rest of this chapter is organized as follows: In Section 2.2 we describe our data set, define our demand flexibility measure and present the results of our demand flexibility analysis. In Section 2.3, we translate the PEV demand data to electric load using the conventional charging policies and analyze its correlation with wind and net load in Texas. In Section 2.4, we introduce our proposed localized policy and compare its performance with the conventional charging policies. In Section 2.5, we introduce anticipative charging behavior and study its impact on PEV load. In Section 2.6, we propose methods for enhancing localized policies introduced earlier to respond to frequency deviations and study the potential of such methods in providing

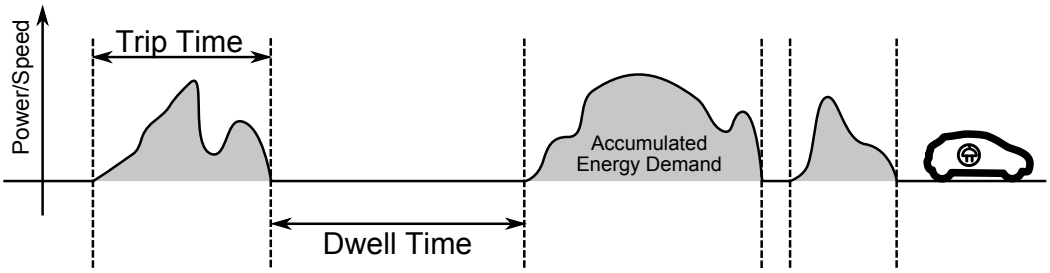

Figure 2.2: Accumulation of energy demand as a PEV is used over time.

ancillary services to the grid. Finally in Section 2.7, we conclude the chapter.

2.2 Demand Flexibility of PEV Load

In this section we analyze PEV demand data and particularly its flexibility in order to assess the potential of PEV demand in affecting electric demand patterns and provision of controllable loads.

2.2.1 Dataset

As PEVs are still not very widespread, finding reliable transportation data sets for analyzing their behavior is a challenging task. To deal with this challenge, similar to other studies [61], we use the publicly available dataset from Traffic Choices Study [75] by the Puget Sound Regional Council which is based on a sample of 449 conventional vehicles. In this study, each vehicle is equipped with a set of sensors including a Global Positioning System (GPS) based location recorder. The public version of the dataset contains compiled results of the raw location data, filtered and combined mainly for privacy purposes, mainly consisting of vehicle speed trajectories over time and trips made

by each vehicle over the course of the survey. The major advantage of this dataset is that the data is collected for more than a year per vehicle and consequently a much better picture of vehicle use can be obtained from it compared to other datasets, e.g. National Highway Travel Survey (NHTS) data set [106], which usually contain a data for periods as short as 24 hours. The transportation dataset in our study is collected in Seattle, Washington area and roughly contains 738,000 usable trips. Table 2.1 summarizes the general statistics of the dataset. While there are other datasets with transportation info based on GPS location of the vehicle, we have particularly chosen this dataset for two main reasons: a) The length of the study as mentioned previously. b) In this dataset, the trips to/from drivers' home and work place are flagged accordingly. No other transportation dataset has these two properties to the best of our knowledge. As demonstrated in the proceeding text, knowledge of stops that happen at home location provides us with very valuable insight about user behavior.

We have assumed no change in driving patterns between the PEVs and conventional vehicles mainly because of lack of data that could help us in the adjustment process. Nonetheless, one would argue that the drivers would prefer no change in their driving patterns too since the purpose of driving is *usually* independent of the vehicle's drivetrain technology.

As will be discussed later, we have scaled the results obtained from this dataset to match the scale of light duty transportation in Texas, so that the results can be interpreted in the contexts of the ERCOT system. While

Table 2.1: Dataset statistics. Averages are per vehicle.

Number of Vehicles	449
Average Data Collection Time Length	360 days
Average Number of Trips	1645 trips
Average Miles Traveled	9711 miles
Data Collection Date Range	11/7/2004 - 4/5/2006
Average Speed	23.5 mph
Percentage of Stops at Home	29.5%

patterns and statistics of driving in Texas might differ from that of Seattle area, we argue that typical driving patterns in large urban areas in Texas and Seattle are similar. Our focus is on major urban areas because they are prime places for PEV adoption. This is because the trips are typically shorter in urban areas, PEVs are much better suited for driving in traffic and the impact of transportation electrification on air quality is more pronounced in dense urban areas. We also had access to and experimented with GPS based transportation dataset for different cities in Texas, including Austin, Houston and San Antonio, although the vehicles where studied for a much shorter period (about a week) and other transportation data, e.g. home location, were not included. Our results, particularly in Austin, did not show any major difference in the overall patterns in cases where comparison was possible. Therefore, we feel confidant to use the Traffic Choices Study dataset as our reference dataset here and interpret the results in the context of the ERCOT system.

In order to deduce the PEV electric demand from the conventional vehicle data, we use the Nissan Leaf specifications. We deduce electrical demand of the vehicle by using its average kWh/mile from its EPA fuel economy specification [38], according to which a Leaf consumes 0.33 kWh/mile on average.[1] Using this conversion rate, we map the trip distance to kWh of accumulated energy demand at the end of the trip (c.f. Figure 2.2). Moreover, we restrict our attention to the trips and vehicles where the trips are viable using the Nissan Leaf's battery capacity. We should note that only less than 1% of the total trips fall under the non-viable category. For charging, we have assumed availability of an AC Level 2 Electric Vehicle Service Equipment (EVSE) with 3.3kW capacity.

In order to establish a comparison to typical load patterns in the grid, we have used the load and wind generation data provided by Electric Reliability Council of Texas (ERCOT) [97] for years 2009 and 2010. Moreover, we have assumed PEV penetration rate of 30% and 15 million vehicles total, which is roughly the number of registered cars and light duty trucks in Texas in 2012.

2.2.2 Measure of Demand Flexibility

Before presenting our results on PEV demand flexibility, we first need to precisely define demand flexibility. In its broad sense, flexible demand is

[1] We are already working on more accurate estimates of energy demand using vehicle road load equations and will report them in our future work.

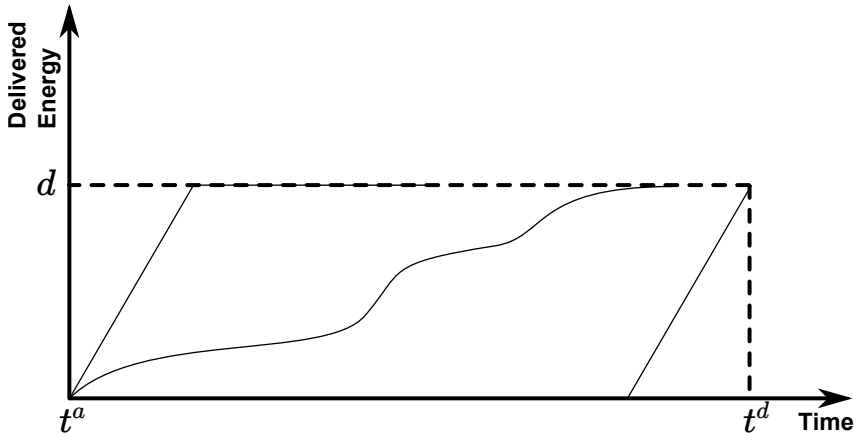

Figure 2.3: Delivered amount of energy to a flexible demand.

electric demand where the energy delivery *rate*, i.e. power, is not bound to a specific trajectory. In many cases such a load can be modeled as one with certain amount of energy demand, d, an availability window of $[t^a, t^d)$ and usually is subject to some rate constraints as depicted in Figure 2.3. Given a maximum power constraint, the upper and lower thin solid curves show immediate and late energy delivery while the middle solid curve shows one other potential energy delivery trajectory over time. This model particularly matches relatively simple loads like PEV charging as it accumulates energy demand while on a trip and satisfies it while dwelling if charging is available and the user desires to do so. We define demand flexibility as:

$$\begin{aligned} \text{Flexibility} &= 1 - \frac{\text{Accumulated Energy Demand}}{\text{EVSE Capacity} \times \text{Dwell Time}} \\ f(d, \overline{x}, t^a, t^d) &= 1 - \frac{d}{\overline{x}(t^d - t^a)}, \end{aligned} \tag{2.1}$$

where $\overline{x}$ represents the EVSE capacity. Basically, (2.1) defines demand flexibility as what portion of charging capacity can be left unused during dwell time. Using this definition, flexibility can vary between $-\infty$ and 1. It is negative if the dwell time is inadequate for completely satisfying the demand, zero if the time is just enough and approaches one as demand becomes more flexible.

2.2.3 Flexibility of PEV Demand

In order to evaluate the charging demand, we also need to identify likely dwell times. In particular, not all the dwell times are suitable for charging. Moreover, a charging station might not be available at the dwell location. Finally, the driver might not connect the vehicle for other non-technical reasons. In this section, to simplify the analysis, we assume the deciding factor for a dwell time suitability is mainly its length and partially its location.

To this end, we assume the driver does not charge at those dwell times shorter than a threshold, say h, and basically continues on accumulating demand until the battery is completely drained or a stop with a dwell time at least h is encountered. For all dwell times at least h, we assume the availability of EVSE as well as the willingness of the driver to charge. The intuition behind this method of categorizing dwell times is the following: First, in short dwell times, there is much less potential in actually charging the PEV as the time is limited. Second, short dwell times can be typically associated with locations where people typically do not stay long and hence a charging station might not be available. Conversely, it is typical to observe the vehicles having

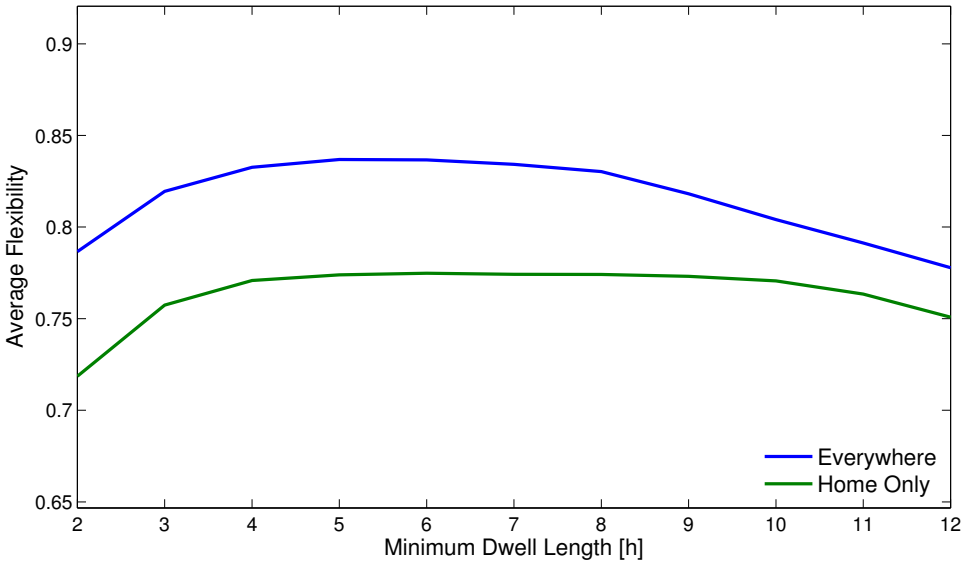

Figure 2.4: Flexibility of EV load at different minimum dwell times.

their longest dwells at the driver's home or work place. Finally, the drivers are less inclined to charge for a short amount of time, simply because the hassle is not worth the amount of energy replenished.

Figure 2.4 shows the average flexibility of PEV load, averaged over the entire potential charging events versus the minimum dwell time i.e. the threshold. We have considered two cases: First, when charging is available at every long enough dwell time. Second, if charging is only available at a long enough dwell time that happens at home. When charging everywhere, although demand flexibility is generally high for the range of minimum dwell times considered, the interesting phenomenon is that it is maximized at around $h = 5$ to $h = 7$ hours. The intuition behind the reduced flexibility at smaller thresholds is the fact that such dwells are basically too short for replenish-

ing the energy demand accumulated in the trip(s) leading to them. As the minimum length of long enough dwell times is increased, however, the dwell time length catches up with energy accumulated, even though there are fewer such dwell times. Finally, if charging happens only at very long (greater than 9 hours) dwell times, the demand flexibility starts to diminish due to the reduced frequency of such dwell times encountered, which is typically one per 24 hours at the driver's home. When charging is available only at home, although the flexibility is reduced as the charging location is much more restricted, the load still shows a substantial amount of flexibility. Also, average flexibility remains almost constant throughout different minimum dwell times since the majority of dwell times at home are typically at least couple of hours long. We will discuss the effects of restricting charging to drivers' home in the proceeding sections as well.

2.3 Impact Analysis of Conventional PEV Charging Policies

In order to analyze the effective demand of PEV charging, we also need to consider the charging policy, which translates the energy demand to power demand on the grid. To this end, in this section, we consider two charging policies common in most PEVs: *immediate* charging and *delayed* charging.

2.3.1 PEV Demand with Immediate Charging

In *immediate* charging, the vehicle starts charging at the nominal EVSE rating as soon as it is connected and continues charging until either the battery is full or the dwell time is finished. That is, the charging rate in immediate charging is given by:[2]

$$x_t = \begin{cases} \overline{x} & t \leq \min\left\{\frac{d}{\overline{x}}, t^d\right\}, \\ 0 & \text{otherwise.} \end{cases} \tag{2.2}$$

Immediate charging is the most natural charging policy when the only available information is the amount of energy required. In other words, in the absence of information like departure time or if there are no incentives such as time-of-use tariffs to vary the timing of charging, and in the absence of demand management/load aggregation mechanisms, there is no incentive except faster availability of the vehicle, which leads to immediate charging at the maximum power.

Figure 2.5 shows the results of immediate mode charging. In this figure and several subsequent figures, demand is shown from the PEVs versus time of day, but averaged across days in the traffic survey data. The PEV demand is scaled to represent 30% penetration of PEVs in the Texas light vehicle fleet of roughly 15 million vehicles [43]. The trip data for the conventional vehicles

[2]Here we are assuming a linear model for the battery, that is, we assume that the rate of charge can remain constant over the whole State of Charge (SoC) range. For typical batteries; however, this is true on about 80% of SoC range and as the battery gets closer to its high SoC region, charging is typically done at a lower rate. We have left investigation of more detailed battery models for future work.

is used to estimate the PEV demand. A minimum dwell time of three hours is assumed for charging. The scale for the PEV demand is on the left of the graph and the PEV demand for 30% penetration is shown as the dashed curve.

The solid curves in Figure 2.5 show the aggregate of ERCOT net load plus PEV load versus time of day, averaged across days in 2010, with the scale on the right of the graph. The lowest solid curve shows ERCOT net load, while the higher curves show ERCOT net load plus PEV load for various PEV penetrations of 10%, 30%, and 70%.

Figure 2.5 shows that the aggregate load can be very correlated with current demand, exacerbating the diurnal patterns of the total ERCOT net load and worsening the capacity factor of the electricity system. Moreover, if there is vehicle clustering in particular areas then high Peak-to-Average Ratios (PAR) can affect the distribution network, even if the PEV load might be relatively small compared to total aggregate load. Clustering is indeed likely. For example, the recently developed Mueller residential area in Austin, Texas, has a very high penetration of electric vehicles.

2.3.2 PEV Demand with Delayed Charging

Some PEVs support *delayed* charging where the PEV owner is required to enter his/her departure time and the PEV automatically starts at the latest time possible to finish charging before the departure time. The PEV is charged at the full charging rate and the charging profile is similar to immediate mode, except that is shifted to the end of the dwell time. Delayed charging rate is

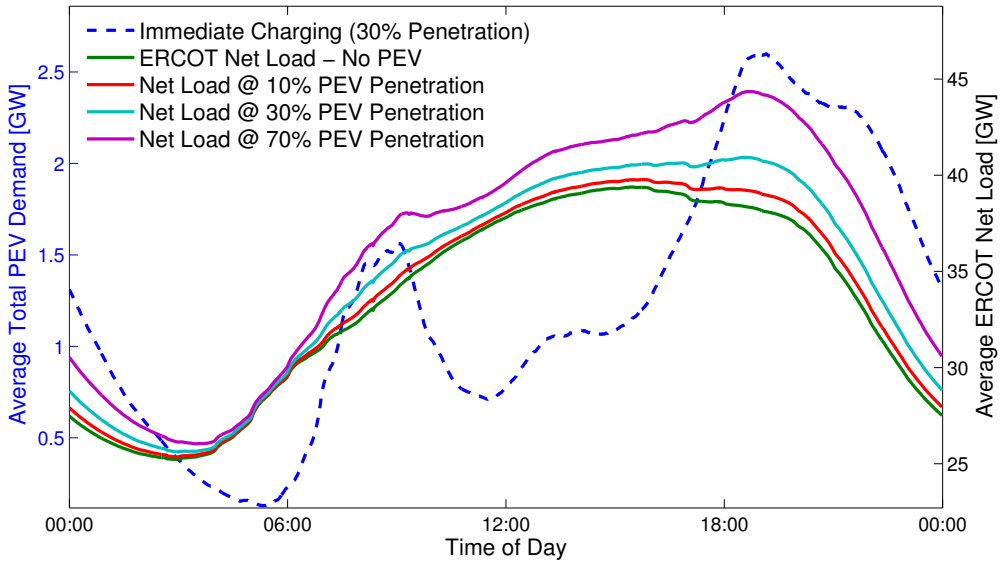

Figure 2.5: PEV load under immediate charging and its effect on ERCOT net load at different penetration levels.

given by:

$$x_t = \begin{cases} \overline{x} & t \geq \max\left\{t^d - \dfrac{d}{\overline{x}}, t^a\right\}, \\ 0 & \text{otherwise.} \end{cases} \tag{2.3}$$

From a PEV owner perspective, providing the departure time allows the car to use grid power to heat or cool the car before departure, which can reduce the load on the battery and therefore increase the distance that can be traveled in comfort. This is attractive in hot and cold climates and consequently it is not unreasonable to expect the owner to provide this information. Alternatively, the car could keep track of driver habits and estimate departure time on a daily basis.

Figure 2.6 shows the average electric demand when delayed charging

is employed by the users. Delayed charging is, in part, designed to avoid synchronization of start times of charging and the consequent high total loads. Therefore, it is somewhat surprising that delayed charging can actually be worse than immediate charging in terms of correlation with peak demand. In particular, the peaks of PEV load that occurred at 19:00 and 9:00 for immediate mode charging as shown in Figure 2.5 are shifted to 7:00 and 17:00, respectively, in delayed mode charging, as shown in Figure 2.6. The PEV load peak at 17:00 coincides with ERCOT typical summer peak demand that is due to air conditioning, increasing the aggregate peak. Again, high PARs can also affect distribution network, even if the aggregate PEV load is relatively small compared to total load. Moreover the morning charging contributes to greater net load ramp rates from 3:00 to 7:00, which can be problematic for thermal generation resources.

2.4 Improved Localized Policies for EV Charging

In this section, we develop localized policies that are aimed at improving the shape of the aggregate demand compared to immediate and delayed charging. We continue to assume, however, that the PEV/EVSE has no information/incentives about time varying electricity prices nor network status. We are also concerned with minimizing the burden on the local distribution network and furthermore observe that lower charging rates may be beneficial to batteries and infrastructure. However, we do not want to sacrifice any convenience for the PEV driver. In the next section, we present a charging policy

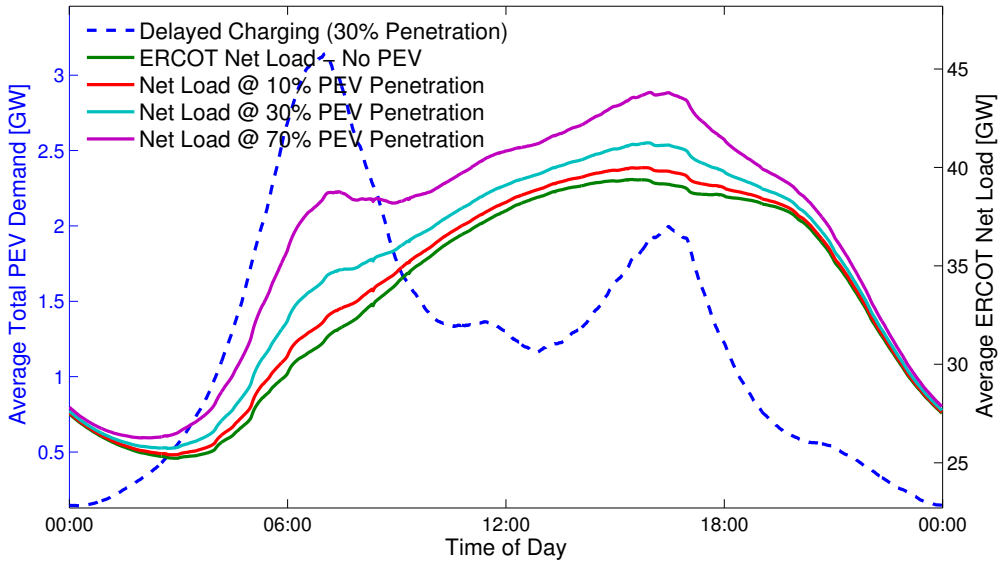

Figure 2.6: PEV load under delayed charging and its effect on ERCOT net load at different penetration levels.

that aids in these goals.

2.4.1 The Average Rate (AR) Charging Policy

Consider the following charging policy: As in delayed charging, upon arrival, the driver is asked for departure time. Charging is carried out at the minimum of: the EVSE capacity, and the ratio of the energy demand divided by dwell time. That is, the rate is chosen such that the dwell time is just enough to finish the charging, subject to EVSE capacity. We call this charging policy the *Average Rate (AR)* charging policy, and the charging rate for this policy is given by:

$$x_t = \min\left\{\frac{d}{t^d - t^a}, \bar{x}\right\}. \tag{2.4}$$

The AR policy requires no information nor incentives about prices or network status. It achieves a full charge by the departure time if possible, and so does not sacrifice convenience compared to immediate or delayed charging.

A variation on all of the localized policies is to restrict charging to periods when the vehicle is at home. In particular, the AR at home policy involves charging only at home, but at the average rate necessary to achieve a full charge between arrival at home and departure from home.

2.4.2 PEV Load vs. Wind Generation

Figure 2.7 compares the average PEV load using immediate, delayed, and average rate policies to the average ERCOT net load and to average ERCOT wind generation. Figure 2.8 shows the corresponding policies when charging is only available at home. Strikingly, the AR policy results in much lower peak rates of charging. As shown in Figure 2.7, the AR charging load is approximately flat throughout the day. As shown in Figure 2.8, the AR at home charging load peaks at night, is correlated with average wind production and is negatively correlated with average ERCOT net load.

2.4.3 Average Rate Policy - Analysis

The average rate policy has several advantages over the other localized policies. In particular, it results in:

- a much smoother local and aggregate load profile;

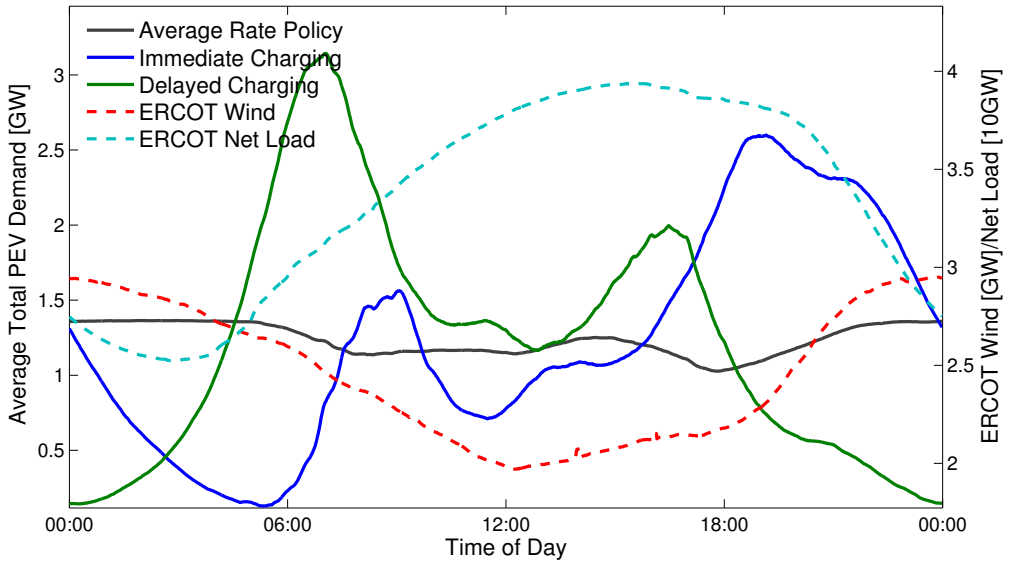

Figure 2.7: Comparison of Average Rate charging with immediate and delayed charging in terms of average daily profile and its alignment with average ERCOT net load and wind generation.

- much better correlation with wind generation;
- lower average state of charge for the battery, which may result in a longer battery life [89].

Like the other localized policies, it does not require communication and control between the PEV and a coordinator, there is essentially no sacrifice of user comfort, and can be readily implemented in current PEVs, possibly through a software update.

As discussed in the Section 2.2, electric vehicles have significantly more flexibility than is being exploited by the AR policy and the question arises as to whether this flexibility can be further exploited. Presumably, policies relying

on non-local information such as market prices would require communication and control to the PEV, but could then be used to track actual net load or system needs, rather than the average. Even policies based on locally available information such as frequency deviations from nominal, would require either incentives such as prices, or standards for frequency response to provide incentives for their adoption.

With communication and control, either explicitly to the vehicle or implicitly through pricing, demand response and coordination with the grid could enable the provision of, for example, ancillary services [25, 55, 58]. However, given that the localized policies like Average Rate charging can achieve significant benefits in terms of average load shaping, the additional cost of implementing communication and control for non-localized policies would need to be justified by significant benefits in terms of value of ancillary services or of matching PEV load to actual wind or net load profiles. The average rate policy sets a "high bar" for cost effectiveness of such non-localized policies.

2.4.4 Average Rate Charging with Minimum Range (ARMR)

While AR charging does not compromise user comfort in expected sense, it is not robust to unexpected changes in future plans. In other words, pure AR charging delivers a full charge by the *expected departure time* and if some emergency happens, the vehicle might not be ready for departure. One of the common examples illustrating such a situation is when a nearly empty PEV battery is needed to be ready by morning for the work commute; how-

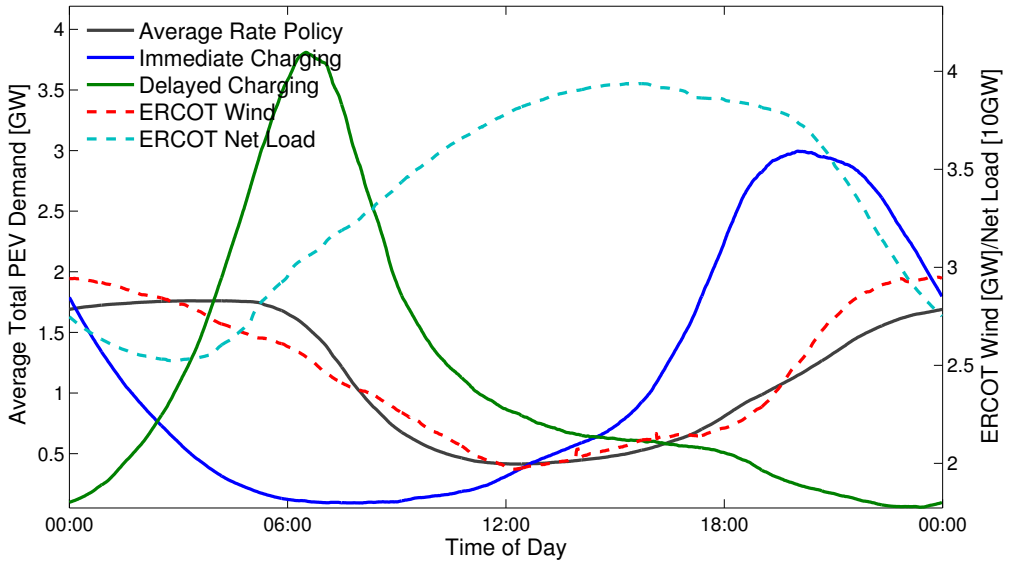

Figure 2.8: Comparison of Average Rate, immediate and delayed charging policies when charging is only available at home.

ever, a need for a trip to hospital might arise in the middle of the night. Yet, the simple solution to this issue, which would be picking a much earlier time for departure would effectively neutralize the benefits of AR charging.

To address this issue, we propose mixed AR policies, or AR policy with Minimum Range (ARMR). Under this policy, the driver is expected to provide a his/her desired minimum range/SoC level. Using this information, the EVSE would charge in immediate mode until that minimum range/SoC is satisfied and continues the charging process in AR mode. Let us denote the desired minimum SoC level, which can be translated to/from minimum desired range, by s° and defining d° as:

$$d^\circ = (d - (\overline{s} - s^\circ))^+, \tag{2.5}$$

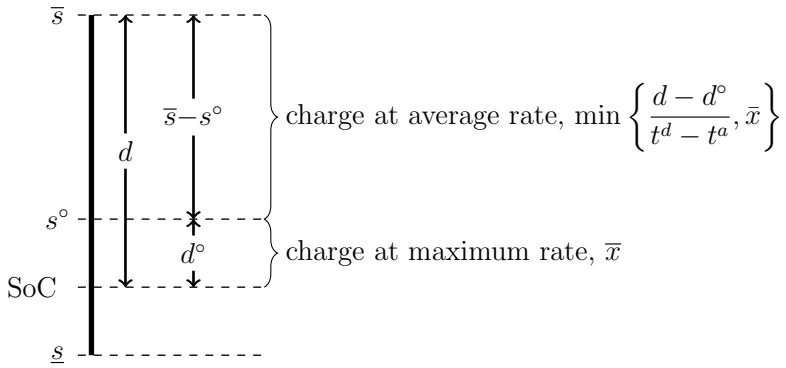

Figure 2.9: Average Rate Charging with Minimum Range when $d^\circ \geq 0$, i.e. $d \geq \overline{s} - s^\circ$. $\overline{s}$ and $\underline{s}$ denote maximum and minimum allowable SoC respectively.

where $\overline{s}$ is the maximum SoC of the PEV battery and $(\bullet)^+ \triangleq \max\{0, \bullet\}$. Then, the rate of charging for AR charging with minimum range is given by:

$$x_t = \begin{cases} \overline{x} & t \leq \min\left\{\frac{d^\circ}{\overline{x}}, t^d\right\}, \\ \min\left\{\frac{d-d^\circ}{t^d-t^a}, \bar{x}\right\} & \text{otherwise.} \end{cases} . \tag{2.6}$$

Figure 2.9, schematically depicts s° and charging rate as prescribed by ARMR in each region of SoC. Note that if SoC upon arrival is above s°, then the immediate mode would never be activated. This policy can be seen as a combination of pure AR and pure immediate charging. The ratio of mixing, however, changes based on demand since the s°, which is independent of d, is constant. Just like AR, ARMR only relies on the local information and hence inherits all implementation advantages of AR charging.

Using the same methodology as before, we investigated the performance of ARMR policy. Figure 2.10 compares the diurnal pattern of the load expected from ARMR with immediate and AR charging for $s^\circ = \overline{s}/2$, i.e. 50%

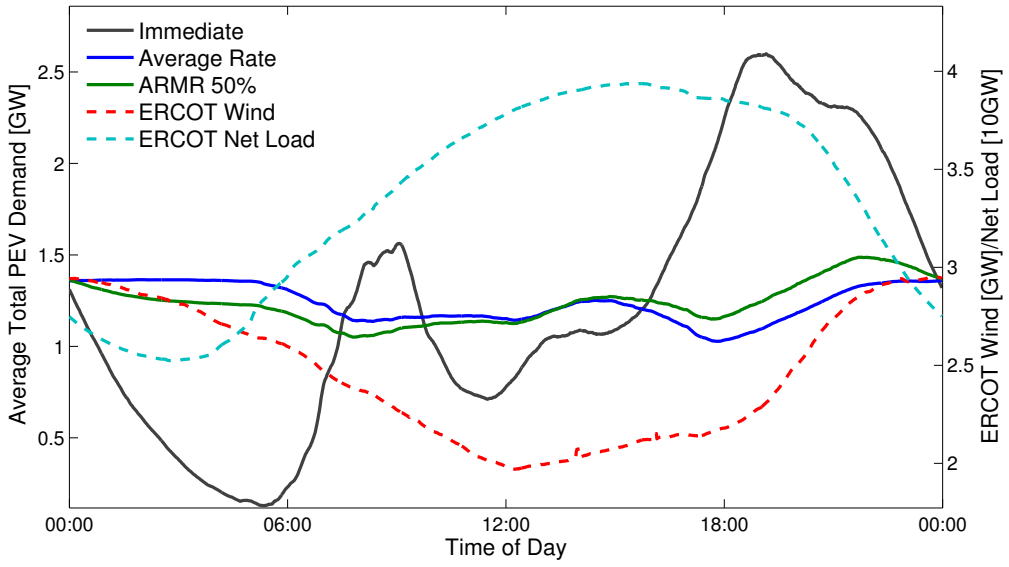

Figure 2.10: Comparison of Average Rate with Minimum Range (ARMR), Average Rate and immediate charging policies.

minimum SoC. Although this threshold seems pretty demanding, about 35-50 miles for a Nissan Leaf, the results show that ARMR maintains most of the benefits of AR charging. This strong performance stems from the fact that typically, PEV SoC upon arrival is above the minimum SoC. Moreover, even when there is need for immediate charging, the immediate charging period is much shorter and hence there is much less chance of coinciding the maximum rate consumption from various PEVs.

Similar to previous cases, we also studied home only charging under ARMR and the results are presented in Figure 2.11. Again, the results are very positive and close to pure AR policy. We find it very interesting that even for a minimum range of 50%, most of the benefits of AR charging are

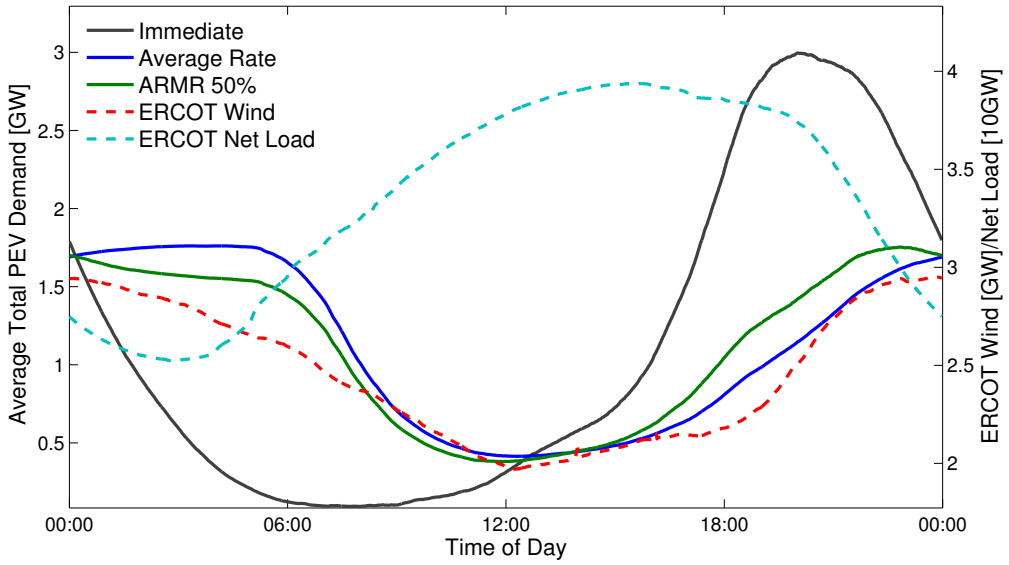

Figure 2.11: Comparison of Average Rate with Minimum Range (ARMR), Average Rate and immediate charging policies when charging is only available at home.

still valid while user comfort is robustly maintained.

2.5 Anticipative Charging and Its Impacts

2.5.1 Anticipative PEV Charging Model

Most previous work and our earlier analysis have studied electrical demand from PEVs as a group of independent charging sessions that randomly occur over time, with potentially time varying probability of occurrence.

In contrast, we argue that an anticipative model needs to be adopted for modeling and optimization of PEV charging load, where user demand and hence charging decisions are made by the driver in anticipation of his/her

future transportation plans. This anticipative behavior particularly has two aspects: First, how does the length of future trips affect the likelihood of charging. That is, the impact of the range needed to complete future trip(s) given the current State of Charge (SoC) and consequently available range of the vehicle. Second, how does the location of future destination(s) affect the charging decision at the current location. That is, whether or not charging is available, economic or convenient at that destination.

Let us illustrate the anticipative behavior with an example. Consider a PEV owner that leaves home in the morning, goes to work and finally visits a store sometime in the afternoon on his way back home. Assume that charging is available at all of these places. In the non-anticipative model, the charging policies would consider three potential charging sessions at each of these locations with energy demand to potentially fill the battery. Under the anticipative model, however, the charging sessions and even user availability for charging at each of these locations, are considered in a correlated fashion. For example, the user may not even plug-in to the charging station at the store, just because the available range of the PEV is enough to reach home, where charging is potentially more comfortable and/or economic. In contrast, if charging is complimentary at the store or work, then the user might be more inclined to charge at the store/work.

The impact of the anticipative model on the performance of charging algorithms and its resulting impact on the grid can be significant. Let us consider a charging cost minimization algorithm similar to what is introduced by

Mohsenian-rad *et al.* [72] to demonstrate this impact. In this charging algorithm the price of electricity is assumed to be time dependent but known. The goal of the algorithm is to find the charging power trajectory that minimizes the total energy cost of charging. To achieve this, the algorithm needs to decide how much to consume at each time slot to minimize the total charging cost subject to the known prices for each time slot, energy demand of the PEV, charging capacity of the EVSE and its availability window. To formalize, the algorithm tries to solve the following optimization problem:

$$\min_{x_t} \quad \sum_{t^a \le t < t^d} c_t x_t + \eta(d - \sum_{t^a \le t < t^d} x_t) \tag{2.7}$$

$$\text{st.} \quad 0 \le x_t \le \overline{x}_t, \quad \forall t \in [t^{a_i}, t^{d_i}) \tag{2.8}$$

$$\sum_{t^a \le t < t^d} x_t \le d, \tag{2.9}$$

where η is the unit cost of unsatisfied demand, t^a and t^d are the arrival and (desired) departure times of the PEV, c_t is the price of electricity over time, d is the desired demand and finally $\overline{x}_t$ is the EVSE capacity at time t. The optimal solution to this problem, $\boldsymbol{x}^*$, is the optimal trajectory which minimizes the total cost. In contrast, if an anticipative model is considered, the objective would still be minimizing the total cost of energy. However, the minimization would take place over the potential future charging sessions so that all the trips can be made while considering price variations across time and location as well as EVSE capacity variations over different locations. This problem can

be similarly formulated as a linear program:

$$\min_{x_t} \quad \sum_{t \in T} c_t x_t + \eta(\overline{s} - s_{t^{\max}}) \tag{2.10}$$

$$\text{st.} \quad 0 \leq x_t \leq \overline{x}_t, \quad \forall t \in T \tag{2.11}$$

$$x_t = 0, \quad \forall t \notin T_a \tag{2.12}$$

$$s_t = s_{t-1} + x_t - d_t, \quad \forall t \in T \tag{2.13}$$

$$\underline{s} \leq s_t \leq \overline{s}, \quad \forall t \in T \tag{2.14}$$

$$\sum_{t' > t} d_{t'} + \underline{s} \leq s_t, \quad \forall t \in T \tag{2.15}$$

where T is the span of time over which the optimization takes place (e.g. the next 24 hours), T_a is the set of times at which the PEV is available for charging, c_t is the cost of electricity at time t and location PEV at time t and, s_t is the State of Charge (SoC), with $\underline{s}$ and $\overline{s}$ as its lower and upper bounds respectively. Also, d_t is the total energy demand accumulated at time t (due to travel – over which the PEV is unavailable for charging). Finally $t^{\max} = \max\{t | t \in T\}$. As mentioned, besides the standard constraints in (2.11)-(2.14), we have constraint (2.15) that enforces the ability of the vehicle to finish all the trips without running out of energy. Note that since constraint (2.15) guarantees feasibility of future trips, if possible, we might want to set η to zero.

While these two optimization problems seem very different at first glance, we argue that the differences are minimal. In fact, the changes in the constraints and model are only there to jointly consider multiple charging

sessions, which are the result of the anticipative behavior. For example, if we have multiple potential charging sessions in the horizon, indexed by i, we would essentially have, $T^a = \bigcup_i [t^{a_i}, t^{d_i})$ and $d_{t^{a_i}} = d_i$. Since the anticipative approach effectively jointly considers multiple instances of the original model, it always yields a better solution. In cases where the anticipative information is not available, the problem will be reduced to the non-anticipative model. However, the future behavior information is typically available, over a reasonable time horizon, due to the routines in the driver's life. This is in fact the basis of many decisions people take. For example, let us consider a typical decision making process for filling up a gas tank. Most people typically fill their tanks in an anticipative fashion, that is, they refill when the level of gas is so low that they might not make their anticipated trips in near future and/or they are at a position when the time/energy cost is relatively low. In other words, drivers do not go to gas station as soon as their level falls below full. Another similar example is the decision process in eating out vs. taking food from home for office workers. In fact, the current models for charging mostly stem from the relatively low capacity of the batteries and the range anxiety perception, which is shown to go away once drivers establish their driving behavior [61].

Anticipative charging behavior can result in a multitude of changes: First, the SoC of the PEV arriving at the charging station would typically be lower because the users do not charge as soon as a charging opportunity is found and there is charging demand; resulting in typically higher energy

demand. Second, anticipating their ability to finish their future trips, the users would skip some charging opportunities. Under the anticipative model, charging sessions will be less frequent and more demanding and hence less flexibility is expected. Yet, while we show this decreased flexibility in the next section based on transportation data, the impact on the overall behavior of the users may or may not be negative and depends on the charging algorithm employed.

2.5.2 Analysis of the Impact of Anticipative Behavior

To model the anticipative behavior, we consider the case where at every stop the driver knows how far away the next potential charging stop, one that is going to be longer than three hours, is and charges only if the remaining range of the PEV is not sufficient to reach this destination. This is of course an extreme case in the sense that this is basically minimal amount of charging stops to keep the normal travel plan feasible.[3] Moreover, information about future trip(s) may not always be available.

Given the fact that longest stops typically happen at home and they are typically before the longest commute of the day, home charging can be considered an asymptotic approximation of the anticipative behavior to some

[3]In fact, this kind of behavior may not *guarantee* feasibility of future plans since it is possible that the trip after the next stop might demand more than what can be charged in the next stop. For this reason, the kind of anticipative behavior we modeled here can be referred as *myopically* anticipative. Yet, this should perhaps be the appropriate behavior since a fully anticipative model requires full information about all future trips, which is a very demanding assumption.

extent. For this reason and the other reasons discussed in previous sections, we pay particular attention to anticipative behavior when charging is restricted to home only.

Anticipative behavior, as modeled here, only affects drivers decision to charge or not charge. Therefore, in order to analyze the impact of the anticipative model, we consider our previously introduced charging policies: immediate and Average Rate.

Let us consider average flexibility as defined in (2.1) for different minimum dwell times for everywhere charging and home only charging under anticipative and non-anticipative models, which is presented in Figure 2.12. The average flexibility presented in this figure is over all charging sessions in the dataset which have occurred under each scenario. For example, setting a minimum dwell length of three hours, under the non-anticipative charging model, all the stops with length more than three hours at the respective locations (everywhere or home only) are considered for charging. Under anticipative model, not only the minimum stop time and location is taken into account, but also charging happens only if the current SoC cannot support driving to the next potential charging stop that satisfies the length and location requirements.

As expected, the average flexibility of anticipative charging is uniformly and significantly below the non-anticipative model. The reduction in average flexibility is roughly 50% across different minimum dwell lengths. We must stress however, that while in most scenarios we have assumed that the whole population shall follow the same behavioral model, in reality, the diversity

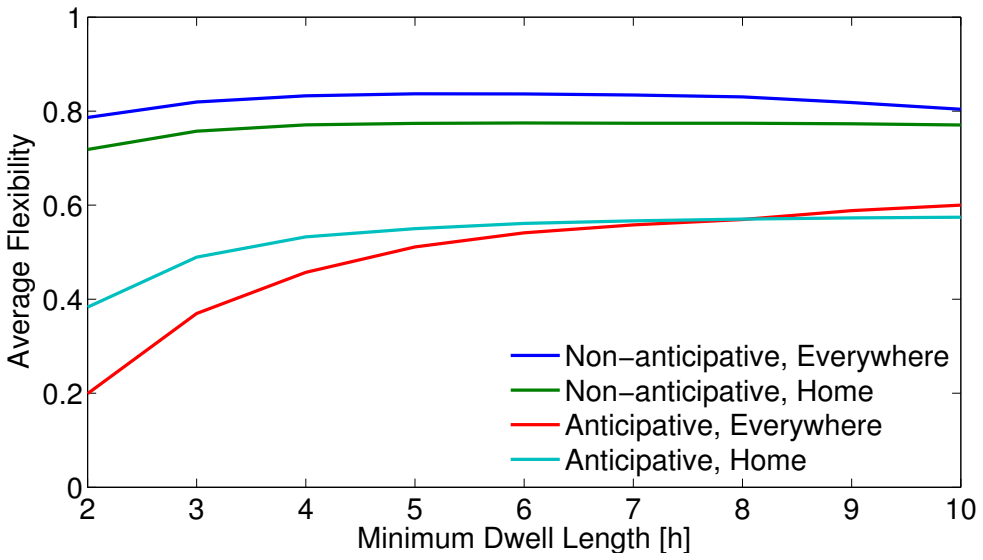

Figure 2.12: Average flexibility of PEV charging under various models.

in the population of drivers and their preferences results in a mixture of the extreme points demonstrated here corresponding to various pure behaviors.

The reduction in flexibility means that the charging optimization problem, irrespective of its particular algorithm, would be more constrained. Consequently, the gains envisioned for PEV charging might not materialize as strongly as suggested in previous studies.

In order to investigate the impacts of the anticipative behavior we compared the charging policies introduced previously under anticipative and non-anticipative behaviors. Figure 2.13 compares the diurnal patterns of immediate and Average Rate charging policies under anticipative and non-anticipative behaviors when charging can happen at every location the PEV stops more

than three hours. The PEV average diurnal load, marked on the left axis, is averaged over all PEVs and all days. Note that it does not represent how a typical PEV load looks over the day, rather, it shows the typical normalized fleet load by PEV. As previously suggested [56], Average Rate charging results in a much smoother impact on the average diurnal load. Our results here show that anticipative charging does not fundamentally change the diurnal patterns of the charging policy and hence the benefits of AR charging are still valid. Interestingly, anticipative immediate charging results in better overall patterns compared to the non-anticipative version by shifting the peak load of PEVs to further times in the evening and reducing coincidence with the net load peak. To demonstrate the impact of the PEV load on the net load, we have also plotted the ERCOT diurnal net load average and augmented it by the expected power load from each scenario in Figure 2.14. Here we have assumed electrification of 30% of roughly 15 million vehicles registered in Texas. As depicted in this figure, anticipative charging actually reduces the negative impact of added PEV load while AR policy works well under both models. Note that even AR charging needs an increase in the total capacity of the grid since it almost uniformly affects the diurnal pattern of the load.

The shift of the load towards later hours of the day as a result of anticipative behavior can be attributed to stops that are not used for charging since a short trip in the evening (perhaps for some shopping or having dinner) is expected and hence the stop between arrival from work and that trip is skipped in favor of the long stop over night; particularly because the next trip

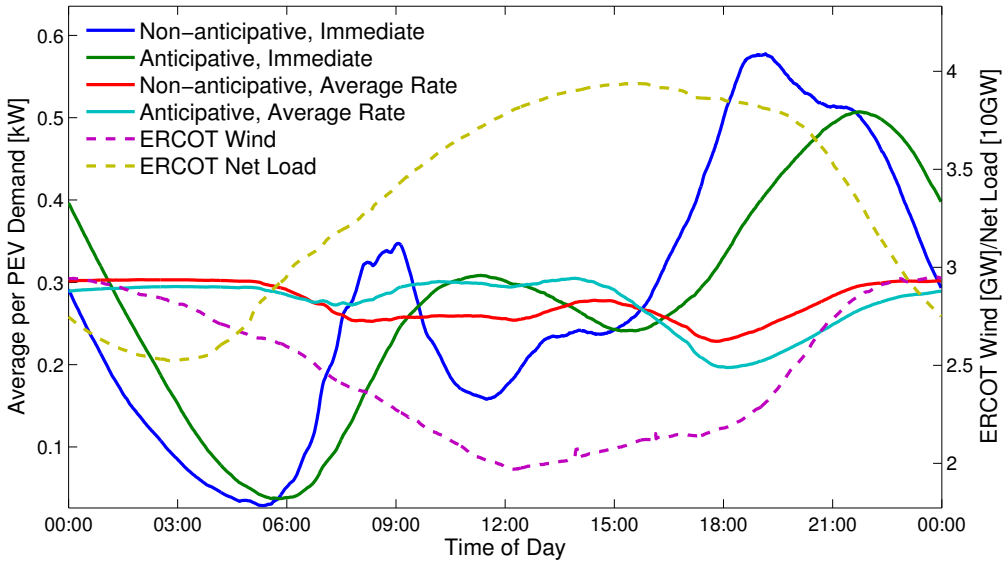

Figure 2.13: The average diurnal pattern of PEV load under various behavioral models and charging policies when charging is available at all stops longer than three hours and its comparison with average diurnal net load and wind generation in ERCOT.

will be the morning trip to work which is typically one of the longest trips taken routinely. As we pointed out in the preceding analysis, this makes the result of anticipative behavior look more like home only charging.

As discussed in the previous sections, home only charging, particularly in presence of financial incentives, presents itself as the dominant place where PEVs are to be charged. Moreover, since stops happening at home tend to be the longest, mostly overnight and before the longest typical trip of the day (e.g. going to work or running errands), home charging can be viewed as the asymptotic limit of anticipative behavior. Therefore, we specifically studied

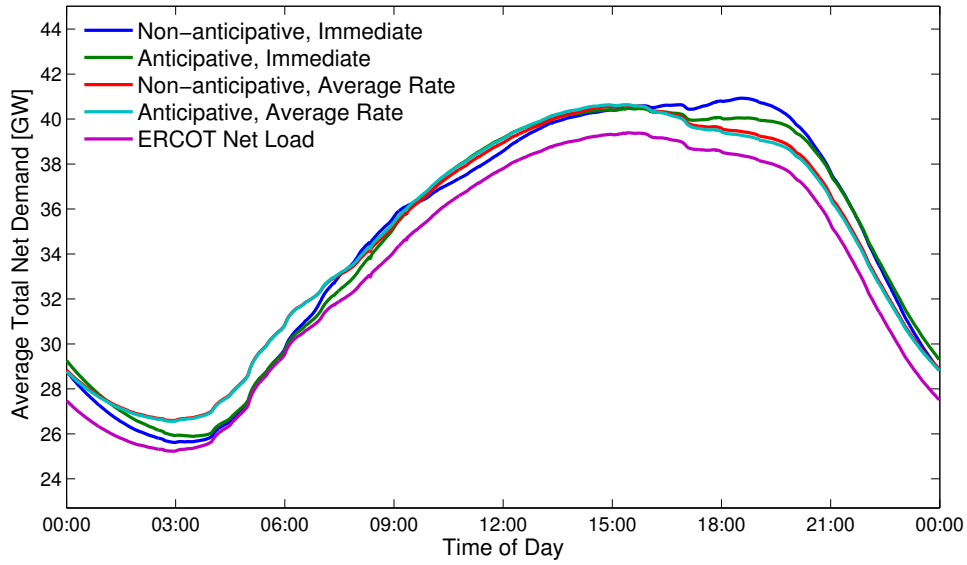

Figure 2.14: The impact of various behavioral models and charging policies on the average diurnal pattern of ERCOT net load when charging is available at all stops longer than three hours.

charging under the same policy set and scenarios assuming that charging can happen only at home. Figure 2.15 compares various policies and scenarios in terms of their average diurnal power load. Similar to everywhere charging, anticipative charging does not have a dominant effect on the overall behavior of the charging policies investigated. A similar shift to later times of the day is observed in case of immediate charging. Affirming our hypothesis on the connection between home charging and anticipative behavior, it can be observed that there is no material difference between the results of the AR policy when users behave anticipatively or not. Similar to Figure 2.14, we have presented the superposition of the expected PEV load in ERCOT assuming

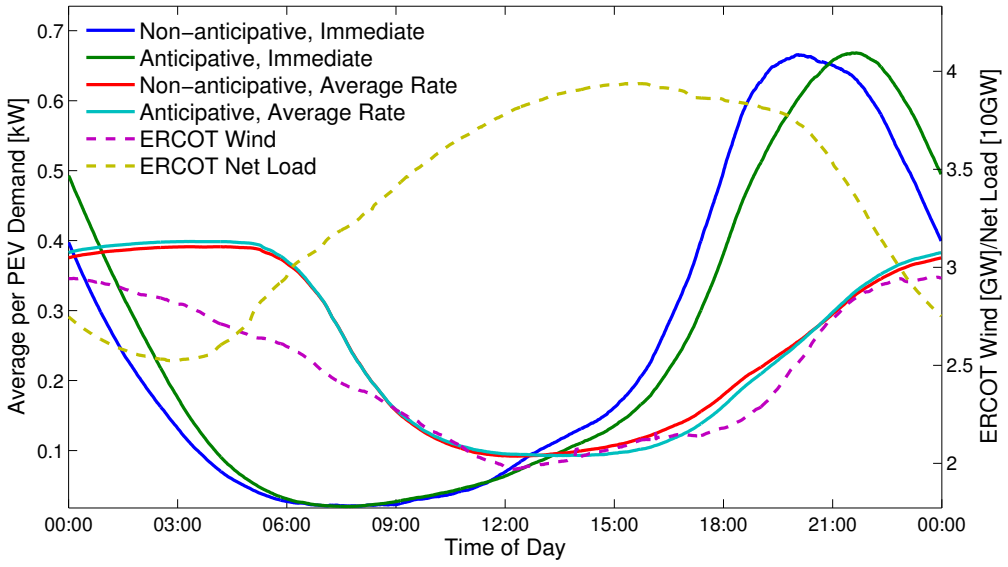

Figure 2.15: The average diurnal pattern of PEV load under various behavioral models and charging policies when charging is only available at **home** (with minimum stop time of three hours) and its comparison with average diurnal net load and wind generation in ERCOT.

30% penetration rate of PEVs on the ERCOT net load in Figure 2.16. It can be observed that the concentration of the load resulting from immediate charging in the early hours of evening shifts and exacerbates the peak hours of load. Moreover, anticipative behavior marginally improves the situation by shifting the load further in the evening hours which would overall help the load pattern. Finally, it is confirmed that AR charging has a very marginal effect, 1.2% to be exact, on the peak of the diurnal pattern. The increase is about 3% for immediate charging under anticipative model and about 5% under non-anticipative immediate charging. This is particularly interesting considering

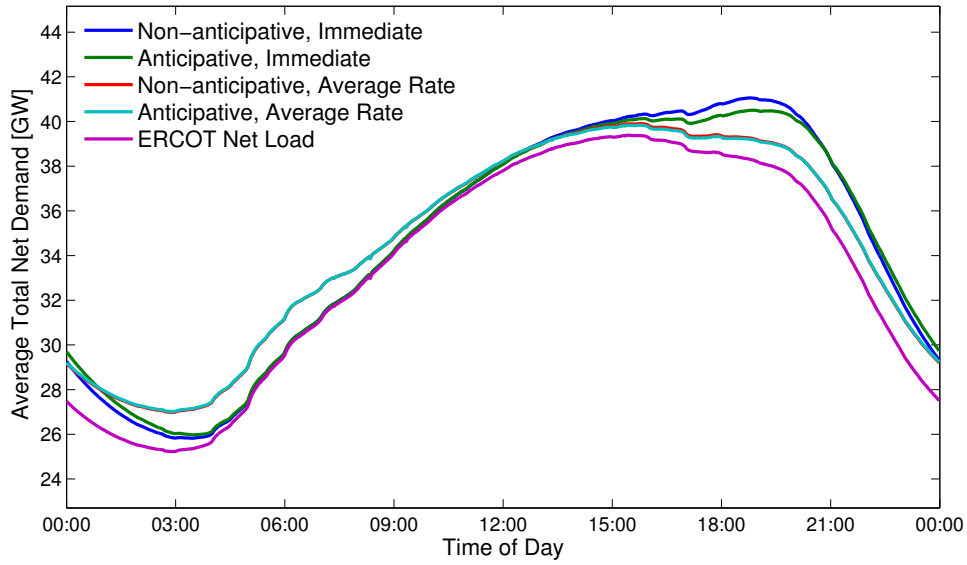

Figure 2.16: The impact of various behavioral models and charging policies on the average diurnal pattern of ERCOT net load when charging is available at all stops at **home** that are longer than three hours.

the fact that anticipative charging generally decreases demand flexibility and hence could have a negative effect on the benefits of the charging algorithm. We believe that this improvement, rather than worsening, is because non-anticipative immediate charging does not utilize flexibility at all.

2.6 Ancillary Service Potential of Localized Charging Policies

2.6.1 Background

Although the grid is a very complex network with different constraints, its stability first and foremost hinges on supply demand balance. Maintaining

this balance at fine grained time steps seems a very challenging task due to the need for coordination; however, in the current grid structure, frequency is the key global indicator that reflects the overall supply demand balance relatively instantaneously. In fact, the rate of change in the system frequency, which is essentially[4] the same quantity at any point in the grid[5], is a strictly increasing function of supply minus demand at the normal operation point. Hence, it can be used as the error signal to locally estimate the imbalance and respond to it. This basically forms the basis for the control system implemented in the governor of most of the generation assets in the current grid and plays a fundamental role in responding to contingencies like unit trips [12]. Therefore, it should be fair to say that frequency is the heartbeat signal of a synchronous grid.

Maintaining supply demand balance and frequency control (a.k.a. frequency regulation) is one of the major tasks of the ISOs and to this end, all North American power markets include products that help this cause, broadly referred to as reserves or Ancillary Services (AS). The variety of the reserve products, at least traditionally, stems from the variety in different events that cause frequency deviations and can be coarsely categorized by their speed of response and magnitude.

[4]Disregarding transients, and putting aside difficulty in defining frequency when the system is not in quasi-steady-state as frequency and its rate of change may vary across the system in that situation.

[5]Here the grid means a wide area synchronous grid, which in the context of the North American grid includes the Eastern, Western, Quebec, Texas and Alaska Interconnections.

Of particular interest in our work is the frequency regulation service (REG), also known as Automatic Generation Control[6] (AGC) and Load Frequency Control (LFC), which is a paid service that is deployed by the ISO to correct frequency deviations in between the market clearing set-points. This service traditionally handles load forecast errors and usually is dispatched in the order of seconds, e.g. every four second in ERCOT. As more wind is integrated into the system, however, REG is used to stabilize the "net-load" deviations and hence used to control (short-term) uncertainties due to wind as well. Various authors [26, 33, 58] have proposed using flexible loads, and particularly PEV load to provide regulation service, however, most of the proposed solutions require communication capability between EVSE and the ISO or a Load Aggregator. Here, our focus is on localized policies that minimize the need for communication with a central management entity.

2.6.2 Frequency Responsive Average Rate Charging

Given that frequency measurement can be done inexpensively at each charging station[7], our work on localized policies for serving flexible demand, can be extended by augmenting the proposed policies to respond to frequency, as yet another localized piece of information. Recent results [113–116] establish that frequency can in fact provide the right signal for re-balancing the system

[6]Technically speaking, AGC is the control system and communication medium through which the REG signal is delivered to the resources.

[7]In fact, there are some charging stations already capable of measuring grid frequency in the market.

after contingencies and such frequency responsive policies can be viewed as a primal-dual algorithm for minimizing the deviations from the desired frequency set-point. Frequency augmented policies can improve the accuracy of the response from flexible loads, particularly PEVs, to the instantaneous status of the grid; and, not only counter balance intermittency of wind, but also, compensate for the "reduced inertia" if they respond fast enough. In its most basic form, using a proportional controller, the frequency responsive average rate policy is given by:

$$x_t = \min\left\{\left(\frac{d_t}{t^d - t} + \alpha_t \Delta f_t\right)^+, \bar{x}\right\}. \tag{2.16}$$

where d_t denotes the remaining demand of the load which is initialized by $d_{t^a} = d$, α_t is the coefficient of response and Δf_t is the measured frequency deviation. In practical settings, Δf_t can be a low-pass and dead-band filtered version of instantaneous frequency deviation measurement which would correspond to a PI controller with dead-band for noise rejection. To maintain user comfort by guaranteeing energy delivery by the desired deadline, the policy needs to respond to deviations of the charging rate from the desired average rate due to frequency deviations and particularly their imbalance.

Determining the proper coefficient of response, α_t, which is analogous the droop characteristic in governors, can play an important role as well. While it can be preprogrammed off-line, it can be adjusted more dynamically based on willingness to cooperate by the PEV owner. It can also depend on time and/or remaining time to depart. Figure 2.17 depicts sample response of

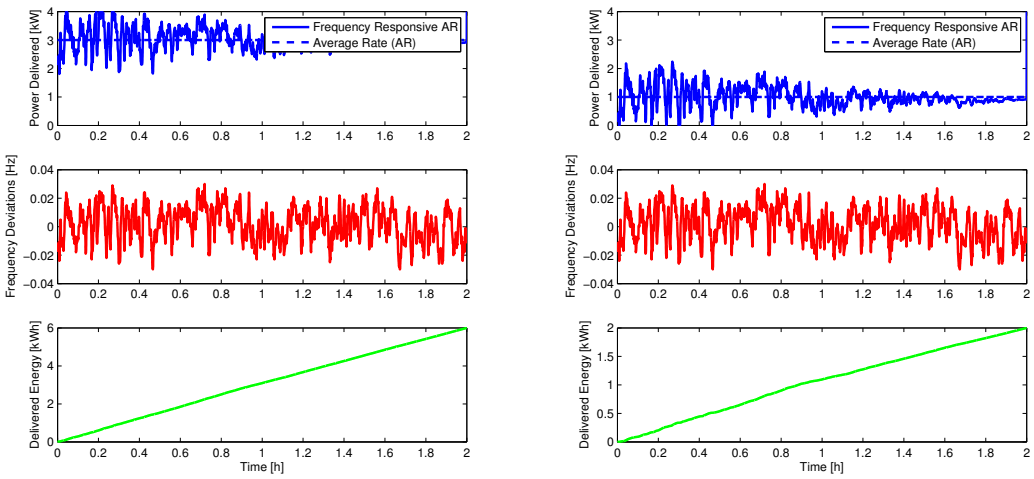

$d = 6$ kWh $\qquad$ $d = 2$ kWh

Figure 2.17: Frequency Responsive Average Rate Charging with high and low demand. (Linear α_t decrease, $\overline{x} = 4$kW)

flexible loads under frequency responsive average rate and compares them with AR policy for high and low demands. Due to the other feedback loops inside the battery charging power electronics, there can be different delays between the actual behavior of the battery and the desired charge rate. Such delays can affect the actual performance of load response to frequency and in pathological cases, when it is mostly out of phase with frequency deviations, it can negatively affect the supply-demand balance.

It should be noted that such localized response can be compensated at some level based on performance since measuring performance and deciding on compensation can be done *ex-post* based on the metered consumption data. Of course the data communication and storage requirements in this case is much

higher as the (time) resolution of the recorded signal significantly increases. For example, moving from a quarter hour metering which is common in most Advanced Meter Reading (AMR) and Smart Grid setups to an every four second metering, equivalently increasing sampling frequency from 1 mHz to 0.25 Hz, results in 225 times more metering data! However, the total amount of data remains very manageable by today's communication and computing capabilities; e.g. a month worth of 4 byte data samples with 1Hz sampling frequency would take only about 10 MB. In line with the rest of this chapter, here we focus more on quantifying the potential of AS that can be provided by PEV demand and leave particular algorithms for designing the optimal response by PEVs for future work.

2.6.3 Symmetric AS Potential of Average Rate Charging

In most markets, regulation products are viewed as (reserve) capacity and are expected as symmetric capacity to move up and down at a minimum specific rate[8]. The symmetry requirement effectively disqualifies immediate and delayed charging, or any charging policy that only uses max rate over its period of activity for that matter, because at maximum rate, there is no room for more consumption. For AR charging, however, there is some headroom that enables provision of AS.

Note that, for PEVs demand response potential, as in the amount of

[8]To the best of our knowledge, ERCOT is the only market in which REG service is traded asymmetrically, i.e. a market participant can provide REG Up, REG Down or both with different capacities and each of these commodities are priced separately.

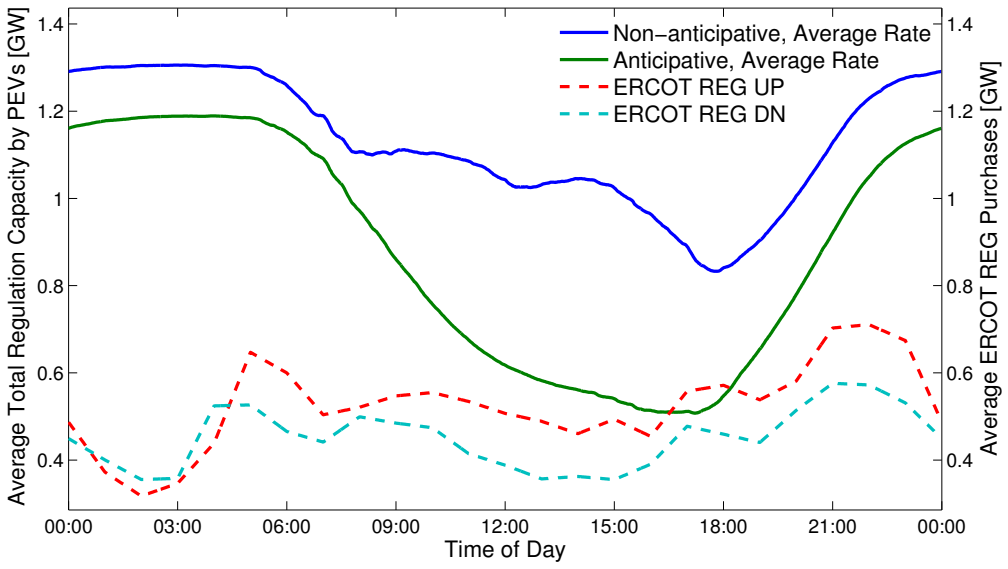

Figure 2.18: The average diurnal pattern of symmetric AS capacity due to PEV load under various behavioral models and Average Rate charging policy when charging is available at all stops longer than three hours and its comparison with average diurnal REG UP and REG DN amounts purchased by ERCOT.

load that can be reduced in relatively short period of time, is roughly equal to the PEV load level. This is because in most cases, the flexibility in PEV load makes it plausible to completely stop consumption without causing noticeable discomfort for the users for short periods of time. Therefore, in the proceeding text, we focus on symmetric capacity of PEV load since most frequency based AS has such requirements.

Based on the symmetry requirement and using the same notation we used in previous sections, the AS capacity of a PEV charging at rate x_t is

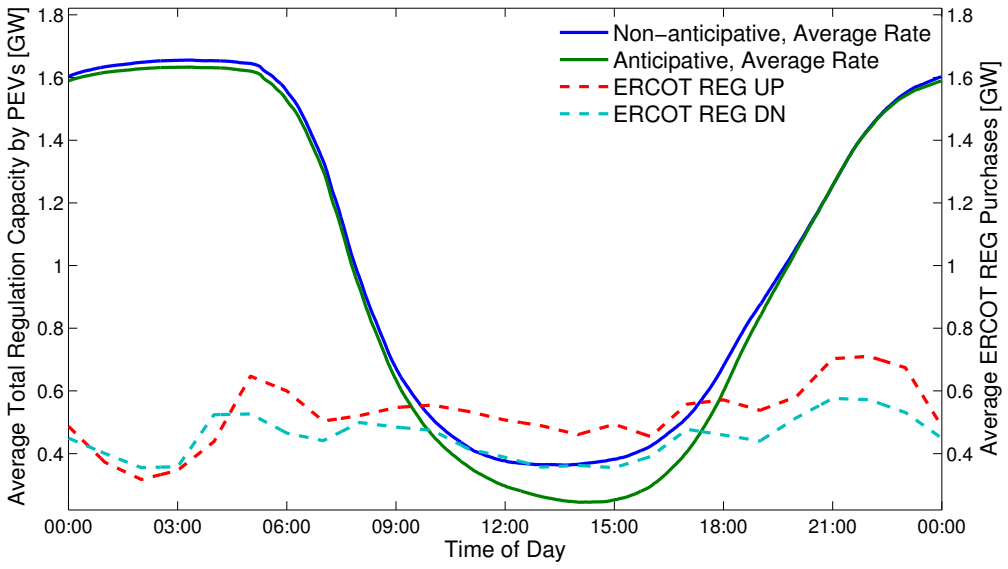

Figure 2.19: The average diurnal pattern of symmetric AS capacity due to PEV load under various behavioral models and Average Rate charging policy when charging is only available at **home** (with minimum stop time of three hours) and its comparison with average diurnal REG UP and REG DN amounts purchased by ERCOT.

given by:

$$c_t = \min\{x_t, \overline{x} - x_t\}. \tag{2.17}$$

Using this measure, we can now analyze the potential symmetric AS capacity of PEVs similar to our analysis in the previous sections, in terms of its average diurnal patterns. To this end, we have presented the results in Figure 2.18 and Figure 2.19 for everywhere and home charging respectively. We have also depicted the patterns for anticipative and non-anticipative models to demonstrate the effect of the anticipative behavior.

It is very interesting that the total AS capacity provided at 30% penetration rate is a pretty sizable number, roughly between 600MW to 1300MW for everywhere charging and 200MW to 1600MW for home only charging, which is comparable to diurnal average of total amount of REG purchased by ERCOT as depicted in dashed lines. Note that even with anticipative charging, the amount of REG potential of average charging stays completely above the current total purchases of REG, suggesting that even if only a fraction of the PEVs adopt the frequency augmented AR, the REG burden of the system can be potentially reduced. Although capturing the reliable amount of this autonomous response, in a way that the ISO can count on, might be hard, the impact of such response on REG deployments would reduce the utilization of such assets and automatically reduce the total amount acquired if the system is designed to decide total purchases based on performance (e.g. ERCOT). Overall, we believe that there is substantial potential in autonomous response and localized ancillary service provision by flexible loads and in particular PEVs.

The other interesting result is that the amount of AS capacity, which unsurprisingly has a similar pattern as the diurnal average load, has close to maximal capability on early hours of day and night. These hours, as suggested by the diurnal patterns of AS purchases, are the hours in which REG is needed most, which is mainly due to the typical wind power fluctuations and uncertainties in those hours. Therefore, AS capacity provided by AR charging is well correlated with the system need. The other positive aspect of this AS

capacity is that particularly in early hours of the day, many generators are ramping up production and providing AS adversely affects their ramp rate; hence, the AS provided by load can open up some ramping capacity for the system.

The impact of increased energy demand and reduced flexibility due to anticipative charging is very vivid, particularly when charging is available everywhere. AS capacity is reduced almost by 40% when anticipative model is adopted. Yet, this is not very surprising given the fact that we already knew that average flexibility of PEV load is almost reduced to half under the anticipative model. In fact, since our flexibility measure and the rate adopted by AR charging have a very similar structure,[9] this result suggests that under non-anticipative charging, charge rates are typically closer to zero, the lower bound in Equation 2.17, rather than the EVSE capacity while under anticipative charging the rates are typically closer to the EVSE capacity. Consequently, charging headroom plays a more important role in setting the AS capacity, similar to what is depicted in Figure 2.17.

2.7 Conclusion

Plug-in electric vehicles are one of the prime examples of flexible loads and expected to have major impact on the grid in terms of overall energy demand. In this chapter, we took a data driven approach to study the impacts

[9]The rate adopted by AR charging is essentially 1-flexibility, subject to EVSE rate limit.

of transportation electrification. We quantified energy needs of PEV charging and its distribution over time under various charging policies. We particularly demonstrated that under conventional consumption, also known as immediate charging, the resulting electrical demand would negatively impact the grid by exacerbating demand peaks. We then proposed Average Rate charging as a simple alternative which would only depend on local information about PEV and showed that it would substantially change the PEV charging load patterns by decreasing its correlation with current net load of the grid and increasing its correlation with wind generation on average, particularly if charging is limited to homes. We then proposed improvements to AR charging to make it more robust to unexpected changes in transportation plans. We also studied more realistic models of user behavior under which drivers may not take advantage of all charging opportunities and showed that while it considerably reduces demand flexibility, it will not have a substantial effect on average diurnal patterns of the load. Finally, we studied ancillary service potential of PEV demand and concluded that, with proper infrastructure and incentives, the PEVs can provide substantial amounts of ancillary services.

Chapter 3

Optimal Response of Flexible Loads to Real-time Stochastic Prices

3.1 Introduction

From the consumers' perspective, the value of demand flexibility can be translated into reduced bills. However, in many cases, there is a trade-off between the level of flexibility and the consumer's comfort. For example, it is typically desired to charge an EV battery as fast as possible, i.e., minimal flexibility; yet, should the right incentives be provided, the consumer would trade-off his/her comfort/desire. The key to achieving this value is not only the right pricing schemes on the utility side, but also optimal algorithms to respond to those schemes with minimal intervention by a user.

Using demand flexibility to improve costs has been considered in various contexts by different authors [22, 25, 58, 72, 79, 103, 104]. Mohsenian-Rad *et al.* [72] propose a price-based residential load scheduling algorithm for smart grids. They consider a combination of real-time pricing (RTP) and inclining block rates (IBR) and model delay aversion by inflating future prices. They first formulated and solved the deterministic model and then extended it to the stochastic case by proposing a price estimation method, essentially run-

ning a certainty equivalence control (CEC) technique. Although their model can be applied to a wide range of scenarios, due to adopting CEC, it fails to capture the opportunistic behavior of load in response to actual variation of prices. Caramanis and Foster [25] consider optimal operation of a load aggregator responding to the spot market and simultaneously offering reserves to the grid by modulating its instantaneous demand by directly controlling each load. A computationally efficient approximate method to solve this problem is later proposed by Kefayati and Caramanis [58]. In another approach to utilize demand flexibility, Papavasiliou *et al.* [79], consider coupling flexible loads with wind generation to reduce the uncertainty of net production. Solutions based on approximate dynamic programming are proposed and used to further analyze the economic merits of the coupling. Neely *et al.* [76] approach the same problem through Lyapunov optimization and obtain a computationally efficient approximate solution that guarantees *order-wise* delay and cost performance.

In this chapter, we study the demand flexibility, particularly translated to time flexibility or delay tolerance by proposing a model for delay tolerant loads which have cost/delay trade-offs subject to uncertain spot pricing. We formulate the problem of energy delivery to such loads as a dynamic program and propose an efficiently computable closed form solution both for the optimal policy and the expected energy delivery cost given price statistics and load preferences. Using our proposed model, we analyze the value of flexibility from the consumers' perspective in terms of the reduction in the expected

cost of demand satisfaction. Finally, we analyze the collective behavior of delay tolerant loads through simulations. We show that, similar to the results by Sioshansi [88], real-time pricing does not always induce desired behavior of the load since opportunistic behavior of demand can exacerbate uneven distribution of the demand and lead to high peak-to-average ratios (PAR) in the aggregate demand.

The rest of this chapter is organized as follows: In Section 3.2 we present our model. Section 3.3 is dedicated to presenting our results on the optimal demand satisfaction algorithm and discussion on its computational efficiency. Section 3.4 is dedicated to a comparative analysis of the performance of our proposed algorithm through simulation as well as its system level impacts. The proofs are moved to appendices for better readability.

3.2 The Model

We consider a flexible consumer with a total energy demand. We desire to satisfy its demand by deciding how much to consume in a discrete time fashion over a finite horizon. We assume that only statistics of the energy cost is known *a priori*. Furthermore, the consumer is assumed to be potentially delay-averse, that is, there is a (subjective) cost to the consumer associated with delaying demand satisfaction.

This model captures the essential features of a delay tolerant demand for the purpose of our analysis. Consider an electric vehicle (EV), for example, under real time pricing (RTP) of electricity at the charger location. This model

essentially captures the cost of charging subject to a deadline. Furthermore, as the vehicle owner may need the car before his stated deadline, there is a tendency to get the vehicle (at least partially) ready before the deadline (potentially by paying more for the energy).

To demonstrate the trade-off between delay and energy cost let us consider the example of a water heater in which the controller is designed to maximize the utility of the consumer by considering energy cost and the temperature deviations simultaneously. Delaying the energy demand translates to temperature deviations. A similar situation holds for most air conditioning systems. The hard deadline in time is when the temperature goes out of the ultimate comfort zone of the user.

To formalize this model, consider the following dynamic programming (DP) formulation: we have a certain amount of energy demand to satisfy, d, through purchasing in an uncertain market as a price taker[1] over T time stages. The time varying stage cost, denoted by $g_t(x_t, u_t, \boldsymbol{\gamma}_t)$, can depend on the remaining demand, x_t, and on the purchased electricity denoted by u_t. The stage cost can include the cost of waiting. The terminal cost is denoted by $g_T(x_T)$. The uncertainty in the market (e.g. random price) is modeled by random vector $\boldsymbol{\gamma}_t$. We assume $\boldsymbol{\gamma}_t$ to evolve over time according to the following Markovian model:

$$\gamma_t = \lambda_t(\gamma_{t-1}) + \epsilon_t, \qquad \gamma_{-1} \text{ given}, \tag{3.1}$$

[1]That is, our actions do not affect the price.

where ϵ_t is the random variable modeling price innovations and $\lambda_t(\bullet)$ is modeling the inter-stage correlation of prices and seasonality. We assume $\epsilon_t \sim F_t(\bullet)$ to be independent, $\lambda_t(\gamma)$ to be monotone to avoid some technicalities, and define $\theta_t \triangleq \gamma_{t-1}$ for notational convenience.

At each stage, u_t is to be decided *after* observing $\boldsymbol{\gamma}_t$. Moreover, u_t is subject to the remaining demand and capacity, $\bar{u}$. The dynamics of the problem is given by:

$$\begin{array}{l} x_{t+1} = x_t - u_t, \qquad x_0 = d, \\ 0 \leq u_t \leq \min\{x_t, \bar{u}\}, \end{array} \tag{3.2}$$

and, the objective is to minimize the total expected net present value of costs:

$$J_0^*(d, \theta_0) = \min \mathbb{E}_{\gamma_t}[\sum_{t=0}^{T-1} c(t) g_t(x_t, u_t, \gamma_t) + c(T) g_T(x_T)], \tag{3.3}$$

where: $c(t) = \prod_{t'<t} \alpha_{t'}$; α_t is the discount factor; and the minimization is over policies that give u_t, denoted by $u_t(x_t, \boldsymbol{\gamma}_t)$ by abuse of notation.

In this work, we consider real time pricing as a method to incentivize automatic demand response and incorporate the consumer desire for shorter delays using the following stage cost structure:

$$g_t(x_t, u_t, \boldsymbol{\gamma}_t) = \gamma_t u_t + \eta_t(x_t - u_t) + \eta_t', \tag{3.4}$$

$$g_T(x_T) = m_T x_T, \tag{3.5}$$

where γ_t is the spot price, η_t is the penalty rate for unsatisfied demand and η_t' is the cost of waiting. In this structure, the first term represents real time pricing. The rest of the cost models delay aversion in an affine fashion. In line

with our real time pricing scheme, through this affine model, at each stage the demand suffers a constant loss due to (precommitted) waiting and a linear loss due to the unsatisfied portion of demand. Of course, the functional form of the delay aversion term generally depends on the actual nature of the demand and consumer preferences but we leave the general case for future investigations.

The model presented in this section and the coming results can be extended to the case where the stage capacities arbitrarily depend on time as well as some cases where there are multiple options for purchasing electricity, with different prices and different capacity implications.

3.3 Optimal Demand Satisfaction Algorithm

In this section we first state our main result which provides a closed form for the value function and the optimal policy that solves our model and yields the optimal demand satisfaction algorithm and then comment on the implications of this result on the trade-off between cost, delay, and arrival time.

Theorem 3.1. *Consider the system described in* (3.1)–(3.5).

(a) The optimal value function is continuous, piecewise linear and convex with $T+1$ *pieces given by:*

$$J_0^*(d,\theta_0)=\sum_{j=0}^{T-1} m_0^j(\theta_0)[(d-j\bar{u})^+\wedge\bar{u}]+m_0^T(\theta_0)[(d-T\bar{u})^+]+C(0), \qquad (3.6)$$

where $a \wedge b \triangleq \min\{a, b\}$, $C(t) = \sum_{\tau=t}^{T-1} c(\tau)\eta'_\tau$ *and* $m_t^i(\theta_t)$ *is given by the following backward recursion:*

$$m_t^i(\theta_t) = \mathbb{E}_{\epsilon_t}[M(\theta_t, \epsilon_t)], \tag{3.7}$$

where,

$$M(\theta,\epsilon)=\begin{cases}\tilde{m}_{t+1}^i(\lambda_t(\theta)+\epsilon) & \hat{m}_{t+1}^i \leq \lambda_t(\theta)+\epsilon \\ \lambda_t(\theta)+\epsilon & \hat{m}_{t+1}^{i-1} \leq \lambda_t(\theta)+\epsilon < \hat{m}_{t+1}^i \\ \tilde{m}_{t+1}^{i-1}(\lambda_t(\theta)+\epsilon) & \lambda_t(\theta)+\epsilon < \hat{m}_{t+1}^{i-1}\end{cases}, \tag{3.8}$$

$\tilde{m}_\tau^i(\theta) \triangleq \alpha_{\tau-1} m_\tau^i(\theta) + \eta_{\tau-1}$, $\hat{m}_T^i = m_T^i(\theta) = m_T$, $\forall i, \theta$, $\hat{m}_t^0 = m_t^0(\theta) = -\infty$, $\forall t, \theta$ *and* $\hat{m}_t^i$ *is the extended solution to the following equation:*

$$\mu = \tilde{m}_t^i(\mu). \tag{3.9}$$

(b) The optimal policy is given by:

$$u_t^*(x, \gamma_t) = (x - i^*\bar{u})^+ \wedge \bar{u}, \tag{3.10}$$

where

$$i^* = \max\{i | \hat{m}_t^i < \gamma_t\}. \tag{3.11}$$

The proof is provided in Appendix A.

Theorem 3.1 establishes a separation structure between remaining demand and price state. In other words, it shows that the shape of the optimal value function only depends on the evolution of prices and consumer's delay aversion and not the demand. Moreover, it shows that the optimal consumption policy is obtained through an extended threshold policy. The extended

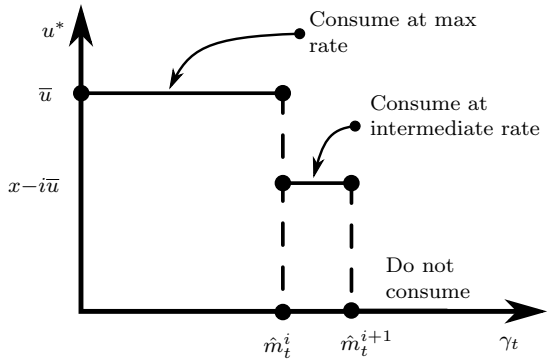

Figure 3.1: Optimal policy assuming $i\overline{u} \leq x_t \leq (i+1)\overline{u}$.

thresholds, denoted by $\hat{m}_t^i$, essentially give the expected opportunity cost-to-go of satisfying their corresponding portions of demand. Therefore, the optimal policy mainly compares these opportunity costs-to-go for each portion and opts for consumption if the current price is below it. This opportunity costs-to-go includes both future prices as well as delay costs. Figure 3.1 depicts the optimal policy and Figure 3.2 depict the form of the extended thresholds or alternatively the slopes of the piecewise linear value function.

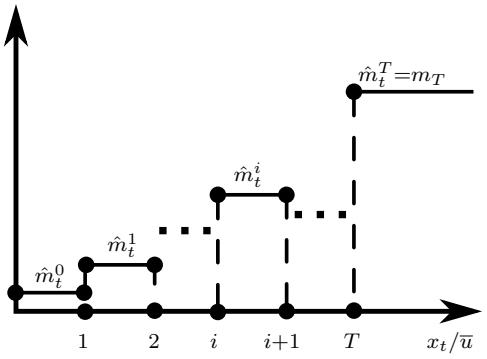

Figure 3.2: Extended thresholds at stage t.

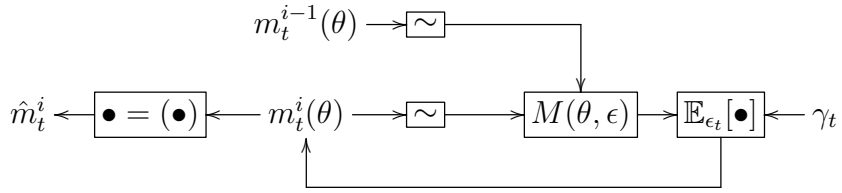

Figure 3.3: Recursive calculation of extended thresholds.

In terms of computation, the result of Theorem 3.1 essentially reduces two dimensional state space to a one dimensional one and only $m_t^i(\theta)$ functions need to be recursively calculated. This still may pose computational overhead if the algorithm is to be implemented in embedded systems. Moreover, there are $O(T)$ fixed point computations per stage due to (3.7) which might be computationally undesirable. Figure 3.3 depicts recursive calculation of the extended thresholds in block diagram form.

Next, we present our result for the independent price case and show that in this case the optimal policy can be considerably simplified and a closed form can be obtained. Moreover we show that this closed form can be efficiently computed.

Theorem 3.2. *Consider the system described in* (3.1)–(3.5) *and assume* $\lambda_t(\theta) = 0$ *for all* t*, then, the optimal value function given in Theorem 3.1 simplifies to:*

$$J_0^*(d) = \sum_{j=0}^{T-1} m_0^j[(d - j\bar{u})^+ \wedge \bar{u}] + m_0^T[(d - T\bar{u})^+] + C(0), \tag{3.12}$$

where m_t^i *is given by:*

$$m_t^i = \tilde{m}_{t+1}^i - G_t(\tilde{m}_{t+1}^{i-1}, \tilde{m}_{t+1}^i), \tag{3.13}$$

in which,

$$G_t(z, z') \triangleq \int_z^{z'} F_t(\zeta)\, d\zeta. \tag{3.14}$$

and $\tilde{m}_\tau^i \triangleq \alpha_{\tau-1} m_\tau^i + \eta_{\tau-1}$ *as defined in Theorem 3.1. Moreover, the optimal policy is given by the same policy as in Theorem 3.1.*

The proof is provided in Appendix B.

Based on Theorem 3.2, it is straightforward to see that the description of the optimal policy is reduced to $\Theta(T)$ storage at each stage and $\Theta(T^2)$ total. Moreover, assuming evaluating the $G(\bullet, \bullet)$ function is $\Theta(1)$, the computational complexity of obtaining each m_t^i is $\Theta(1)$ and hence the overall computational complexity of obtaining the solution is $\Theta(T^2)$, which can be implemented in parallel from according to (3.13) for higher efficiency. Figure 3.4 shows the simplified block diagram for calculation of the extended thresholds under independent price assumption.

Theorems 3.1 and 3.2 also quantify and demonstrate the cost-delay trade-off. To capture delay aversion, we assume $\eta, \eta' \geq 0$ and $\alpha_t \geq 1$ which translates to a non-decreasing threshold going backwards unless the negative

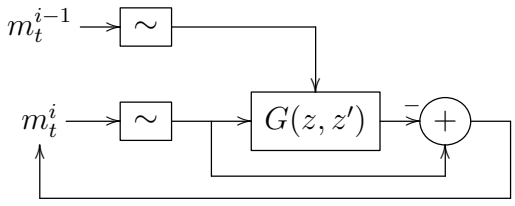

Figure 3.4: Simplified recursive calculation of extended thresholds under independent prices.

term in (3.13) overweighs the increase. Hence, the extended thresholds are not guaranteed to be increasing in t and in most cases become decreasing at some point. This leads to existence of a soft deadline for demand satisfaction which depends on delay aversion parameters. Moreover, non-stationary prices enable the consumer to further optimize its utility by jointly choosing its *arrival time* and *availability interval* subject to its constraints.

A consequence of piecewise linear value function (which is essentially the demand function of the load) is that it automatically matches most of the current bidding models in electricity markets where offers consist of price-quantity pairs. In other words, if instead of simple consumption, the load is supposed to make an offer, there is no lack of optimality by constraining the offers to be a set of price-quantities.

Since the demand is only decreasing over the horizon, the effective number of m coefficients to compute depends on d. In particular, if the initial demand is below the capacity, $\bar{u}$, the optimal value function becomes linear and the optimal policy transforms to a threshold type one, and in case of independent prices, we obtain the following simple corollary:

Corollary 3.3. *If the initial demand is less than the stage capacity, i.e. $d \leq \bar{u}$, the optimal value function and policy for the system are given by:*

$$J_0^*(d) = m_0 d + C(0), \tag{3.15}$$

$$u_t^*(\gamma_t) = \mathbb{1}\{\gamma_t \leq \tilde{m}_{t+1}\}d, \tag{3.16}$$

where $\mathbb{1}\{A\}$ *is the indicator function of event* A *and* $\{m_t\}$ *is given by the following backward recursion:*

$$m_t = \tilde{m}_{t+1} - G_t(-\infty, \tilde{m}_{t+1}). \tag{3.17}$$

Moreover, the probability of failure in meeting the demand is given by $\prod_{t=0}^{T}(1 - F_t(\tilde{m}_{t+1}))$.

Proof. Only the last part is not immediate from Theorem 3.1 so we only prove the last claim. Observe that at each stage the demand remains unsatisfied if the price, γ_t is greater than the threshold m_{t+1}, which happens with probability $1 - F_t(\tilde{m}_{t+1})$. The desired product form follows from the independence assumption on prices. ■

Note that load capacity is the maximum energy load can consume over a decision interval. So Corollary 3.3 can be realistic or not depending on how fast prices are updated (and hence decisions are made). It roughly holds if the load usually runs shorter than the length of the decision interval. In this case, the problem essentially transforms to a stopping problem where all the demand is satisfied at once. Moreover, the probability of failure in meeting the demand can be made arbitrarily small by setting a large enough terminal cost, m_T.

3.4 Numerical Results and Network Level Impacts

In this section, we present the result of a case study to demonstrate the performance of the proposed optimal policy and study its impact on the

network when a group of flexible loads adopt such algorithm.

For each scenario we consider a group of 1000 PEVs which show up over a 24 hour period of time. To have the most realistic arrival, energy demand, and departure patterns, we use the results of our study in Chapter 2 based on the transportation dataset we discussed in that chapter. We considered the charging sessions realized as the result of a non-anticipative model when charging is available everywhere. We further truncated the availability length of the PEVs to 24 hour for ease of calculations.

Price statistics are based on the real-time market prices in the Houston Load Zone for year 2012. For easier analysis, we have only considered the independent case here. The prices are assumed to be normally distributed with mean from average Houston Load Zone prices for each hour and simulations are done for various price uncertainties reflected in the standard deviation of price realizations, denoted by σ. Price uncertainty here can be interpreted as Gaussian price estimation error from the flexible loads perspective.

We have compared the optimal algorithm against the policies we previously studied, i.e. immediate and average rate, as well as a Certainty Equivalent Control (CEC) based algorithm adopted by other authors previously (e.g. [72]) under which, the optimal consumption is solved as a deterministic program where stochastic prices are replaced by their estimates. In this case, CEC based policy would essentially solve a linear program with expected prices over the availability horizon as cost coefficients and unrolled version of system dynamics, i.e. (3.2) as constraints. Note that the CEC approach ignores price

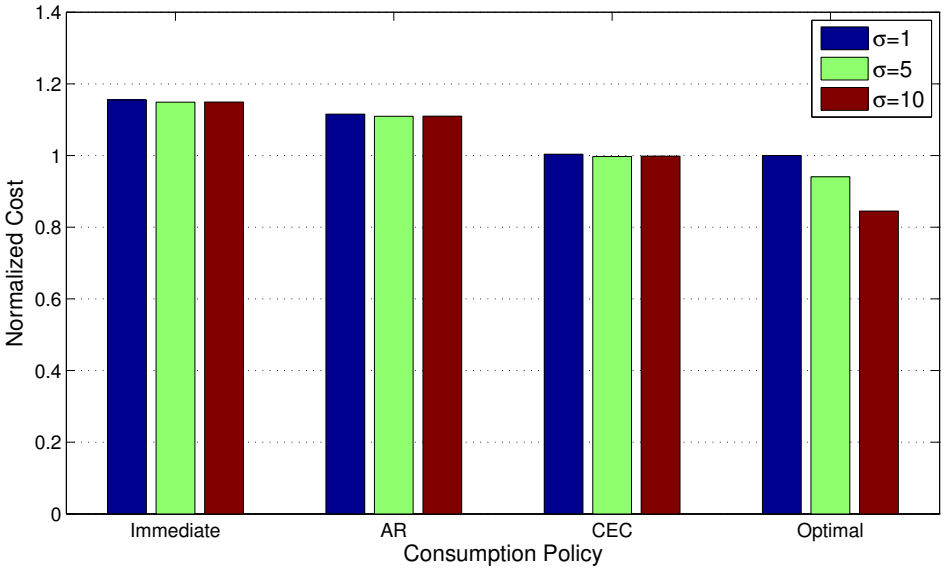

Figure 3.5: Cost comparison between various consumption policies under different levels of uncertainty.

uncertainty. Yet, it responds to the general trend (expected value) of prices, while immediate and average policies are completely oblivious to prices. The optimal policy on the other hand takes advantage of the uncertainty as well as the trend.

Finally, to reach statistical consistency, the simulations are repeated 10,000 times.

From the consumers' perspective, the projected savings suggests a strong case. As depicted in Figure 3.5, adopting the optimal policy by the consumers results in roughly 14%-30% reduction in cost on average, compared to immediate consumption, depending on the level of uncertainty, as measured by σ. As previously mentioned, all policies except the optimal policy are oblivious

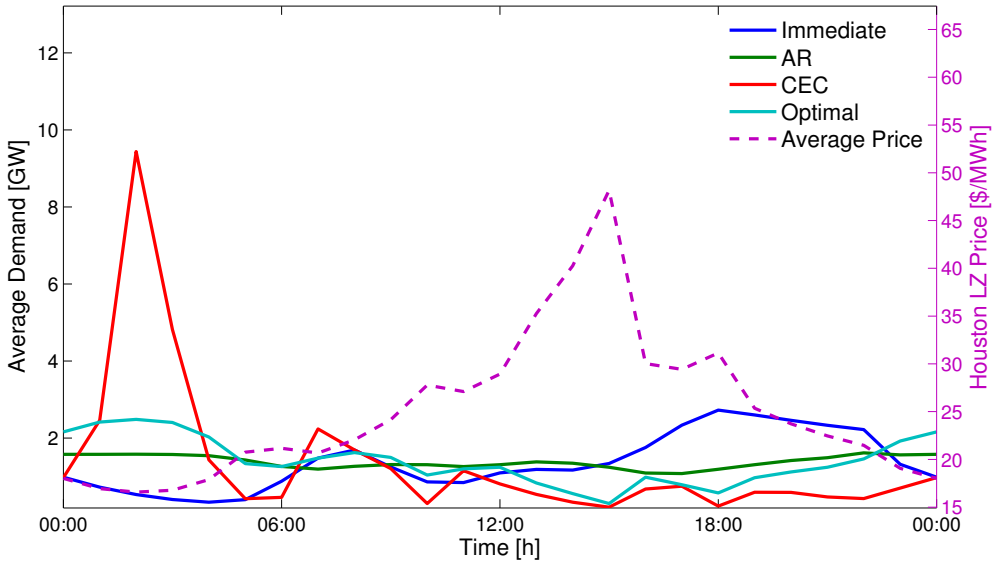

Figure 3.6: Average diurnal load comparison between various consumption policies ($\sigma = 10$).

to the stochastic nature of the prices and hence cannot adapt to it. The most interesting comparison here is between CEC and the optimal policy. While both result in the same cost at low levels of price uncertainty, the difference grows with uncertainty, to about 10% for $\sigma = 10$. Combined with the fact that the computational cost of obtaining the optimal policy is not very different from the CEC, we conclude that the optimal policy should be adopted by the loads, if cost is the most important factor to them.

To study the impact of wide spread adoption of the optimal policy and compare it with other policies, in line with our results in the previous chapters, we considered the average diurnal pattern of the load produced by each of these policies which is presented in Figure 3.6. Note that this diurnal

pattern is formed by averaging almost 10 million charging sessions (10,000 scenarios each with 1000 charging sessions). Moreover, the curves are less smooth compared to the figures presented in Chapter 2 since the curves are based on hourly data as opposed to minutely curves presented previously. For a better comparison, the expected price is also depicted in dashed lines.

Each policy results in its own unique diurnal pattern. As expected from our previous results, immediate consumption produces its maximum consumption at peak hours in the evening, while Average Rate consumption results in an almost flat consumption. Price responsive policies, i.e. CEC and optimal, shift the load towards the *locally low price* times, i.e. times in which the price is lower than its neighboring times, which typically happen over night. Their response, however, are quite different on average sense. In particular, CEC creates a huge peak at the lowest expected price while the peak created by the optimal method is lower and more spread over night, almost as high as the peak in the evening by immediate consumption. This is mainly due to the fact that the optimal policy looks for (and usually successfully finds) the *realized* locally low price while the CEC policy only considers expected values, and hence the consumption is concentrated around the *expected* low prices for all scenarios. Since the uncertainty in the price changes the exact time of the low prices, the average result of the optimal behavior does not show its sample behavior properly.

To study the behavior of the optimal policy more carefully, let us consider a sample path realization of the response. Figure 3.7 compares the aggre-

gate load of a single scenario for different uncertainty levels. In these figures, it is evident that as the time of the locally low price changes due to increased uncertainty, the optimal policy tracks the realized low price successfully and creates a similar pattern as CEC around it. Note that the height of the peak does not change much because the minimal price typically happens sometime over the night, when the expected price is also typically low and there is not much change in availability of the demand at the particular locally low price time versus the expected locally low price. This is also confirmed by our measured Peak-to-Average Ratios presented in Table 3.1. Consequently, we can observe an indirect synchronization of load around the realized low prices. As expected, PAR values for CEC does not depend on σ. The interesting observation, however, is that PAR values for the optimal policy are also pretty constant and close to the values for CEC, both in terms of maximum and average values (across scenarios.). This affirms that the multi-threshold form of the optimal policy is more sensitive to the time of the locally low prices rather than their magnitude.

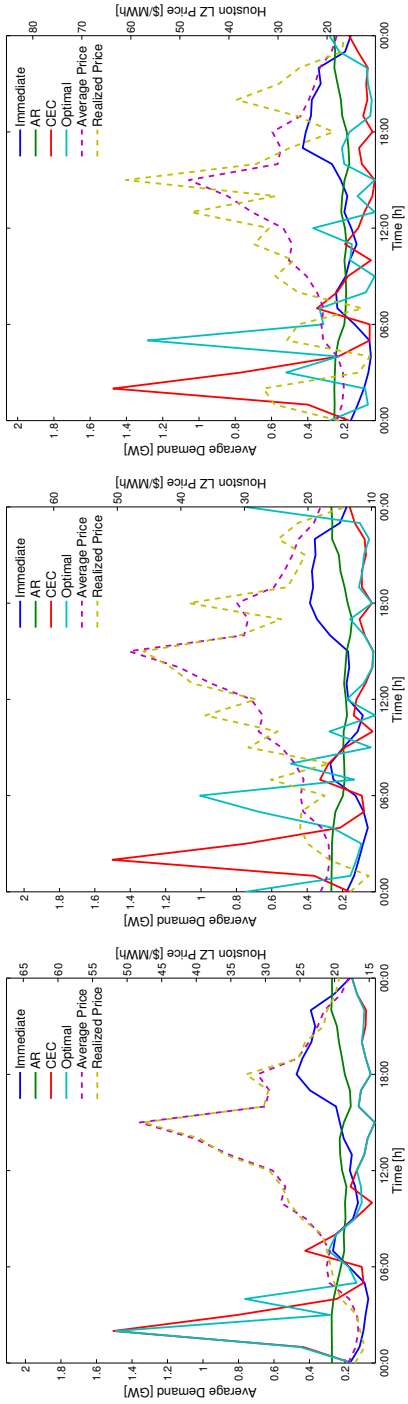

(a) $\sigma = 1$ (b) $\sigma = 5$ (c) $\sigma = 10$

Figure 3.7: Sample aggregate behavior at difference price uncertainty levels overlaid on price.

As discussed, interestingly, yet not surprisingly, the increased volatility/uncertainty in prices leads to lower relative costs, which essentially shows that the optimal policy efficiently adapts to market uncertainty. On the other hand, at the transmission and distribution network level, the consequence of such opportunism is not necessarily desired. One key driver for real-time pricing is to shift consumption to low price and hence low load times (i.e. off-peak) and hence get a smoother overall load profile. Our simulation results, however, show that load profiles may be less smooth than expected because of opportunism as depicted in Figure 3.7 and Table 3.1.

Although such behavior from the load can eventually affect the behavior of the price over time towards a more flat one, our results show that it would not fundamentally change the undesirable behavior of the flexible loads if uncertainty persists. The uneven aggregate load behavior is mainly due to opportunism from the load side which is triggered by local price minima. In other words, locally low prices act as synchronization signals to the loads. For example, in Figure 3.7(c), some peak loads happen at a low price for which the expected price is high. Moreover, the market response to such concentrations

Table 3.1: Peak to Average Ratio of Aggregate Load vs. price uncertainty.

σ	CEC		Optimal	
	Average	Max	Average	Max
1	6.9	7.9	6.8	7.9
5	6.9	7.9	6.2	7.9
10	6.9	7.9	5.9	7.7

does not happen in a timely manner, and hence, cannot control it. Moreover, the prices at wholesale may not be affected if a relatively small number of opportunistic loads (with respect to the total system load) are clustered under the same distribution feeder.

Considering the structure of the optimal consumption policy, one fundamental reason behind the undesired behavior of the aggregated load can be attributed to the linear pricing scheme. The linear pricing effectively transforms the optimal consumption to a pseudo-stopping problem where the demand usually consumes as much as it can when the price is low enough. Nonlinear pricing can better distribute the load over the availability interval of the demand; however, with the prospect of bidirectional energy exchange, such proposals should be considered more carefully.

Another approach which can effectively enforce distribution level congestion constraints is to utilize the bidirectional communication mechanism of the smart grid and have local auctions at the distribution network level. Our early results in this direction suggest that using the thresholds in our proposed algorithm as bids, and selecting highest bids up to network capacity, can result in a better solution. We leave detailed consideration of this setting to future work.

3.5 Conclusion

In this chapter, we presented a model for delay-averse flexible demands and the optimal solution for minimizing the average cost of energy consump-

tion by them under uncertain prices. We showed that the solution to our model which is a stochastic dynamic program admits a closed form which is efficiently computable.

We also investigated the energy cost savings and network level behavior of a flexible demands adopting our proposed optimal policy through simulation. We concluded that, while the optimal policy achieves considerable cost savings, contrary to common belief, network level impact of wide spread adoption of price responsive algorithms for electricity consumption might not be as desired under simple dynamic pricing. Therefore, we concluded that further coordination should be necessary to prevent undesired demand patterns at network level. We will be investigating such methods and architecture in the later chapters of this thesis.

Chapter 4

Optimal Policies for Simultaneous Energy Consumption and Ancillary Service Provision for Flexible Loads under Stochastic Prices

4.1 Introduction

As discussed in previous chapters, smart grids are expected to bring about fundamental changes in terms of information availability to electricity networks and provide bidirectional communication and energy exchange even to the end points of the distribution network. Although it is generally understood that the closed loop of information/energy exchange can improve the overall energy exchange process in many ways (e.g. reducing cost, increasing reliability), models to quantitatively understand the fundamental benefits of the information availability over smart grids are relatively lacking.

A considerable portion of the current electricity demand is inherently flexible i.e., electric power need not be delivered to the load at a very specific trajectory over time. For these loads, an amount of energy is needed by some (potentially recurring) deadline. In other words, over the operation time of the load, the trajectory of the delivered power only needs to satisfy some constraints instead of exactly following a specific trajectory. Such loads include most heating/cooling systems and electric vehicles (EV). The most recent EIA

statistics [107] suggest that such loads comprise more than 50% of average residential electricity consumption. The prospect of such loads comprising a considerable portion of emerging loads urges us to investigate the benefits obtained from such flexibility utilizing the infrastructure provided by smart grids.

In Chapter 3, we considered flexible loads responding to real-time prices from the grid as a signal to reflect the more realistic cost of energy consumption. Yet, if the communication infrastructure and the dynamics of the loads allow, their flexibility can be further utilized by the grid. This would be achieved by the loads not only participating in the market for purchasing energy they need, but also for providing ancillary services. Under such scenarios, loads would not only respond to energy prices but also to requests for adjusting their consumption, at rates much faster than market or pricing intervals, which are typically issued by the ISO. Such adjustment signals are typically designed to fine tune supply demand mismatches by regulating system frequency, as we discussed them in Chapter 2. This form of service, however, needs much faster communication and capability but as we previously discussed, are well within rates available to residential and commercial Internet users. Such ancillary services are typically traded as *capacity*, that is, the operator pays for the ability to adjust the current rate (consumption of generation) of the provider within a specified range (i.e. capacity).

In this chapter, we consider an extension of the problem we considered in Chapter 3 by adding the potential for offering ancillary services to the

problem of optimal energy consumption by a flexible load. We first examine the model carefully and show that multiple cases are possible depending on the form of capacity constraints to which the load is subjected when changing consumption at paces faster than the decision interval. We then show that our previous techniques to obtain the optimal policy can be extended to joint optimization of energy consumption and AS provision and the optimal policy has a very similar multi-threshold form. We also show that the optimal policy can be computed efficiently in a similar recursive fashion and the complexity order of computations stays the same. Considering joint energy consumption and AS provision is not only a natural extension of the optimal consumption problem, but also play as a bridge towards the work we present in later chapters, where an Energy Services Company (ESCo) is in charge of solving the optimal energy delivery and AS provision for a group of flexible loads.

The rest of this chapter is organized as follows: In Section 4.2 we present and analyze our model and the optimal demand satisfaction algorithm. In Section 4.3 we present our proposed optimal joint consumption and AS provision policy for the case that AS provision does not need capacity reservation. Section 4.4 is dedicated to analysis of network level performance of our proposed algorithm through simulation as well as its system level impacts, similar to Chapter 3. We conclude this chapter and comment on our future directions in Section 4.5. The proof of the theorems are moved to the appendices for better readability.

4.2 System Model

We model a consumer with a flexible load subject to a total energy demand and energy rate limits. Assuming a discrete time model, our objective is to find out how much energy the consumer should consume towards its total demand so that its total expected cost is minimized. The consumer can also offer some of its flexible capacity for use as reserve in return for some reward.

Let us first introduce the price model which is very similar to the price model we considered in Chapter 3. We assume a Markovian price structure for energy and reserve prices, denoted by π_t^e and π_t^r respectively. Defining $\boldsymbol{\pi}_t \triangleq (\pi_t^e, \pi_t^r)$:

$$\boldsymbol{\pi}_t = \boldsymbol{\lambda}_t(\boldsymbol{\theta}_t) + \boldsymbol{\epsilon}_t, \qquad \boldsymbol{\theta}_0 \text{ given}, \tag{4.1}$$

where $\boldsymbol{\epsilon}_t \triangleq (\epsilon_t^e, \epsilon_t^r)$ is the random vector capturing price innovations, $\boldsymbol{\lambda}_t(\boldsymbol{\theta_t}) \triangleq (\lambda_t^e(\boldsymbol{\theta_t}), \lambda_t^r(\boldsymbol{\theta_t}))$ models inter-stage correlation of prices and seasonality and $\boldsymbol{\theta}_t$ represents the state of the Markov process and throughout this work we assume $\boldsymbol{\theta}_t = \boldsymbol{\pi}_{t-1}$, i.e. the previous prices form the state of the price process. We denote the distribution function of $\boldsymbol{\epsilon}_t$ by $F_t(\bullet)$ and assume independent price innovations over time, i.e. $\boldsymbol{\epsilon}_t \perp\!\!\!\perp \boldsymbol{\epsilon}_{t'}$, $\forall t \neq t'$. Note that the prices are assumed to be non-stationary, generally distributed and arbitrarily correlated (between energy and reserves). Moreover, we assume $\boldsymbol{\lambda}_t(\boldsymbol{\theta}_t)$ to be monotone but otherwise arbitrary to avoid some technicalities.

We model the cost minimization problem faced by the consumer as a Dynamic Program (DP) (a.k.a. Markov Decision Process). Under this model,

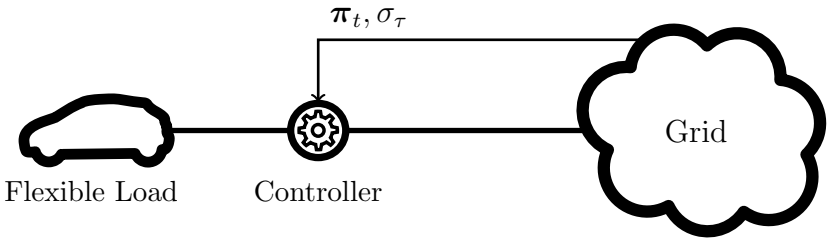

Figure 4.1: System model.

which is schematically depicted in Figure 4.1, the consumer is assumed to have a certain amount of energy demand at time $t = 0$, and needs to make decisions about exactly how to consume electricity in the next T time periods with the knowledge of past and current prices and (remaining) energy demand. In other words, the consumer has a deadline of T time slots and seeks an optimal demand satisfaction policy. We assume that the consumer acts as a price taker; consequently, the optimal policy alternatively captures the consumer's bid for purchasing energy and offer for providing reserves. The consumer is also subject to consumption rate limits; that is, its consumption at every stage cannot exceed a certain amount. This models the capacity limits that a typical consumer is facing, from local transformer capacity limits to the rate supported by the device (e.g. charging capacity of a charger).

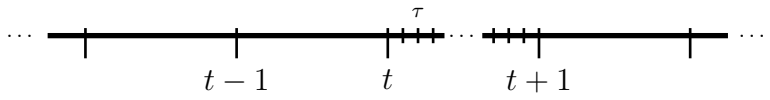

Figure 4.2: Timeline of decisions versus reserve deployments.

The consumer is also assumed to sell its flexibility, i.e. its ability to change its consumption rate, as a reserve capacity to the grid too. By modulating its output in a time frame faster than the decision intervals, see Figure 4.2, it provides a balancing service (a.k.a. reserve) to the grid. An example of such a situation in ERCOT is providing Regulation (REG) service in intervals of four seconds while the market (and hence energy prices) is cleared every five minutes. Since the fast deployments of the reserves is usually designed to manage the uncertainty between the anticipated supply demand balance and its actual behavior, it is fair to expect that reserve deployments have a zero mean and balance out over (relatively) long periods of time. Figure 4.3 demonstrates a sample path of this operation where e_t, energy consumption by the flexible load, is modulated by reserve deployments (σ_τ). Note that the reserve deployments happen at about two orders of magnitude higher frequency and hence the time indexes are different. Since the consumer is assumed to be solely capable of consuming energy and not injecting it back, the amount of reserves offered by the consumer cannot exceed its consumption in that time slot. On the upper bound on consumption rate however, the actual constraint on the instantaneous rate depends on the underlying limiting factor and can be either an average rate constraint (over the time slot) or an instantaneous rate limit similar to the lower bound on consumption. For example, if the constraint on the maximum consumption rate is due to thermal limits, like a transformer, then typically the capacity can be modeled as an average rate limit per time slot. Consequently, while instantaneous changes in consumption

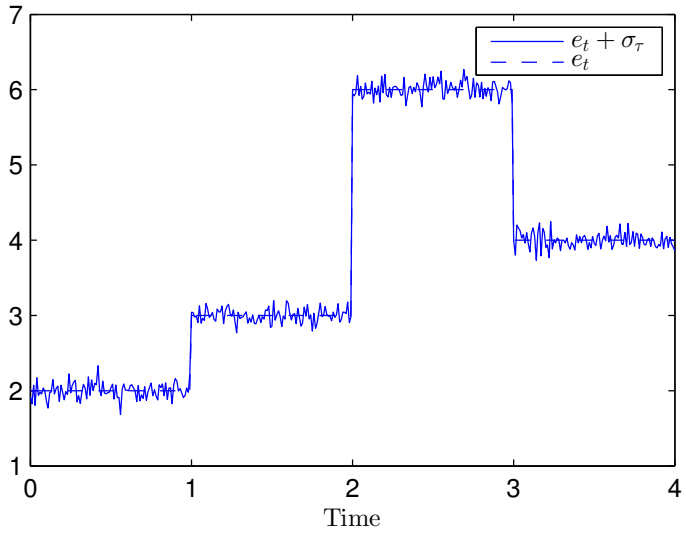

Figure 4.3: A sample path of energy consumption by the consumer while providing reserves.

(due to the summation of designated consumption and reserve deployments) can exceed the upper bound of the consumption rate, the average rate of consumption remains within desired limits since reserve deployments are assumed to be zero mean. This is the model we adopt in this chapter.

Alternatively, the rate limit could be due to a hard limit and hence, the total consumption rate (the sum of designated energy consumption rate and reserve deployments) cannot exceed the rate limit. This alternate model basically asks the consumer to reserve some capacity for reserves that could otherwise be used for energy consumption and will result in a more complex optimal policy. We leave this case for future work.

With this model and denoting the remaining energy demand of the

consumer by d_t, and the amount of consumed energy and offered reserve by e_t and r_t, respectively, we have the following dynamics:

$$\begin{aligned} &d_{t+1} = d_t - e_t + s_t, \qquad d_0 \text{ given}, \\ &0 \leq r_t \leq e_t \leq \min\{d_t, \overline{e}\}, \end{aligned} \tag{4.2}$$

where d_0 denotes the initial energy demand of the flexible load, $\overline{e}$ denotes the maximum amount of energy the consumer can consume in one time slot, $s_t = \sum_\tau \sigma_\tau$ denotes the sum of reserve deployments over the time interval. Generally, s_t is assumed to be a zero mean independent process, i.e. $\mathbb{E}[s_t] = 0, \forall t$ and $\boldsymbol{\epsilon}_t \perp\!\!\!\perp s_t \perp\!\!\!\perp s_{t'}, \forall t \neq t'$; in this work, however, we assume $s_t = 0, \forall t$ as a simplifying assumption. That is, we assume that reserve deployments over each time slot are balanced and sum up to zero. Note that in some jurisdictions, there are balanced reserve products that ensure a balanced property.

The objective of the problem is to minimize the expected cost, i.e. to obtain $J_0^*(d_0, \boldsymbol{\theta}_0)$:

$$J_0^*(d_0, \boldsymbol{\theta}_0) = \min_{\substack{e_t(d_t, \boldsymbol{\pi}_t), \\ r_t(d_t, \boldsymbol{\pi}_t)}} \mathbb{E}_{\boldsymbol{\epsilon}_t}[\sum_{t=0}^{T-1} g_t(e_t, r_t, \boldsymbol{\pi}_t) + g_T(d_T)], \tag{4.3}$$

where the minimization is over policies that give e_t and r_t upon observing $(d_t, \boldsymbol{\pi}_t)$, which we denote by $e_t(d_t, \boldsymbol{\pi}_t), r_t(d_t, \boldsymbol{\pi}_t)$ by abuse of notation. Finally, we need to define our stage and final cost:

$$g_t(e_t, r_t, \boldsymbol{\pi}_t) = \pi_t^e e_t - \pi_t^r r_t, \tag{4.4}$$

$$g_T(d_T) = \hat{m}_T d_T, \tag{4.5}$$

where m_T is basically the marginal cost of unsatisfied energy demand which depends on the type of the load. For example, for plug-in hybrid vehicles, $\hat{m}_T$

is on the order of the equivalent price of gasoline. This model can capture a wide range of flexible loads. The prime example of such loads are battery charging loads like plug-in electric vehicles.

4.3 Optimal Energy Consumption and Reserve Provision Policy without Capacity Reservation

First, we present our main result which gives the optimal joint energy consumption and reserve provision policy. Then, we present the algorithm to recursively calculate the parameters of this optimal policy derived from the main theorem and discuss its implications and complexity. Finally, we establish another theorem which considers the result for the uncorrelated price case.

Theorem 4.1. *Consider the system described in* (4.1)–(4.5).

(a) The optimal value function is continuous, piecewise linear and convex with $T+1$ *pieces given by:*

$$J_0^*(d_0, \boldsymbol{\theta}_0) = \sum_{j=0}^{T-1} m_0^j(\boldsymbol{\theta}_0)[(d_0 - j\overline{e})^+ \wedge \overline{e}] + m_0^T(\boldsymbol{\theta}_0)(d_0 - T\overline{e})^+, \qquad (4.6)$$

where $a \wedge b \triangleq \min\{a, b\}$ *and* $m_t^i(\boldsymbol{\theta}_t)$ *is given by the following backward recursion:*

$$m_t^i(\boldsymbol{\theta}_t) = \mathbb{E}_{\boldsymbol{\epsilon}_t}[M_i(\boldsymbol{\theta}_t, \boldsymbol{\epsilon}_t)], \qquad (4.7)$$

where,

$$M_i(\boldsymbol{\theta}_t, \boldsymbol{\epsilon}_t) = \begin{cases} m_{t+1}^i(\boldsymbol{\pi}_t) & \hat{m}_{t+1}^i \leq \pi_t^a, \\ \pi_t^a & \hat{m}_{t+1}^{i-1} \leq \pi_t^a < \hat{m}_{t+1}^i, \\ m_{t+1}^{i-1}(\boldsymbol{\pi}_t) & \pi_t^a < \hat{m}_{t+1}^{i-1}, \end{cases} \tag{4.8}$$

$\boldsymbol{\pi}_t = \boldsymbol{\lambda}_t(\boldsymbol{\theta}_t) + \boldsymbol{\epsilon}_t$ *by* (4.1), $\pi_t^a = \pi_t^e - (\pi_t^r)^+$, $m_T^i(\boldsymbol{\theta}_t) = \hat{m}_T^i = \hat{m}_T$, $\forall i$, $m_t^0(\boldsymbol{\theta}_t) = \hat{m}_t^0 = -\infty$, $\forall t$ *and* $\hat{m}_t^i$ *is given by:*

$$\hat{m}_t^i = \{m_t^i(\mu_1, \mu_2) | m_t^i(\mu_1, \mu_2) = \mu_1 - (\mu_2)^+\}. \tag{4.9}$$

(b) The optimal policy is given by:

$$e_t^*(d, \boldsymbol{\pi}_t) = (d - i^* \overline{e})^+ \wedge \overline{e}, \tag{4.10}$$

$$r_t^*(d, \boldsymbol{\pi}_t) = e_t^*(d, \boldsymbol{\pi}_t) \mathbb{1}\{\pi_t^r \geq 0\}, \tag{4.11}$$

where $\mathbb{1}\{\bullet\}$ *is the indicator function and,*

$$i^* = \max\{i | \hat{m}_t^i < \pi_t^e - (\pi_t^r)^+\}. \tag{4.12}$$

The proof is provided in Appendix C.

The value function obtained in Theorem 4.1 shows an interesting property of the problem under study: even with arbitrary prices and correlation, the value function remains not only piecewise linear, but also, all the pieces have the same length, namely $\overline{e}$. More importantly, the number of pieces scales only linearly with the number of available time slots, T, as opposed to exponential scaling which typically happens in dynamic programming problems [13]. Consequently, a relatively simple multi-threshold optimal policy for

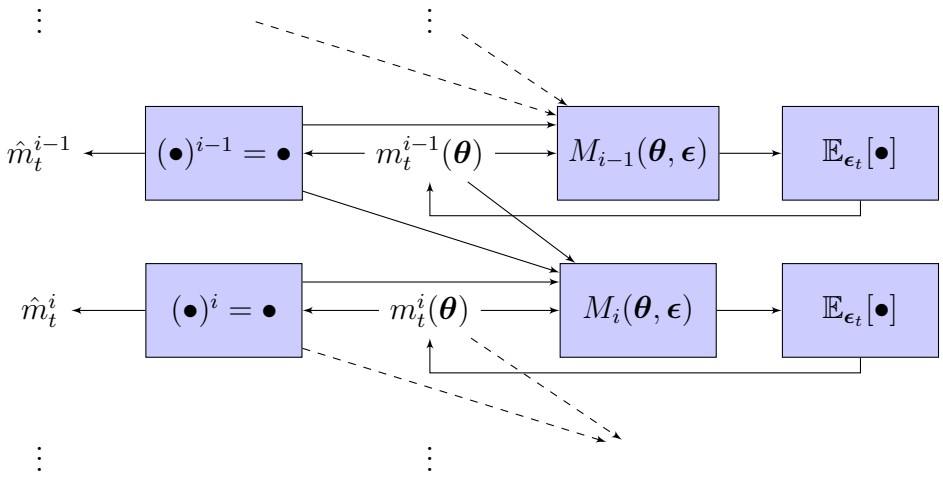

Figure 4.4: Recursive calculation of value function coefficients and thresholds in block diagram form. Note that recursions are backward on t and $(\bullet)^j = \bullet$ represents the corresponding solution to (4.9).

joint demand satisfaction and reserve provision can be obtained. Since such a policy is either to be implemented in embedded devices such as the EVSE, PEV, Home Energy Management System (HEMS) or thermostat or used to control a large group of flexible loads by a load aggregator, such scalability is very important.

While Theorem 4.1 gives a closed form optimal policy and value function, it also encapsulates the essential richness of the problem due to the general price structure into the coefficients of the value function and the corresponding thresholds obtained through (4.9). Whether a closed form can be attained for these thresholds depends on the assumed price statistics. Nevertheless, Theorem 4.1 gives a straightforward algorithm for calculating these

thresholds. Figure 4.4 depicts the recursive algorithm that is used to calculate the coefficients and corresponding thresholds in a block diagram form, mainly around the ith element. This block diagram basically depicts (4.7), (4.8) and (4.9). Let us go through these steps for more clarity, assuming time t at the beginning:

1. Using $m_t^j(\boldsymbol{\theta})$, obtain $\hat{m}_t^j$ using (4.9) for all j.

2. For all j form the corresponding $M_j(\boldsymbol{\theta}, \boldsymbol{\epsilon})$ using $m_t^j(\boldsymbol{\theta})$, $m_t^{j-1}(\boldsymbol{\theta})$, $\hat{m}_t^j$, $\hat{m}_t^{j-1}$ obtained in previous step and (4.8).

3. For all j take the expected value of $M_j(\boldsymbol{\theta}, \boldsymbol{\epsilon})$ and obtain $m_{t-1}^j(\boldsymbol{\theta})$ as in (4.7).

4. Repeat these steps letting $t = t - 1$.

A considerable advantage of the above algorithm for obtaining the optimal thresholds is that it can be implemented in parallel very efficiently. In particular, at each time t, all the T pieces, indexed by j can be calculated in parallel. This is implicitly reflected also in the steps described above, noting that each step happens for all j simultaneously for a given time slot t, without using any of the information corresponding to other time slots. This parallelism can also be seen in the parallel branches of the block diagram in Figure 4.4.

The computational complexity of obtaining the optimal policy using Theorem 4.1 is $O(\frac{T^2}{\delta})$, assuming the operations in equations (4.7), (4.8) and

(4.9) are $O(1)$ and the resolution of $m_t^j(\boldsymbol{\theta})$ in $\boldsymbol{\theta}$ is $O(\delta)$. Note that $m_t^j(\boldsymbol{\theta})$ is a function of $\boldsymbol{\theta}$ and, hence, at worst, it needs to be calculated and stored numerically. Given the above discussion on the parallel computation of the optimal policy, establishing this bound is straight forward. Note that we have at most $O(T)$ pieces and T time slots. Bear in mind that assuming $O(1)$ computation time on each operation only implies that these computations do not depend on T and hence, do not scale with the problem.

In terms of storage complexity of the optimal policy, Theorem 4.1 gives an even better result. Note that once (4.9) is solved, there is no need to store $m_t^j(\boldsymbol{\theta})$ since $\hat{m}_t^j$ is enough to run the optimal policy. Therefore, the storage complexity of the optimal policy is $O(T^2)$, which is great for embedded systems or when the optimal policy is computed in the cloud and should be transferred to the controller.

Another advantage of the proposed computational structure becomes vivid when multiple flexible loads are involved and an aggregator is controlling all the loads simultaneously. In such setups, the load aggregator can reuse the calculated coefficients and thresholds for the loads which share the same (absolute) deadline and capacity. To observe this property, first note that the loads with the same per stage capacity have the same break points in their value function. Now, consider two loads with potentially different demands, say d and d' and potentially different dwell lengths, e.g. T and T', but with the same deadline, i.e. $t_d = t'_d$. Now, for calculating the optimal coefficients backward, the actual statistics seen by these loads are the same for all times

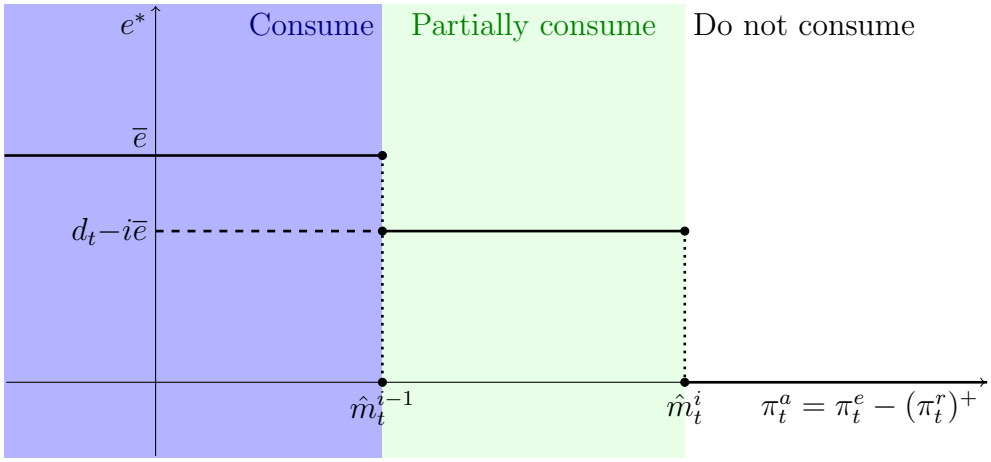

Figure 4.5: Optimal policy.

between $t_d = t'_d$ and $t_d - \min\{T, T'\}$ since their deadlines are equal. Note that since the times are measured relative to arrival times, the time indexes for these two loads might not be the same. For the period where both loads share the same statistics, i.e. between $t_d - \min\{T, T'\}$ and t_d, the coefficients obtained in backward recursion discussed in the above algorithm are the same. Note that the coefficients, $m_t^j(\boldsymbol{\theta})$, do not depend on the demand. Hence, the load aggregator essentially needs to calculate these coefficients and optimal thresholds only once per deadline and load capacity, for the maximum amount of load dwell time. Moreover, in case a new load arrives sharing deadline and capacity with another load but staying for more time, computations are needed to be performed only for the extra amount of steps this load stays compared to longest staying load with the same deadline and capacity. That is, the optimal policy parameters only get augmented by the ones that are not calculated before arrival of a new load.

The optimal coefficients in the value function and their corresponding thresholds also have a very interesting economic interpretation. Consider a load with demand d and capacity $\overline{e}$ and let us define $i = \lfloor \frac{d}{\overline{e}} \rfloor$, then for any t, $m_t^i(\boldsymbol{\theta})$ basically gives the expected effective marginal cost of energy for this load, noting that the expected value function is the expected cost to go for such a load. This economic interpretation of the optimal coefficients results in a very intuitive interpretation of the optimal policy: It basically says consume if the effective price, π_t^a, i.e. energy price minus reserve price if positive, is better than what you believe as the expected effective marginal cost of consumption (at the level of remaining demand upon finishing consumption). If the effective price is only better than the current expected effective marginal cost to go, then only consume enough to satisfy the partial demand. Finally, if the effective price is higher than the current expected effective marginal cost, then do not consume. Figure 4.5 depicts this interpretation. Note that the price axis in this figure, and the price considered in the optimal policy, is the effective price which depends on price of energy as well as price of reserve. Figure 4.6 depicts price regions corresponding to the three effective price regions in Figure 4.5 more vividly. Note that these regions are exactly the ones defined by the conditional function $M_i(\boldsymbol{\theta}, \boldsymbol{\epsilon})$ in (4.8).

If further assumptions are made about the price statistics, the computational complexity of the optimal policy can be further improved. An interesting case in this direction is the independent price case, which also covers deterministic prices. We address the independent case in the following

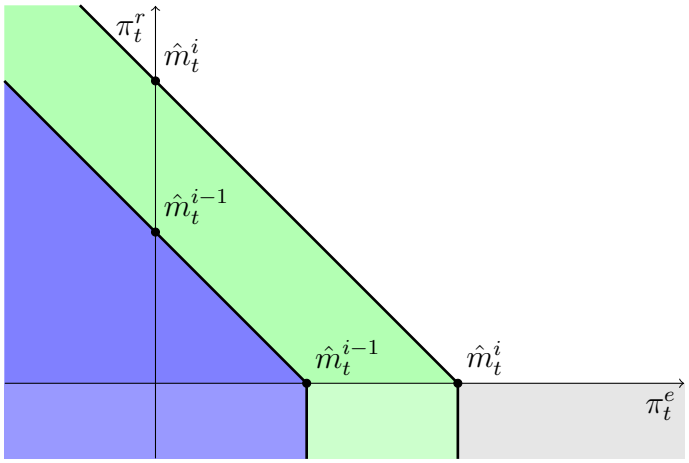

Figure 4.6: Price regions.

theorem:

Theorem 4.2. *Consider the system described in* (4.1)–(4.5) *and assume* $\boldsymbol{\lambda}_t(\boldsymbol{\theta}) = 0$, $\forall t, \boldsymbol{\theta}$, *then, the optimal value function given in Theorem 4.1 simplifies to:*

$$J_0^*(d_0) = \sum_{j=0}^{T-1} \hat{m}_0^j [(d_0 - j\overline{e})^+ \wedge \overline{e}] + \hat{m}_0^T (d_0 - T\overline{e})^+, \tag{4.13}$$

where m_t^i *is given by:*

$$\hat{m}_t^i = \hat{m}_{t+1}^i - G_t(\hat{m}_{t+1}^{i-1}, \hat{m}_{t+1}^i), \tag{4.14}$$

in which,

$$G_t(z, z') \triangleq \int_z^{z'} F_t^a(\zeta)\, d\zeta, \tag{4.15}$$

where $F_t^a(\bullet)$ *is the marginal probability distribution function of the effective price random variable defined as* $\pi_t^a = \epsilon_t^a \triangleq \epsilon_t^e - (\epsilon_t^r)^+$.

Moreover, the optimal policy is given by the same policy as in Theorem 4.1.

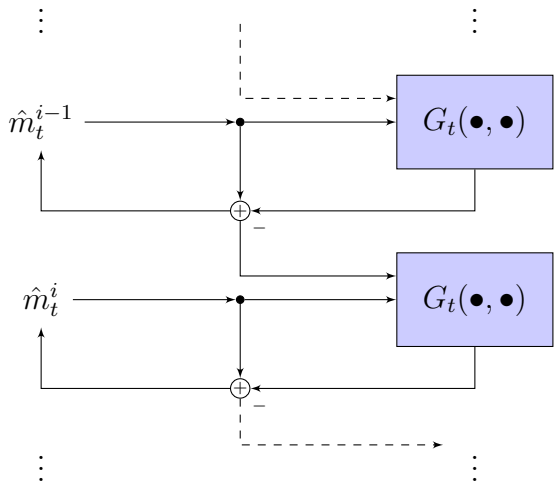

Figure 4.7: Recursive calculation of optimal thresholds under price independence assumption as described by (4.14).

The proof is provided in Appendix D.

A corollary of Theorem 4.2, is that the computational and storage complexity of the description of the optimal policy and value function is $\Theta(T)$ for each t, and hence $\Theta(T^2)$. This is assuming that evaluating $G_t(\bullet,\bullet)$ function is $\Theta(1)$, which is in line with other assumptions we had in the general case.

Similar to the general case, this solution can be implemented in T parallel processes in a very straightforward way essentially resulting in a $(T+1)\times(T+1)$ table that represents the optimal thresholds for every i and t. The implementation complexity of each branch, however, is reduced dramatically. Figure 4.7 depicts the block diagram form of the optimal threshold calculation algorithm.

As discussed, the independent case covers the deterministic price case. In deterministic case finding the optimal consumption and reserve provision amounts is a straightforward optimization problem, Theorem 4.2 gives a quick, recursive and parallel method to obtain the optimal policy independent of the actual amount of demand. This is particularly useful for an aggregator which would calculate the policy once and reuse it for many loads as discussed in the general case. Note that in deterministic case, $G_t(\bullet, \bullet)$ can be calculated in closed form very easily as:

$$G_t(z, z') = (z' - (z \vee \epsilon_t^a))^+, \tag{4.16}$$

where $(a \vee b) \triangleq \max\{a, b\}$ and $\epsilon_t^a = \epsilon_t^e - (\epsilon_t^r)^+$ is a given deterministic number.

4.4 Numerical Analysis

Although we have proven the optimality of the proposed algorithms mathematically, we still need to establish the improvements of optimal response and also compare it to the no AS case we studied in Chapter 3. To this end, we use a similar setup as in Chapter 3 where we studied the cost improvements for PEV loads based on the dataset and charging session patterns obtained in Chapter 2.

In a same setup as in Chapter 3, we considered 10,000 scenarios in which a group of 1000 PHEVs which show up over a 24 hour period of time. Energy demand, arrival and departure patterns are based on the results of our study in Chapter 2 based on the transportation dataset with minimum

dwell time of three hours and availability of charging everywhere under a non-anticipative model. Dwell times of the loads are truncated to 24 hour for ease of calculations.

Energy price statistics are based on the real-time market prices in the Houston Load Zone for year 2012 and only independent case is considered for simplicity. The prices are assumed to be normally distributed with mean from average Houston Load Zone for each hour and simulations are done for various price uncertainties reflected in the standard deviation of price realizations, denoted by σ. Price uncertainty here can be interpreted as Gaussian price estimation error from the flexible loads perspective. AS prices are based on average of ERCOT REG Up and REG Down prices and are assumed to be known to the load because AS prices are typically obtained in the day-ahead market and hence are available at real-time.

For the comparative cost performance study, we have depicted the normalized per charging session costs in Figure 4.8, normalized by the no-AS case. The comparison is done against no-AS optimal algorithm, the static price responsive CEC based method we introduced in Chapter 3, as well as price oblivious methods we studied in Chapter 2: immediate and AR charging. Moreover, to compare the network level impact of AS providing optimal response, we have plotted the average diurnal pattern of load produced by the above mentioned charging policies in Figure 4.9.

Figure 4.8 demonstrates considerable reduction in total cost due to AS provision, roughly about 10% to 15%, for all uncertainty levels. Since this

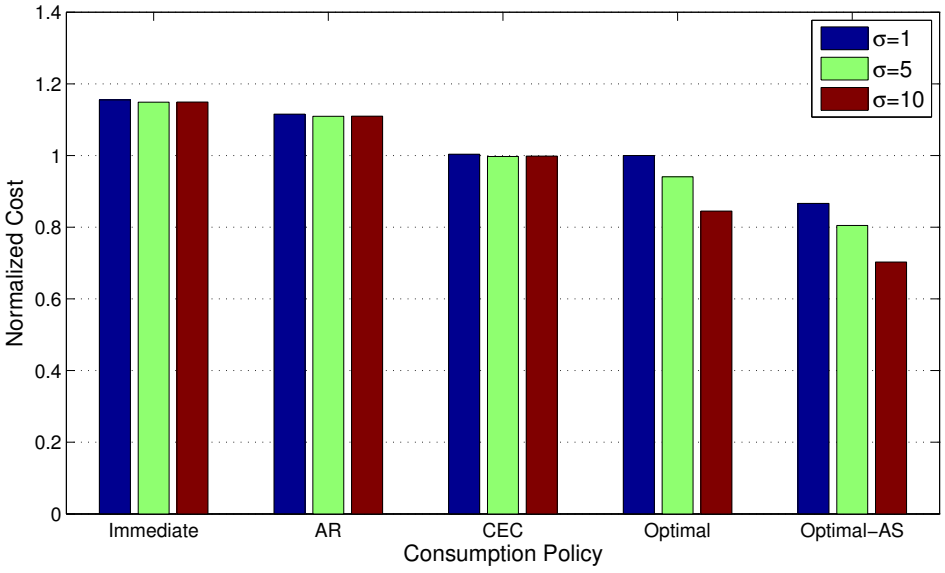

Figure 4.8: Cost comparison between various consumption policies under different levels of uncertainty.

cost savings is accompanied by AS capacity offered to the grid equal to the amount of load served (since AS prices are always positive in practice and hence optimal amount of AS to offer is equal to the amount of consumption due to Theorem 4.1 and Equation 4.11), it is in the best interest of both load and the grid to adopt this method versus the optimal consumption, if possible. On the other hand, the added cost of infrastructure for receiving AS commands and reporting back to the grid, or localized AS provision in case of autonomous response, should be considered. Finally, Figure 4.9 compares the average diurnal pattern of load induced by various consumption policies. Based on this figure, we observe no significant change in the pattern of load, mainly because the pattern of AS prices is very similar to the pattern of energy

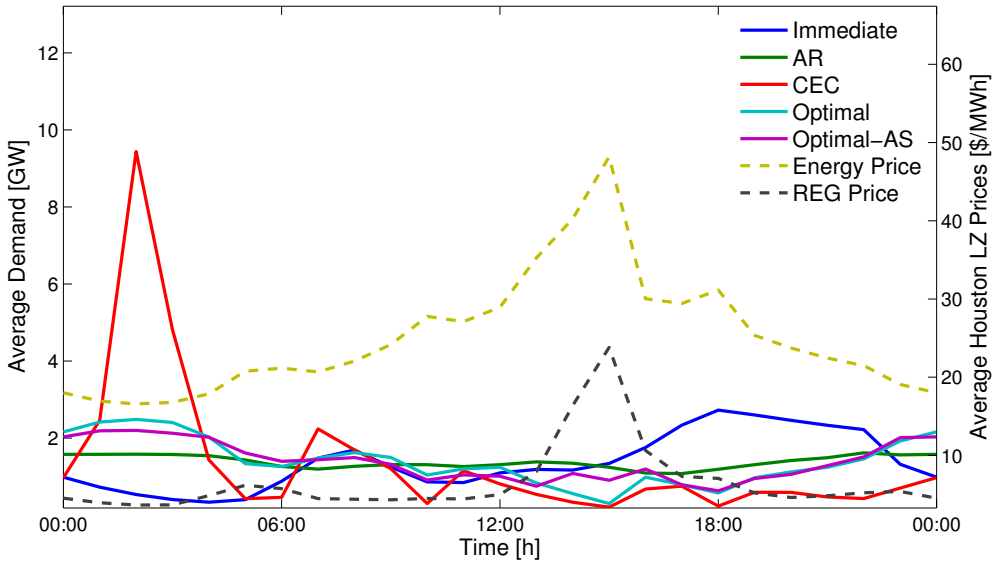

Figure 4.9: Average diurnal load comparison between various consumption policies ($\sigma = 10$).

prices as depicted in the figure.

4.5 Conclusion

In this chapter we extended our results in Chapter 3 for optimal response of flexible loads to the case where the loads can provide ancillary services in sub-market interval time frame and showed that a similar optimal policy structure holds. We particularly considered the case where no capacity reservation is needed for AS provision. Considering the case with capacity reservation is an ongoing future work.

Based on our performance evaluation on PEV load, we observed similar network load patters due to the high correlation of energy and AS prices.

Moreover, we observed consistent cost reduction across the studied levels of uncertainty. Combined with the fact that AS provided by the flexible loads can ultimately help the grid, we conclude that AS providing optimal response should be adopted when communication infrastructure is readily available or economically justifiable.

As a natural direction for this work, we are already working on the case with capacity reservation requirement. Our preliminary results suggest that the same multi-threshold optimal policy structure holds and there exists a similar efficient method for calculating the thresholds. We plan to perfect this case as our future work. To extend this work further, we also consider AS providing optimal response as building block for approximating the coordinated energy delivery problem we study in later chapters. This is another direction we are planning to work on in the future.

Chapter 5

Optimal Operation of Storage Devices under Stochastic Market Prices

5.1 Introduction

The need to maintain continuous supply demand balance in electric grid, and the increased variability and stochasticity in demand, and more recently supply due to intermittent renewables has exacerbated the need for energy storage in the grid. This need has resulted in a trend in development of storage assets at different levels of the grid and in different sizes.

As these assets become mainstream, a key question that needs to be addressed is how to efficiently operate them. For most of the current assets, efficient and optimal operation is defined with respect to the asset owners objective. For example, in some cases, the storage is used to displace the energy generated by renewables from the time they are more abundant to the time they are more needed, i.e. high demand times. The time scale in such cases can vary from a day to a season. In other cases, such assets are primarily geared towards grid stabilization and provision of ancillary services, and some newer applications involves firming intermittent sources. At micro grid and consumer level, storage assets have been used to increase reliability and more

recently, shaping the load profile to reduce the overall energy bill; e.g. by reducing demand charges.

What ultimately drives operation of an asset; however, is the economic value it provides to its operator. Hence, it is conceivable for the owner to operate the asset to maximize its economic benefit. This economic value depends on the structure of the underlying energy market. In other words, the optimal operation of the asset, and hence its impact on the overall power system is directly influenced by the incentives provided by the market.

In restructured electricity markets, the grid is operated as an open market in which power is traded while grid reliability and supply demand balance is maintained by the Independent System Operator (ISO). The incentives in such markets, also known as the restructured electricity markets, are mainly prices that are formed as a result of market clearance based on the bids submitted by participants. Given the stochastic nature of demand and most renewable supplies, market participants, particularly smaller ones, effectively respond to market prices. Hence, for a storage asset operator, optimal operation of the asset is equivalent to optimal response to real-time stochastic prices and this is our focus in this chapter.

Potential benefits and applications of the storage assets in power systems has been investigated in the past by various authors. Eyer and Corey [39] aim at giving a broad perspective of the value of energy storage in power systems, one that is most suitable for assessment of long term benefits and investment purposes. Many authors have proposed optimizing the storage operation

to stabilize the combined output of an intermittent generation source, like a wind farm, and the storage asset. Korpaas *et al.* [63] investigate optimal operation of a combination of a storage asset and a wind farm and propose using the storage asset to meet the output schedule which has been formed based on a forecast model. Along the same lines, Teleke [96] considered control strategies for smoothing wind farm output using battery storage. Denholm and Sioshansi [35], examined co-locating wind farms with Compressed Air Energy Storage (CASE) to assess the value of energy storage. Divya and Østergaard [36] investigate various applications of battery storage in power systems. They discuss firming wind power as well as using battery for energy arbitrage between high and low price times. Qin *et al.* [85] studied the arbitrage value of storage assets under locational marginal prices. Secomandi [87] studied optimal commodity trading with a capacitated storage asset and showed that a multi-threshold policy (buy, idle, sell) is optimal under some conditions. Faghih *et al.* [40] studied economic value of ramp-constrained storage assets and particularly showed that storage assets can improve price elasticity near average prices.

In this chapter, we present our preliminary results on optimal operation of the energy storage device as an independent asset in response to stochastic real-time market prices. We first present our generic model for an storage asset and then formulate the optimal operation problem as a dynamic program whose objective is to maximize the net present value of the profit achieved by operating the asset. Our main contribution in this work is to give the

exact optimal operation policy under fairly generally distributed stochastic prices and demonstrate that under some conditions, the optimal policy can be computed and stored in a computationally efficient manner. Our approach is not limited to grid scale storage devices and can be applied to micro grid or even consumer level storage assets, e.g. Vehicle to Grid (V2G), if they are under the same pricing structure.

The rest of this chapter is organized as follows: In Section 5.2 we present our generic storage asset model. Section 5.3 is dedicated to presenting our main result on optimal operation of the storage assets. We conclude the chapter and comment on our future directions in Section 5.4.

5.2 System Model

In this section, we first introduce our general model for energy storage assets and the objective of the optimization problem. We then make some simplifying assumption and prepare the ground for our results on optimal operation of the proposed model in the proceeding section.

We consider an energy storage asset which is being operated under real-time prices where the asset owner aims at maximizing its profit through buying and selling energy over time. We assume the storage operator participates as a price taker; i.e. its decisions does not impact the prices. Considering a discrete time setup, at each time slot, the storage operator needs to decide how much energy to buy or sell given the price of energy over that time slot. Note that due to lack of market power assumption, obtaining the optimal

policy for energy trading is equivalent to finding the optimal bidding strategy.

Similar to Chapter 3, we assume a Markovian model for prices whose statistics are available to the operator. Following a similar model as in [57], we assume stochastic prices evolving as:

$$\pi_t = \lambda_t(\pi_{t-1}) + \epsilon_t, \tag{5.1}$$

where ϵ_t is the random variable modeling price innovations and $\lambda_t(\bullet)$ is modeling the inter-stage correlation of prices and seasonality. We assume $\epsilon_t \sim F_t(\bullet)$ to be independent with respect to t, $\lambda_t(\bullet)$ to be monotone to avoid some technicalities, and define $\theta_t \triangleq \pi_{t-1}$ for notational convenience. Note that the price innovation statistics is assumed to be completely general with arbitrary mean and distribution.

Our objective is to find the optimal policy which can be employed by the storage operator, or operator in short, to maximize its expected profit from operating the storage asset. To this end, we need to model the dynamics of the storage asset. Storage assets come in wide variety depending on their size and technology. Examples range from batteries based on different chemistries and in various sizes to flywheels, thermal storages, pumped hydro assets and Compressed Air Energy Storage (CAES). Although the dynamics of each of these storage technologies are different, they share some common fundamentals. From grid's perspective, all of these assets have a State of Charge (SoC) which is basically the amount of energy stored in them. For efficient operation of the asset, its SoC is bounded to a specific range. Moreover, the operator

can control the flow of energy in and out of the asset and similar to SoC, for efficient operation of the asset, there are upper and lower bounds on the rate of energy flow. The operator pays for flows going in, i.e. consuming electricity and is paid for flows out.

We formalize this model as follows. Let us denote the state of charge by x_t and the total energy transfered in/out of the storage asset at time t by u_t, then the dynamics of the asset can be described as:

$$\begin{aligned} &x_{t+1} = x_t - (\eta^+(u_t)^+ + \eta^-(u_t)^-), \\ &\underline{u} \leq u_t \leq \overline{u}, \\ &\underline{x} \leq x_t \leq \overline{x}, \end{aligned} \tag{5.2}$$

where η^- and η^+ capture inefficiencies in energy storage and retrieval respectively; and, $\underline{x}$, $\overline{x}$, $\underline{u}$ and $\overline{u}$ represent the upper and lower bounds on feasible SoCs and energy flow per time slot respectively. Also, we define: $(\bullet)^+ \triangleq \max\{0, \bullet\}$ and $(\bullet)^- \triangleq \min\{0, \bullet\}$. Note that for a physical system where losses are always non-negative:

$$0 \leq \eta^- \leq 1 \leq \eta^+. \tag{5.3}$$

Moreover, the bi-directional flow of energy implies that:

$$\underline{u} \leq 0 \leq \overline{u}. \tag{5.4}$$

At each time step, the utility of the operator is given by its energy sales to the grid:

$$g_t(x_t, u_t, \pi_t) = \pi_t u_t, \tag{5.5}$$

and final stage utility at stage T, which captures the effect of remaining energy in the storage device is given by:

$$g_T(x_T) = m_T(x_t - \underline{x}). \tag{5.6}$$

where m_T is the price for energy remaining in the storage asset after final stage. The objective is to maximize the total expected net present value of the profits:

$$J_0^*(x_0, \theta_0) = \max \mathbb{E}_{\pi_t}[\sum_{t=0}^{T-1} a(t) g_t(x_t, u_t, \pi_t) + a(T) g_T(x_T)], \tag{5.7}$$

where $a(t) = \prod_{t'<t} \alpha_{t'}$; α_t is the discount factor; and the maximization is over all policies that admit a feasible u_t, denoted by $u_t(x_t, \pi_t)$ by abuse of notation. Here, we consider a finite horizon model due to the non-stationary statistics of prices and the infinite horizon case can be approximated by picking a large enough T.

5.3 Optimal Operation of Storage Assets

In this section, we state our main result which provides a closed form optimal policy and value function for the no-loss case and then show that under price independence assumption, the optimal policy can be computed and stored computationally efficiently. We then discuss the technical challenges with the lossy case and shed some light on sufficient conditions on tractable cases.

For the sake of brevity and notational clarity, let us define some notation and make some simplifying assumptions. We define $a \wedge b \triangleq \min\{a, b\}$ and

$a \vee b \triangleq \max\{a, b\}$. Also, we assume symmetry in the rate limits in and out of the storage device from the grid perspective, i.e.:

$$\underline{u} = -\overline{u}. \tag{5.8}$$

Also, defining $r_P = \frac{\overline{x}-\underline{x}}{\overline{u}}$ and $n_P = \lfloor r_P \rfloor$, we assume:

$$r_P \in \mathbb{Z}, \tag{5.9}$$

which implies that state space range is divisible by the per time step limit of energy transfer and $r_P = n_P$. Moreover, without loss of generality, we assume:

$$\underline{x} = 0. \tag{5.10}$$

Finally, for the ideal case, we assume:

$$\eta^- = \eta^+ = 1. \tag{5.11}$$

Now we are ready to present our first result, which gives the optimal operation policy under correlated prices:

Theorem 5.1. *Consider the system described in* (5.1)–(5.11).

(a) The optimal value function is continuous, piecewise linear and concave with $n_P + 1$ pieces given by:

$$J_0^*(x, \theta) = \sum_{j=0}^{n_P} m_0^j(\theta)[(x - j\bar{u})^+ \wedge \bar{u}] + c_0(\theta)\bar{u}, \tag{5.12}$$

where $m_t^i(\theta_t)$ is given by the following backward recursion:

$$m_t^i(\theta_t) = \mathbb{E}_{\epsilon_t}[M(\theta_t, \epsilon_t)], \tag{5.13}$$

where,

$$M(\theta_t,\epsilon_t)=\begin{cases}\tilde{m}_{t+1}^{i+1}(\pi_t) & \pi_t<\hat{m}_{t+1}^{i+1}\\ \pi_t & \hat{m}_{t+1}^{i+1}\leq\pi_t<\hat{m}_{t+1}^{i-1}\\ \tilde{m}_{t+1}^{i-1}(\pi_t) & \hat{m}_{t+1}^{i-1}\leq\pi_t\end{cases}, \tag{5.14}$$

$\pi_t \triangleq \lambda_t(\theta)+\epsilon$, $\tilde{m}_\tau^i(\theta) \triangleq \alpha_{\tau-1}m_\tau^i(\theta)$, $\hat{m}_T^i = m_T^i(\theta) = m_T$, $\forall i,\theta$, $\hat{m}_t^0 = m_t^0(\theta) = +\infty$, $\forall t,\theta$ *and* $\hat{m}_t^{n_P} = m_t^{n_P}(\theta) = -\infty$, $\forall t,\theta$, *and* $\hat{m}_t^i$ *is the extended solution to the following fixed point equation:*

$$\mu = \tilde{m}_t^i(\mu), \tag{5.15}$$

and, $c_t(\theta_t)$ *is given by:*

$$c_t(\theta_t) = \mathbb{E}_{\epsilon_t}[C(\theta_t,\epsilon_t)], \tag{5.16}$$

where $\pi_t = \lambda_t(\pi_{t-1}) + \epsilon_t$.

$$C(\theta_t,\epsilon_t)=\alpha_t c_{t+1}(\pi_t) + \begin{cases}\tilde{m}_{t+1}^i(\pi_t)-\pi_t & \pi_t<\hat{m}_{t+1}^i\\ \pi_t-\tilde{m}_{t+1}^{i-1}(\pi_t) & \hat{m}_{t+1}^{i-1}\leq\pi_t\end{cases}. \tag{5.17}$$

(b) The optimal policy is given by:

$$u_t^*(x,\pi_t)=\begin{cases}\underline{u} & \pi_t\leq\hat{m}_t^{i+1},\\ x-(i+1)\overline{u} & \hat{m}_t^{i+1}<\pi_t\leq\hat{m}_t^i,\\ x-i\overline{u} & \hat{m}_t^i<\pi_t\leq\hat{m}_t^{i-1},\\ \overline{u} & \hat{m}_t^{i-1}<\pi_t.\end{cases}, \tag{5.18}$$

where

$$i = \lfloor\frac{x}{\bar{u}}\rfloor. \tag{5.19}$$

The proof is provided in Appendix E.

Theorem 5.1 demonstrates that the optimal operation policy follows a multi-threshold form in the sense that for any given x and its corresponding i, the thresholds can be obtained. Moreover, the number of these thresholds are limited to n_P which is basically the minimum number of time steps needed to span the SoC state space.

Moreover, one main result of this theorem is the structure of the optimal value function. Equation (5.12) basically shows how the price state and SoC state interact. In particular, the optimal value function is piecewise linear in SoC state and the price statistics only affect the coefficients of the pieces.

Intuitively, these coefficients correspond to the expected marginal net present value of the storage at different SoCs. That is, at given SoC, x, these coefficients represent the expected marginal change in the profit of operation given the price statistics forward, adjusted by the discount rate. This marginal profit involves both selling and buying energy forward in time. $c_t(\theta)$, on the other hand, is the constant profit obtained from the operation at stage t independent of x, or basically the base profit.

Since we have assumed that the storage operator acts as a price taker, it is not hard to see that the optimal policy obtained also corresponds to the optimal bidding strategy by the operator. Therefore, the piecewise linear structure of the optimal value function means that using piecewise linear marginal cost specification which is common in many energy markets does not impact opti-

mality of the bidding for the storage operator, and Theorem 5.1 indeed gives the optimal bidding strategy under assumptions given in (5.1-5.11).

Although Theorem 5.1 simplifies the structure of the value function by decomposing the role of SoC and prices and giving $O(n_P)$ fixed point calculations for SoC recursions, price expectation recursions still pose a computational challenge due to correlations. Taking this lead, in the next theorem, we show that there recursions can be much simplified and the optimal policy can be computed and stored in a computationally efficiently under price independence assumption.

Theorem 5.2. *Consider the system specified by* (5.1)–(5.11) *and further assume* $\lambda_t(\theta) = 0$ *for all* t*, then, the optimal value function given in Theorem 5.1 simplifies to:*

$$J_0^*(x) = \sum_{j=0}^{n_P} m_0^j [(x - j\bar{u})^+ \wedge \bar{u}] + c_0 \bar{u}, \tag{5.20}$$

where m_t^i *is given by:*

$$m_t^i = \tilde{m}_{t+1}^{i+1} - G_t(\tilde{m}_{t+1}^{i-1}, \tilde{m}_{t+1}^{i+1}), \tag{5.21}$$

and c_t *is given by:*

$$c_t = \alpha_t c_{t+1} + G_t(-\infty, \tilde{m}_{t+1}^i) + \bar{G}_t(\tilde{m}_{t+1}^{i-1}, \infty), \tag{5.22}$$

in which,

$$G_t(z, z') \triangleq \int_z^{z'} F_t(\zeta)\, d\zeta, \tag{5.23}$$

$$\bar{G}_t(z, z') \triangleq \int_z^{z'} (1 - F_t(\zeta))\, d\zeta, \tag{5.24}$$

and $\tilde{m}_\tau^i \triangleq \alpha_{\tau-1} m_\tau^i$. *The optimal policy remains the same as given in Theorem 5.1.*

The proof is provided in Appendix F.

According to this result, the description of the optimal value function, and hence optimal policy, which essentially consists of m_t^i and c_t can be stored in vector of $n_P + 1$ elements per time step and hence is $\Theta(n_P)$. For any given T, the total size of the optimal policy description would be $\Theta(Tn_P)$. Computationally, assuming $G(\bullet, \bullet)$ and $\bar{G}(\bullet, \bullet)$ are $\Theta(1)$, we have the same result computationally. Moreover, the per stage computation can be parallelized into $n_P + 1$ independent computations for higher efficiency.

5.4 Conclusion

In this chapter, we extended our results on flexible loads to storage assets and proposed a generic model for energy storage assets. We then formulated the profit maximization problem for the asset owner under stochastic prices. We also obtained the exact optimal policy for operation of such assets under no-loss assumption and further demonstrated that if prices are not correlated, the optimal policy and value function can be computed and stored in a computationally efficient manner.

Chapter 6

Energy Delivery Transaction Pricing for Flexible Electrical Loads

6.1 Introduction

Price signals are considered by many authors as the key demand-response method to coordinate supply and demand and induce demand elasticity, especially to shift load to off-peak hours. Various dynamic pricing methods such as Time of Use (ToU) pricing [4], Real-Time Pricing (RTP) [50, 82], Critical Peak Pricing (CPP) [32, 110] have been proposed, studied and experimentally evaluated, and optimal algorithms for responding to such prices have been designed [72]. Various authors [17, 18, 66, 73, 105] have taken a game-theoretic approach and sought existence of Nash-Equilibria (NE), its stability, convergence and efficiency, and prices supporting it. Nevertheless, as shown in [57], exposing flexible consumers to real-time prices can induce undesired aggregate load profiles with high peak-to-average ratios (PAR) that can be particularly detrimental to the distribution network.

Alternatively, recent work such as [6, 8, 9, 11, 14, 15, 25, 44, 45, 48, 58, 60, 74, 86, 91–94, 102] suggest that more coordination among flexible loads can provide benefits beyond merely shifting and distributing the load over time by

providing ancillary services to the grid. This coordination is usually achieved by an Energy Service Company (ESCo) which is delegated the control of the energy delivery process by the consumer in return for a low flat energy price to the consumer. The ESCo utilizes aggregate demand flexibility to minimize total energy delivery cost by offering some of the load as responsive reserves in the market while keeping the aggregate load profile under capacity constraints of the distribution network (DN). Increasing penetration of uncertain generation sources, emergence of new flexible loads, and the inefficiency of existing reserve provisioning methods make such proposals very appealing. Consequently, some authors [7, 19, 76, 79, 90] have considered direct coupling of uncertain renewables, e.g., wind, with flexible demands. However, since methods similar to ones in [25] and [58] charge users at a fixed flat rate independent of demand flexibility and time, they fail to efficiently incentivize users to reveal their flexibility and may face fundamental challenges in real world implementations.

In this chapter, we aim to fill the gap between dynamic pricing and coordinated energy delivery approaches by proposing a novel interaction and pricing scheme in which the *process* of energy delivery has a central role, and demand flexibility and system state play major roles besides market prices and demand amount.

We define an *Energy Delivery Transaction (EDT)* as the process of delivering a certain amount of electric energy subject to given power trajectory and time constraints. The trajectory constraints may involve maximum and

minimum limit but implicitly assumed to provide some flexibility. Although our method can be used in most EDT classes, for more clear demonstration, here we focus on a particular class of EDTs in which a certain amount of energy should be delivered by some deadline subject to rate constraints. EVs constitute a natural, and perhaps the most important, example of this class where, upon plugging in, the battery needs to be charged over a given period of time subject to the charger power constraints.

Building on our previous work in [58], we consider an ESCo as a central entity which receives EDT requests from users, and prices them according to market prices, demand amount and flexibility, and congestion level of the distribution network. The ESCo also makes decisions necessary for purchasing and delivery process to minimize energy delivery cost while observing distribution network constraints. At the system level, the ESCo plays an important role in stabilizing the uncertainty in the system through aggregating and controlling the flexible demands and coupling them with the uncertainties in distribution load level and supply demand balance in the market. The response to distribution load level uncertainty is achieved by only using the excess capacity of the distribution network. Response to uncertainty in the wholesale market is accomplished through responding to reserve prices, which are expected to go up as supply demand mismatch in the wholesale market becomes more uncertain. At the user level, the ESCo simplifies demand response participation and increases its efficiency by managing user schedules, and hedges the risk of real-time prices for the users. Our focus in this work

is to design a pricing mechanism that reflects the value of flexibility to the users so that they can make clear cost-comfort trade-offs and are incentivized to reveal their true flexibility. Our main contributions can be summarized as follows:

- Introducing the concept of *Energy Delivery Transaction* and using it as the commodity which is priced and exchanged, and analyzing the effects of trading such a commodity besides the real time electric power.
- Proposing and analyzing a new pricing scheme for EDTs, and particularly showing that it provides efficient incentives to flexible users in a coordinated energy delivery context and can be implemented in a computationally efficient manner.
- Verifying, through simulation, the effectiveness of the method under different distribution network load levels, and analyzing network level user response to such a scheme and its efficiency in competition with opportunistic response under RTP and conventional consumption.

The rest of this section is organized as follows: In Section 6.2 we present the model according to which the ESCo interacts with the users, the market and the distribution network. In Section 6.3 we introduce and discuss energy delivery transaction pricing. In Section 6.4 we present our simulation results and compare the performance of transaction pricing with optimal user response to real-time prices and conventional consumption. Finally, in Section 6.5 we conclude the chapter.

6.2 Preliminaries and Model

6.2.1 The Energy Services Company (ESCo)

We consider a model similar to that discussed in [58] where the ESCo acts as a mediator between the wholesale market and the end-users and therefore has a role similar to the retailers or retail electricity providers (REPs). The main difference, however, is that the ESCo offers a different type of service, targeted at delay tolerant demands. Instead of committing to deliver at a certain rate, the ESCo provides the requested amount of energy by the requested deadline. In case of failure in delivery, the ESCo reimburses the load at a pre-negotiated inconvenience price, denoted by s. This service is either provided at end-points called smart plugs which are capable of communication and control with the ESCo or using Home Energy Management Systems (HEMS), which collaborate with the ESCo on energy delivery control process in smart grid environments. The ESCo also contracts with the distribution network operator to only use the excess capacity of the distribution network and in return receives a discount on the distribution costs. Table 6.1 summarizes the interactions of the ESCo with the other entities in the system and Figure 6.1 visualizes them.

To satisfy its commitment to the users, the ESCo should receive the user energy demand information and decide the amount of electricity purchases on behalf of each user over time. For notational convenience, we arrange the user energy demands into a column vector denoted by $\tilde{\boldsymbol{d}}_t$ and $\tilde{\boldsymbol{d}} = \sum_t \tilde{\boldsymbol{d}}_t$, where the subscript t allows for capturing user arrivals at different times. The user

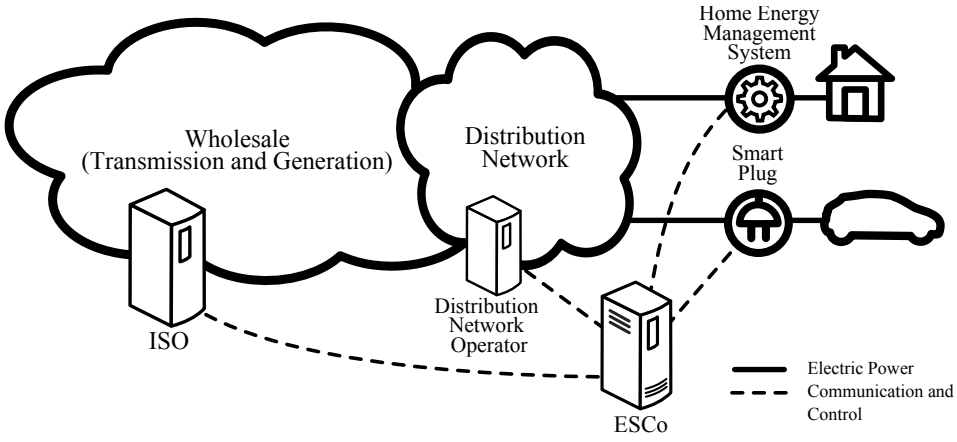

Figure 6.1: ESCo interactions.

arrival and departure times (based on their deadlines) are similarly denoted by $\boldsymbol{t}^a$ and $\boldsymbol{t}^d$. We also arrange ESCo power purchase decisions on behalf of users at each time t in $\boldsymbol{x}_t^e$ and corresponding decisions for the amount of reserves to offer in $\boldsymbol{x}_t^r$, and define $\boldsymbol{x}_t = (\boldsymbol{x}_t^e, \boldsymbol{x}_t^r)$ for notational convenience.

Table 6.1: ESCo interactions with different entities.

Entity	Interactions
ISO	Wholesale market participation: Purchasing electricity and offering reserves.
Distribution Network Operator	Obtaining the excess capacity information.
Smart Plugs	Obtaining demand information, user selections and controlling the energy delivery schedule.
Home Energy Management Systems (HEMS)	Obtaining demand information, system preferences and selection, communicating the energy delivery schedule.

The ESCo participates in the wholesale electricity market for purchasing electricity. Besides conventional participation, just like other load serving entities, the ESCo utilizes the flexibility of the delay-tolerant loads at its disposal to offer reserve services in the market. To keep the model simple and manageable, we assume a single time scale for the market clearing interval, Δt, essentially assuming the real-time market; however, this model can be generalized to multiple time scales as done in [26]. We assume that the market requires bi-directional reserve offers, where, the reserve provider offering x amount of reserves should be able to modulate its consumption around its nominal value up and down up to x. Furthermore, we assume that reserve deployment requests are net zero over the decision period. Assuming the ESCo participating as a price-taker, it should decide bid/offer prices u^e, u^r, u^s corresponding to electricity purchases, reserve deployment, and reserve standby prices, respectively. Denoting the market clearing prices for energy and reserves by p^e and p^r, similar to [58] and [25], the indicators for the events of winning the bids for electricity and reserve offers are obtained as $w_t^e = \mathbb{1}\{u_t^e \geq p_t^e\}$ and $w_t^r = \mathbb{1}\{|p_t^e - u_t^r| + u_t^s \leq p_t^r\}$ respectively, as a result of co-optimization of energy and reserves, where $\mathbb{1}\{\bullet\}$ is the indicator function. We assume that reserves are paid p^r for being standby, while deployment remunerations are calculated according to real-time energy price, p^e. We also define $w_t = (w_t^e, w_t^r)$ and $u_t = (u_t^e, u_t^r, u_t^s)$.

As treated more extensively in [58], the problem of minimizing the total cost of energy purchases for the users subject to market uncertainties can be

formulated as a Dynamic Program (DP) with the following dynamics:

$$\boldsymbol{d}_{t+1}=\boldsymbol{d}_t+\tilde{\boldsymbol{d}}_t-\boldsymbol{w}_t^e \circ \boldsymbol{x}_t^e \Delta t, \quad t=0,\ldots,T-1, \tag{6.1}$$

where $\circ$ denotes element-wise product and $\boldsymbol{d}_t$ is the vector of remaining demands. The step and terminal cost functions, $g_t(\cdot)$ and $g_T(\cdot)$, are given by:

$$g_t(\boldsymbol{x}_t,\boldsymbol{u}_t) = \mathbf{1}^\top(p_t^e \boldsymbol{w}_t^e \circ \boldsymbol{x}_t^e - p_t^r \boldsymbol{w}_t^r \circ \boldsymbol{x}_t^r)\Delta t, \tag{6.2}$$

$$g_T(\boldsymbol{d}_T) = s\mathbf{1}^\top \boldsymbol{d}_T, \tag{6.3}$$

where $\mathbf{1}$ is the all ones vector of appropriate length. The decision variables, $\boldsymbol{x}_t$ and $\boldsymbol{u}_t$ are subject to the following constraints:

$$\mathbf{1}^\top(\boldsymbol{x}_t^e+\boldsymbol{x}_t^r) \leq C_t, \quad \forall t, \tag{6.4}$$

$$\boldsymbol{x}_t^r \leq \boldsymbol{x}_t^e, \quad \forall t, \tag{6.5}$$

$$\boldsymbol{x}_t^e+\boldsymbol{x}_t^r \leq \bar{\boldsymbol{x}}, \quad \forall t, \tag{6.6}$$

$$\Delta t\ \boldsymbol{x}_t^e \leq \boldsymbol{d}_t, \quad \forall t, \tag{6.7}$$

$$x_{t,i}^e, x_{t,i}^r = 0, \quad \forall i,\ ,\forall t \notin [t_i^a, t_i^d], \tag{6.8}$$

$$\boldsymbol{x}_t^e, \boldsymbol{x}_t^r \geq \mathbf{0}, \quad \forall t, \tag{6.9}$$

where index i indicates the ith user, C_t denotes distribution network excess capacity, which we refer to as capacity for short, and $\bar{\boldsymbol{x}}$ encompasses maximum input rates. Note the positivity constraint on $\boldsymbol{x}_t^e$ implies no reverse power transfer back to the grid unlike what is suggested in [59] and dubbed as "Vehicle-to-Grid" (V2G). The objective of the ESCo then can be formulated as:

$$\text{DP}: \ J^*(\tilde{\boldsymbol{d}},\boldsymbol{t}^a,\boldsymbol{t}^d)=\min \mathbb{E}_{p_t}[\sum_{t=0}^{T-1} g_t(\boldsymbol{x}_t,\boldsymbol{u}_t)+g_T(\boldsymbol{d}_T)], \tag{6.10}$$

where the minimization is over the policies which give $\boldsymbol{x}_t$ and $\boldsymbol{u}_t$ as a function of the current state, $\boldsymbol{d}_t$.

6.2.2 The LP Scheduler

As discussed in [58], the problem in (6.10) cannot be solved in a computationally efficient manner; nevertheless, a computationally efficient approximate solution can be obtained by using a mixture of certainty equivalence control [13] for obtaining $\boldsymbol{x}_t$, and a heuristic method for obtaining $\boldsymbol{u}_t$. This solution is called the *LP Scheduler* since it casts the approximate problem in a Linear Programming (LP) model to approximate the expected cost-to-go function. The LP Scheduler is implemented in a rolling horizon fashion, i.e., at each step, the next stage solution is implemented and the system state is updated based on the evolution of the system. By some abuse of notation, from the LP Scheduler's perspective, $\tilde{\boldsymbol{d}}$ captures the system state as the demand currently owed to each load, i.e., all loads arrived before the current stage are treated like loads arrived just now with demand equal to their remaining demand and $\boldsymbol{t}^a$ and $\boldsymbol{t}^d$ are modified similarly. Denoting the estimated market prices by $\hat{p}^e$ and $\hat{p}^r$, the LP Scheduler obtains the solution for $\boldsymbol{x}_t$, denoted by $\hat{\boldsymbol{x}}_t$ at each step by solving:

$$
\begin{aligned}
\hat{J}(\tilde{\boldsymbol{d}}, \boldsymbol{t}^a, \boldsymbol{t}^d) = \min_{\boldsymbol{x}} \; & \mathbf{1}^\top [s\tilde{\boldsymbol{d}} + \textstyle\sum_{t=0}^{T-1} (\hat{p}_t^e - s)\boldsymbol{x}_t^e - \hat{p}_t^r \boldsymbol{x}_t^r] \\
\text{st. } & \Delta t \textstyle\sum_t \boldsymbol{x}_t^e \leq \tilde{\boldsymbol{d}}, && \forall \tau \leq t, \\
& \mathbf{1}^\top (\boldsymbol{x}_t^e + \boldsymbol{x}_t^r) \leq C_t, && \forall \tau \leq t, \\
& \boldsymbol{x}_t^e + \boldsymbol{x}_t^r \leq \bar{\boldsymbol{x}}, && \forall \tau \leq t, \\
& -\boldsymbol{x}_t^e + \boldsymbol{x}_t^r \leq \mathbf{0}, && \forall \tau \leq t, \\
& x_{t,i}^e, x_{t,i}^r = 0, \;\; \forall i, \;\; , \forall t \notin [t_i^a, t_i^d], \\
& \boldsymbol{x}_t^e, \boldsymbol{x}_t^r \geq 0, && \forall \tau \leq t.
\end{aligned}
\tag{6.11}
$$

Now let us define the conditional one step forward solution, denoted by $\hat{J}_{+1}(\cdot|\boldsymbol{x}^e, \boldsymbol{x}^r)$, as the next stage solution cost, assuming the state, $(\tilde{\boldsymbol{d}}, \boldsymbol{t}^a, \boldsymbol{t}^d)$, is updated by $(\boldsymbol{x}^e, \boldsymbol{x}^r)$. Then $\hat{\boldsymbol{u}}_t$ is obtained by the approximated opportunity cost of losing the corresponding bid:

$$\begin{aligned} \hat{u}^e_{0,i} &= \frac{\hat{J}_{+1}(\cdot|\hat{\boldsymbol{x}}^e - \hat{x}^e_{0,i}\boldsymbol{e}_i, \hat{\boldsymbol{x}}^r) - \hat{J}_{+1}(\cdot|\hat{\boldsymbol{x}}^e, \hat{\boldsymbol{x}}^r)}{\hat{x}^e_{0,i}}, \\ \hat{u}^r_{0,i} - \hat{u}^s_{0,i} &= \frac{\hat{J}_{+1}(\cdot|\hat{\boldsymbol{x}}^e, \hat{\boldsymbol{x}}^r - \hat{x}^r_{0,i}\boldsymbol{e}_i) - \hat{J}_{+1}(\cdot|\hat{\boldsymbol{x}}^e, \hat{\boldsymbol{x}}^r)}{\hat{x}^r_{0,i}}, \end{aligned} \tag{6.12}$$

and setting $\hat{u}^r_{0,i} + \hat{u}^s_{0,i}$ to the minimum possible (by market rules) where $\boldsymbol{e}_i$ is the standard unit vector in the ith dimension as discussed in more detail in [58].

Since the LP scheduler is a linear program at heart, it can be solved in a computationally efficient (polynomial time) manner and there are already free and commercial software packages available for that purpose. The effective number of variables in (6.11) is $\frac{2}{\Delta t}\sum_{i\in I}(t^d_i - t^a_i)$ where I is the set of active users in the system. To obtain offer prices, a problem similar to (6.11) should be solved at most $2|I|$ times; however, such subproblems can be solved with less effective complexity due to availability of the solution of (6.11).

6.3 Energy Delivery Transaction Pricing (EDTP)

6.3.1 Motivation

In the energy delivery model proposed in [25] and [58], the users are charged at a pre-negotiated flat rate for their demands independent of their arrival and departure times and distribution network congestion level. Such

pricing scheme effectively makes the users insensitive to market prices and distribution network congestion and hence reduces demand elasticity; essentially restoring the problematic situation of inelastic demand. Due to the inherent desire of most users in minimizing their energy acquisition time, the users have no incentive to declare their actual desired deadline or alternatively, no way to find it out through cost-comfort analysis.

To address this issue, we propose a new user interaction method for the ESCo that reflects the value of flexibility to the user by pricing the energy delivery transaction request based on the arrival time, deadline, and requested demand for various deadlines. This approach essentially balances between RTP settings which can result in overreaction by loads, and flat rates which result in inelastic demand.

6.3.2 User Interactions Model

To accommodate differentiated service offerings and user choice on smart plugs, the user interaction model should be changed. The following shows the step by step process through which each user is offered prices and potentially commits to a deadline:

1. The user communicates its demand amount, d, and maximum acceptable delay, $\tau_{\max}$, i.e., its transaction request.

2. The ESCo responds with the vector of energy delivery costs for all feasible deadlines, i.e., the transaction prices vector.

3. The user does the cost-comfort analysis and potentially picks the desired deadline, τ.

4. The ESCo commits to deliver the requested energy or pay the inconvenience fee at rate s.

5. The ESCo communicates proper control commands necessary to complete the energy delivery transaction schedule as well as potential updates in response to reserve calls to the smart plug.

In case of HEMS, there is not a fundamental change in the interaction scheme at the negotiation phase. However, the actual implementation of the schedule commands are delegated to the HEMS. The same negotiation framework can be used with proper generalization of fixed and flexible parameters for more general energy delivery transactions. HEMS are advantageous in terms of privacy by limiting ESCo's access to appliances as well as further optimization by appropriately grouping appliances and serving them under different transactions.

6.3.3 Scheduling Algorithm and Transaction Pricing

The LP Scheduler is employed by the ESCo to jointly solve the market participation and user scheduling problem in a computationally efficient manner, minimizing the total cost of satisfying the energy delivery to the users. Therefore, the ESCo has an estimate of the expected cost-to-go given the time and current initial state of the system with respect to problem (6.10), com-

posed of (remaining) user demands and arrival and departure times. Let us define the unperturbed evolution of the system as the situation where the desired decisions are implemented at each step and no arrival or early departure happens. The ESCo also can use the LP Scheduler to obtain estimates of the potential perturbed evolutions of the state, as used for obtaining offer prices for the market.

Using this methodology, the ESCo calculates the estimated cost of energy delivery for an arriving user by obtaining the differential estimated cost of the current schedule versus a new schedule obtained from perturbing the system state with the new demand included in the schedule assuming it leaves at deadline τ:

$$c(d,\tau) = \hat{J}([\tilde{\boldsymbol{d}}\ ;\ d], [\boldsymbol{t}^a\ ;\ 0], [\boldsymbol{t}^d\ ;\ \tau]) - \hat{J}(\tilde{\boldsymbol{d}}, \boldsymbol{t}^a, \boldsymbol{t}^d), \tag{6.13}$$

where semicolon denotes vertical augmentation. In other words, the ESCo prices energy delivery cost to each new user as the estimated extra cost due to the perturbations in the initial state caused by the new arrival.

The vector $\boldsymbol{c}(d) = [c(d,1)\ \ldots\ c(d,\tau_{\max})]$ forms the prices offered by the ESCo to the incoming user and, as discussed, it can form a basis for the user to make cost-comfort analysis as depicted in Figure 6.2. Note that it is implicitly assumed that the user arrives at $t = 0$ since the LP Scheduler is running in rolling horizon manner and hence $t = 0$ is the current time for the scheduler.

A key aspect of such pricing scheme is that it is incentive revealing.

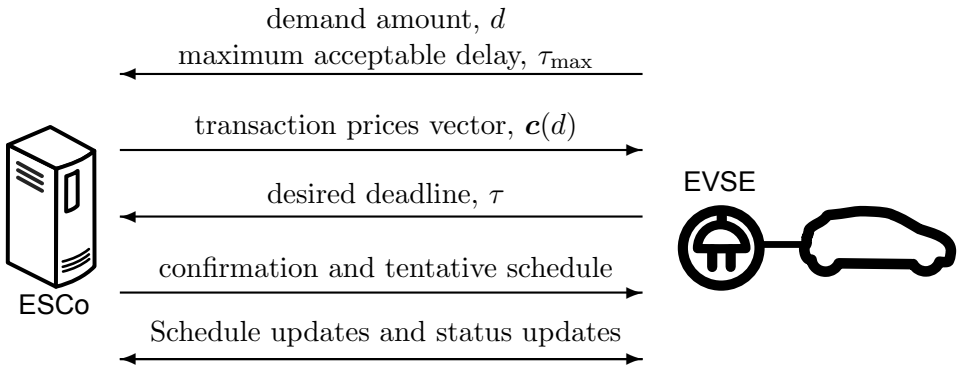

Figure 6.2: Interactions between a PEV and the ESCo.

Inspecting the LP Scheduler formulated in (6.11), the new arrival effectively translates to addition of $2\tau_{\max}$ variables and their corresponding constraints. In this setting, obtaining $c(d, \tau)$ is equivalent to adding more constraints to the problem enforcing the corresponding $x^e_{\tau'}$ (and consequently $x^r_{\tau'}$) to zero for $\tau' > \tau$; hence, $c(d, \tau) \geq c(d, \tau + 1)$. In other words, the more flexible the new user is, the less would be its energy delivery cost.

More generally, since the cost of initial state perturbation is directly reflected to the arriving user we can conclude that a rational incoming user has incentives that are aligned with the ESCo in minimizing its cost and hence desires the same decisions. This property of differential pricing addresses the admission control problem, another main issue with the flat pricing model discussed in [25]. As pointed out in [58], the cost of serving the new demand, d, approaches sd with increasing demand irrespective of demand flexibility and the demand will be left unserved due to congestion. This is because the total amount of demand approaches the maximum ultimate capacity of the

system, $\Delta t \sum_t C_t$. New arrivals have no way to respond to such a situation since flat prices do not reflect the system load level and the ESCo cannot reduce congestion by blocking users. An interesting property of transaction pricing is to reflect the effect of system load. Consequently, transaction pricing incentivizes the incoming users to join the system at the right time, preventing congestion and automatically and gracefully handling the admission control problem. In other words, the pricing dynamically combines market prices (as in dynamic pricing) and distribution level congestion cost.

The drawback of differential pricing for the ESCo is that, at least in this most simple form, the total amount collected from the new users and the cost of energy procurement (generation and transmission) in the market balance out, hence leaving the ESCo with almost no profit. We address this issue, by considering the total cost of energy delivery and including the distribution cost which roughly accounts for 20% to 40% of a typical residential electricity bill. By factoring in the gains to the distribution network, we assume that the ESCo gets 50% discount on the distribution network costs and collects it as profit. That is, the ESCo is able to potentially undercut competing retailers in the total delivered price to consumers, in part, because it guarantees to the distribution network provider that it will not overload distribution network capacity.

Similar to obtaining offer prices, energy delivery transaction pricing can be implemented in a computationally efficient manner. Although it seems that roughly $\tau_{\max}$ instances of (6.11) type problems should be solved in the

formation of each $\boldsymbol{c}(d)$ vector, the effective complexity of such instances are substantially reduced noticing that the solver can warm start from the current scheduler solution.

6.4 Simulation Results

Two sets of data is used for the simulations: A set of synthetic data, and another set based on the dataset introduced in Chapter 2.

6.4.1 Results Based on Synthetic Data

In order to evaluate EDTP, we considered a group of total 300 users randomly arriving according to a non-homogeneous Poisson process whose rate of arrival is proportional to market prices over 24 hours to simulate the effect of more arrivals at peak hours. Maximum deadlines are selected uniformly over 24 hours and upon joining the system, the user selects its deadline as the first one which achieves the minimum cost. Each user selects its demand uniformly over $[0, \frac{1}{2}\bar{x}_i(t_i^d - t_i^a)]$, half of user's maximum total capacity, taking into account that people typically expect their waiting time proportional to their demand and would not ask for an amount that is infeasible to receive. Market prices over the 24 hours are obtained from perturbing average ERCOT real-time market prices for the Houston zone over the 2009 year by Gaussian perturbations with standard deviation of roughly 10% of the average prices. Excess distribution network capacity is inversely affected by the general consumer demand. To model this effect, distribution network excess capacity is obtained by scaling

of the difference of a constant capacity and the estimated consumer demand, where the latter is estimated from market prices. To model different traffic scenarios, we scale distribution network capacity appropriately. Each scenario is run 10 times and the results are appropriately averaged for further statistical consistency.

We compare the performance of EDTP with the conventional consumption and opportunistic consumption. Conventional consumption, which is similar to immediate charging in PEVs, is defined as the setting in which an incoming load starts its consumption at its arrival time with its maximum rate and continues until its total demand is satisfied. Opportunistic consumers, on the other hand, optimally respond to real-time prices using the algorithm derived in Chapter 3. In order to obtain an upper bound on the performance of the opportunistic consumers, they are assumed to be subject to the same real-time prices on generation, transmission and distribution as the ESCo is, while *not* being constrained by distribution network capacity. Hence, opportunistic consumption is the best alternative users could have and the strongest competitor for EDTP. As will be shown, however, it occasionally results in overloads of the distribution system.

Table 6.2 summarizes our macro level results for the three load level scenarios we considered named as high, medium, and low load conditions corresponding to different total requested demand divided by the total (energy) capacity available to the ESCo, i.e., $\frac{\mathbf{1}^\top \tilde{\boldsymbol{d}}}{\Delta t \sum_t C_t}$.

Considering the total G&T cost for the ESCo, there is not much dif-

Table 6.2: Simulation results for EDTP, opportunistic and conventional methods based on synthetic load.

Scenario	Low Load	Med. Load	High Load
Total capacity (MWh)	31.05	20.7	13.8
Demand/Capacity ratio	31%	46%	72%
ESCo G&T cost	$182	$182	$224
Reserves offered by ESCo	78%	75%	36%
Average delay reduction	7.6%	7.8%	8.6%
Total G&T Cost (Opportunistic)	$229	$218	$226
Total over-capacity by opportunistic loads	0%	3%	20%
Peak over-capacity by opportunistic loads	0%	30%	96%
Total G&T (Conventional)	$317	$319	$317
Total over-capacity by conventional loads	2%	5%	11%
Peak over-capacity by conventional loads	43%	104%	233%

ference in the total cost between the low and medium load scenarios which is remarkable considering roughly 50% utilization factor of the distribution network capacity. As expected, the cost increases under heavy load as capacity becomes scarce; yet, we never encountered any unserved demand. In comparison, the ESCo keeps a relatively good margin, roughly 46% to 77% versus the conventional, and 1% to 20% versus opportunistic methods. There are two main reasons enabling the ESCo keep its margin despite working under distribution network constraints: First, its ability to sell back portions of its

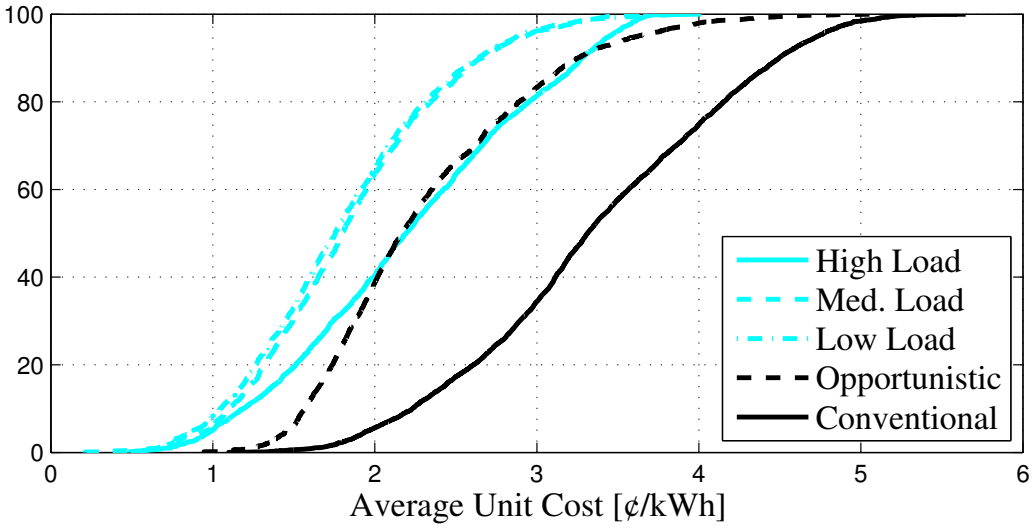

Figure 6.3: Empirical cumulative distribution function of unit costs experienced by users assuming synthetic demand patterns.

load as reserves and second, its ability to run centralized scheduling over the active users which leads to more efficient scheduling.

In order to get a more detailed view, let us consider Figure 6.3 where the empirical cumulative distribution function (CDF) of the unit cost experienced by users is depicted. Comparing EDTP and opportunistic consumption, at low and medium load levels, shows a uniform unit cost difference of roughly 0.4¢/kWh in average unit cost of 2¢/kWh (i.e. roughly 20%) in advantage of EDTP, demonstrated by the horizontal difference between the corresponding curves at different levels of the vertical axis. However, the competition gets very tight under the low capacity/high load regime. The shape of the CDF for heavy load conditions suggests that although there is moderate concentration at relatively low prices, the competition gets tight between EDTP

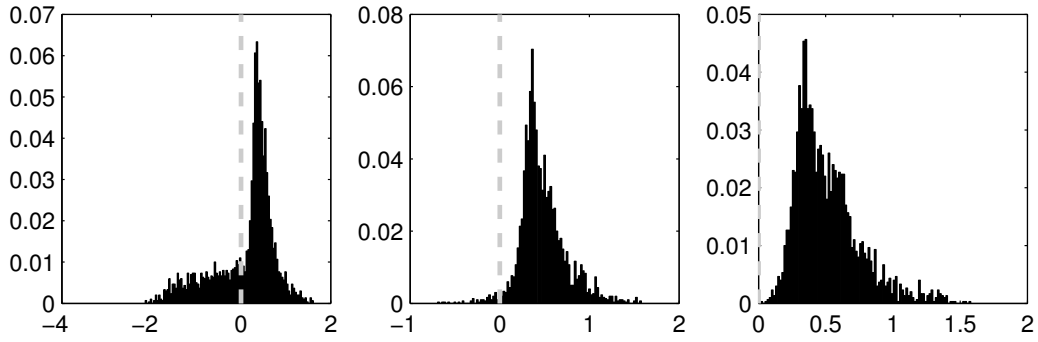

(a) High Load (b) Med. Load (c) Low Load

Figure 6.4: Histogram of unit cost differences between EDTP and opportunistic consumption, i.e. $\frac{\text{cost}^{\text{Opp}}-\text{cost}^{\text{EDTP}}}{d}$, in ¢/kWh, for synthetic demand patterns.

and opportunistic methods for a considerable portion of the users. To have a better comparison from users perspective, we analyzed the cost difference between opportunistic consumption and EDTP for each user and normalized it by the total energy demand of the user to obtain the users unit cost difference. Figure 6.4 provides a histogram of the unit cost advantage of EDTP whose formula is given in the caption of the figure. This figure gives a more vivid comparison of the two methods. More mass on the positive side of the horizontal axis basically means that more users will be happier with EDTP rather than opportunistic consumption. Unsurprisingly, as the load levels increase, EDTPs ability to offer better prices is reduced since it is subject to capacity constraints. Having in mind that high load levels happen are unlikely in well designed distribution networks, we conclude that EDTP is in fact very robust to capacity constraints and performs well even under heavy congestion.

Conventional and opportunistic consumers are insensitive to load level

as reflected in their total costs because these methods are oblivious to the distribution network capacity; that is, some consumption is at the expense of overloads in the distribution network. The total overcapacity load, served while the distribution feeder has been overloaded, can be as large as 11% for conventional and 20% for opportunistic loads, which essentially asserts the potential overreaction issues of exposing flexible demands to real-time prices. More concerning situations are observed in peak demand capacity violations. In conventional settings the overcapacity situation mostly happens at peak hours; however, in opportunistic settings, overcapacity situations happen during off-peak hours corresponding to lowest prices in the market as a result of overreaction to such prices.

The amount of reserves offered, which generally depends on distribution network capacity, load flexibility and reserve prices, is a key social value proposition for the ESCo's operation. Our results show that the ESCo can handle the flexibility of the demand quite well and offer up to 75% of the load back to the market as reserves. Moreover, as a consequence of positive correlation of the amount of offered reserves with reserve prices over time, these reserves are offered at the time they are needed most. Remarkably, even at high load settings, the ESCo manages to offer 40% of its load back while other methods only overload the capacity by 10%-20%.

We also analyzed how the offer vector provided by the ESCo is used by the users to do cost-comfort analysis and its impact on both parties. We have assumed that users choose the smallest deadline among the ones which give

the least cost. Interestingly, in many situations, minimum cost choice may not result in the maximum delay as the gains from more flexibility can become very marginal to the total schedule cost of the ESCo and consequently the cost offered to the user. This is exhibited at user level by the amount of delay reduction with respect to maximum delay allowed by the user. As shown in Table 6.2, roughly 8% delay reduction, compared to maximum allowed delay, is observed independent of the congestion level.

Although EDTP provides many benefits to the grid and distribution networks, its fate is ultimately decided by user adoption. For this matter, perhaps the number of users who benefit from adopting it is more important than their total cost reduction. Figure 6.3 illustrates the big picture showing the strong performance of EDTP, especially at medium to low congestion levels. We believe this advantage stems from offering reserves as the value of the advantage is roughly about the average price of the reserves in the market. A more detailed comparative view is given in Figure 6.4, where average normalized advantage of EDTP versus opportunistic consumption is depicted. Here we can particularly see the effect of capacity as it becomes scarce: More users are pushed to the negative tail of the distribution although the main concentration exhibits a steady 20% difference between the two since the average unit price is roughly 2¢/kWh from Figure 6.3 and the average difference in unit cost is about 0.4¢/kWh. However, it should be emphasized that the users in the negative tail typically correspond to cases where opportunistic consumption overloads the distribution system. That is, this apparent price

advantage of opportunistic consumption is not sustainable.

6.4.2 Results Based on PEV Energy Demand

In order to obtain more realistic results, particularly in case of PEVs, we repeated our numerical experiments with the PEV dataset we introduced in Chapter 2. We also used more recent ERCOT load and price data for the experiments presented here. In particular, we used the minutely total overall ERCOT load as the existing load in the system and obtained the base capacity available to the ESCo as the excess capacity left after subtracting this average existing load from a constant capacity of 120% of max average demand over the 24 hour period. This base capacity pattern is then scaled for the various level of load to obtain the target energy demand to capacity ratios presented in Table 6.3. With this method, we basically assumed that the pattern of the capacity available to the ESCo follows the constant capacity of the circuit minus the average existing system demand; consequently, we did not have to use prices as proxy to system demand as we did in the synthetic case. For prices, we used Houston Load Zone prices for energy and ERCOT wide REG prices for Ancillary Services, averaged over year 2012. To obtain symmetric REG price, we averaged REG UP and REG DN prices for each hour.

Similar to the previous section, the simulations were limited to a 24 hour arrival period with maximum 24 hour dwell time, to obtain PEV demand for such a profile, we randomly sampled the PEV charging request that would arise from a non-anticipative everywhere charging model and truncated their

maximum desired dwell time to 24 hours. It is worth pointing out that the maximum capacity of each load in the PEV based setup is set to 3.3kW, consistent with the capacity assumed in previous chapters, which is roughly one third of the capacity assumed under the synthetic demand model. Moreover, while the energy demand for the synthetic model was almost uniform, our observations show that the energy demand from PEVs has a non-uniform, almost exponential, empirical distribution. Finally, we have assume minimum dwell time of two hours.

For each high, medium and low load scenario, similarly defined as in the synthetic case, the model is run 160 times and the average results are presented in Table 6.3, in a similar format as in Table 6.2. Similar to the synthetic demand case, each scenario consisted of 300 users with their arrivals following the arrivals of PEVs. The prices in each scenario are obtained from perturbing average ERCOT prices as discussed above by Gaussian perturbations with standard deviation of roughly 10% of the average prices. Similar to the synthetic case, and in line with the previous chapters, we compare the performance of EDTP with the conventional consumption and opportunistic consumption.

Table 6.3 compares the performance of EDTP with opportunistic and conventional consumption. As previously observed, EDTP adapts to tight network constraints very well and its total cost is not heavily affected by the level of load, about 10% change in cost for 40% change in demand to capacity ratio. In other words, EDTP packs the flexible loads pretty efficiently. More-

Table 6.3: Simulation results for EDTP, opportunistic and conventional methods based on PEV induced demand.

Scenario	Low Load	Med. Load	High Load
Total capacity (MWh)	4.6	2.8	2
Demand/Capacity ratio	30%	50%	70%
ESCo G&T cost	\$96	\$102	\$106
Reserves offered by ESCo	75%	74%	50%
Average delay reduction	15.0%	16.7%	19.0%
Total G&T Cost (Opportunistic)	\$109	\$109	\$109
Total over-capacity by opportunistic loads	5%	16%	23%
Peak over-capacity by opportunistic loads	60%	200%	269%
Total G&T (Conventional)	\$120	\$120	\$120
Total over-capacity by conventional loads	0%	8%	17%
Peak over-capacity by conventional loads	32%	111%	205%

over, the total cost remains below the best total cost achievable to energy only methods even in higher load levels. That is, EDTP outperforms opportunistic consumption in terms of total cost, which is mainly due to the gains from offering ancillary services. In fact, considering the percentage of load offered back as AS, which varies between 50% to 75%, the cost performance of EDTP comes as no surprise. This significant amount of load offered as AS also strengthens the benefits of EDTP versus other methods. The third main advantage of EDTP shows itself comparing the overcapacity consumptions of

the aggregated demand. In particular, it is observed that the cost advantage of opportunistic consumption vs. conventional consumption, which is roughly 10%, comes at the cost of increased overcapacity consumption, roughly 1.5 to 2 times both on average and at peak. Note that EDTP always observes the capacity constraints and hence no overcapacity is observed. In fact, since EDTP typically reserves some capacity for AS provision, its consumption is typically below the full network capacity. So, as concluded before, EDTP presents a strong case for managing load in the overall sense.

In comparison with the results based on synthetic load data, as presented in Table 6.2, first we observe that the general trend of EDTP's performance advantage is maintained. Although it may appear that the total costs are drastically changed, it should be noted that this change is mainly due to the reduced total energy load, rather than the change in demand patterns. To observe this, note the reduced total capacity available at each load level, which is almost six times. Also, less importantly, the change in the base prices in the two cases contributes to the change in absolute values of total cost. Overall, we conclude that the results in the two cases are consistent while EDTP shows slightly higher advantage for the PEV users.

EDTP is designed to attract users to the ESCo's program and address incentive compatibility issues in coordinated energy management. To evaluate its success in this goal, we need to compare the cost offered to the users. As expected, the reduction in total cost may not be uniformly passed down to the users due to their diverse preferences and demands. Similar to the pre-

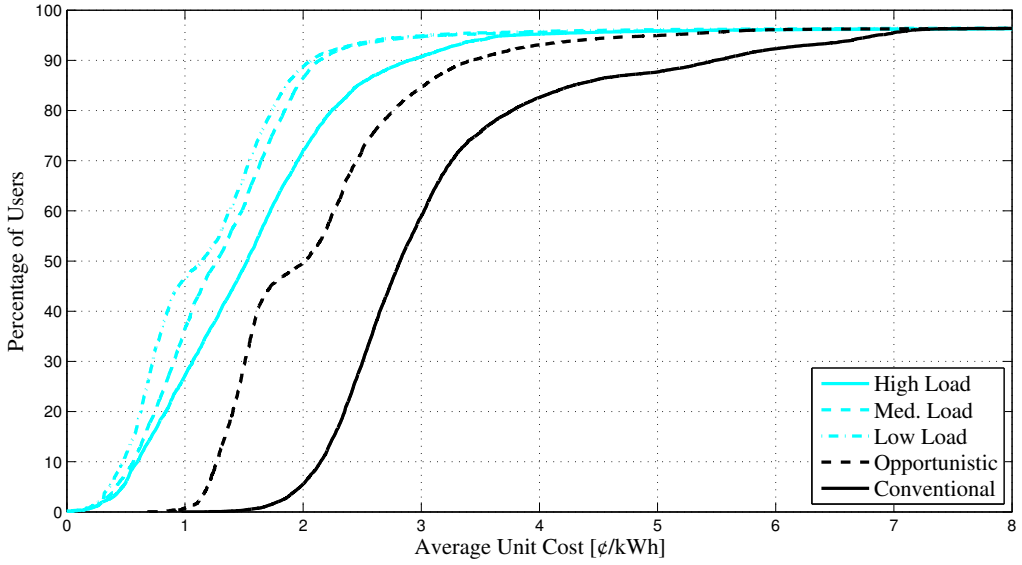

Figure 6.5: Empirical cumulative distribution function of unit costs experienced by PEV users.

vious section, we have used empirical CDF of the unit cost to the users and the histogram of unit cost advantage of EDTP versus opportunistic consumption. Figure 6.5 and Figure 6.6 present our results on these two measures. As observed before, Figure 6.5 shows a considerable cost advantage in favor of EDTP, demonstrated by the horizontal difference between the corresponding curves at different levels of the vertical axis, and as the capacity gets tighter, this cost advantage diminishes. An interesting observation is the comparison between the empirical distribution of the low load case and the opportunistic case which shows the same change pattern and almost a uniform horizontal difference. Interestingly, this pattern goes away as the capacity gets tighter. We believe that the pattern is induced by the prices, and basically the signifi-

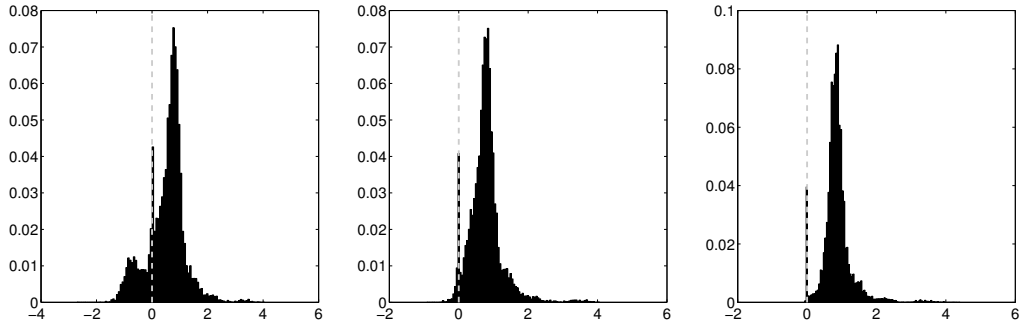

(a) High Load (b) Med. Load (c) Low Load

Figure 6.6: Histogram of unit cost differences between EDTP and opportunistic consumption, i.e. $\frac{\text{cost}^{\text{Opp}} - \text{cost}^{\text{EDTP}}}{d}$, in ¢/kWh, for PEV users.

cant cost difference between consumption in on-peak hours and off-peak hours. The similarity between low load curve and opportunistic curve shows that the total capacity constraint of the network does not heavily constrain the overall schedule under low load situations. Consequently, similar load patterns should be expected under EDTP and opportunistic consumption and the cost difference, demonstrated by the horizontal difference between the curves, is mainly due to the added value of AS provision. As the load level is increased, the effect of network constraint becomes more pronounced and we see a complete change in the empirical CDF in the high load regime.

The unit cost advantage of EDTP versus opportunistic consumption, as depicted in Figure 6.6, shows that for most PEV users, EDTP offers superior costs particularly at low and medium load levels. We believe that the users who prefer opportunistic consumption at high loads are mainly the ones that cause distribution network overloads and since EDTP pushes them to other

hours, they are essentially subject to an increased cost to comply with network constraints. For these particular users, the benefits of AS provision is not large enough to compensate for the change in cost induced by their shifted load.

In comparison with Figure 6.4, Figure 6.6 shows higher advantages for EDTP, roughly about two times. This observation suggests that PEV demand patterns are more fitting to the EDTP scheduling structure and hence PEV users would be more inclined to EDTP based programs. This is a very positive result since it translates to EDTP's ability to incentivizes PEV owners to subscribe to programs that are more advantageous to the rest of the power system without adding much more complexity.

6.5 Conclusion

In order to address the need for incentive revealing schemes to ensure successful implementation of coordinated energy delivery solutions for flexible and delay-tolerant loads, we took a fresh look at the problem by viewing the complete process of delivering the requested energy to a load over time as a single transaction. This approach helped us propose a natural dynamic pricing scheme for such transactions which provides efficient incentives to the users as well as substantial benefits to the grid and distribution network. We showed that Energy Delivery Transaction Pricing not only reduces the total cost of energy delivery compared to optimal response to real-time prices, but also, provided with moderate distribution network capacity, gives a roughly 20% better unit cost for most users and very few may actually find it not beneficial.

Such gains are provided to the users while the ESCo protects distribution feeder from overloading and offers roughly 75% of the load back to the market as reserves.

Chapter 7

Scheduling Flexible Loads for Ancillary Service Provision in Multi-settlement Electricity Markets

7.1 Introduction

Demand flexibility is one of the key enablers of demand response. Flexible loads, i.e. loads not bound to a specific instantaneous power consumption trajectory, comprise a considerable portion of the current load and are hence potential demand response providers. Moreover, plug-in electric vehicle (PEV) charging, which is projected to be a considerable future load, has shown to be very flexible [56]. This flexibility not only enables displacement of electric energy consumption by flexible loads to the time when it is more abundant and hence cheaper, but also helps counterbalance the intermittency and uncertainty of renewable sources, should the proper communication, control and service infrastructure be in place. Furthermore, flexibility can be used to match renewable generation to maximize its utilization without need for expensive storage.

Utilizing demand flexibility and instigating demand response, however, is a challenging task. As restructured electricity markets become standard

in the US and around the world, economy becomes the main driver of supply demand balance. However, a considerable portion of flexible demand has been shielded from market prices through utilities and Retail Energy Provider Companies (REPCo) for technical and non-technical reasons. The major infrastructure challenges, i.e. fine grained measurement of consumption over time and communication of prices to the consumer, are being addressed by smart grids and other innovative communication mechanisms like OpenADR [101]. However, new services should be offered over this infrastructure to enable full utilization of demand side assets. Due to the diversity in flexible loads and their preferences, as discussed in Chapter 6, common pricing of electricity such as Time of Use (ToU) and dynamic pricing cannot fully utilize the potential of flexible loads and may result in undesired behavior at network level, as demonstrated in Chapter 3.

In this context, an Energy Services Company (ESCo) or Load Aggregator (LA), which can be a part of a REPCo, can orchestrate flexible demands and aggregate them to a level that can participate in the electricity market at the wholesale level. The motivation for such organization of flexible loads goes beyond facilitation of operations and market participation to more control on the aggregate level load, avoiding distribution network (DN) congestion, and enabling provision of Ancillary Services (AS) in a reliable manner, which is required by most Independent System Operators (ISO) as a part of market rules. Ancillary Services, and particularly frequency regulation service (REG), are basically reserves provisioned by the system operator to cover supply-demand

imbalances and maintain system stability. By modulating the instantaneous consumption of a large enough group of flexible loads, the LA can operate flexible loads as a REG provider while they are actually net consumers.

Aggregating flexible loads by the LA, however, is a technically challenging problem due to the wholesale market structure and inherent uncertainties in the process. Most wholesale electricity markets are organized in a multi-settlement fashion [21, 52, 70, 77, 84, 99] with at least two stages: The forward stage, which we refer to as the day-ahead market (DAM), plays an operations planning role. It is also where the reserves and unit commitment decisions are usually made, in co-optimization with energy decisions, to ensure reliable operation of the grid. Most markets also incorporate a "real-time" market (RTM), acting as a recourse stage, which is usually implemented as an adjustment market.

The DAM is usually cleared hours before the actual operation time, when information about flexible loads is available. Although LA can solely participate in the RTM for energy purchases, offering AS usually requires participating in the DAM. Moreover, participating in DAM can potentially result in better total costs of energy to LA, if it can buy energy at a lower cost. On the other hand, making day-ahead commitments are challenging as there are various uncertainties faced by the LA in real-time in addition to load arrivals and departures, including changes in real-time prices and distribution network congestion situation.

Scheduling and participation in multi-settlement markets have been

studied by many authors in the past and using various approaches. The major part of the past work [10, 29, 54, 78, 109, 111, 112] has focused on the strategic behavior of generation entities and firm resources in multi-settlement markets and how various aspects, like risk, offering ancillary services and market rules affect the results. Various approaches have been taken by the authors, from Supply Function Equilibria (SFE) [10, 78] methods to simulation based approaches [112]. However, optimal participation of collections of demand side resources in multi-settlement markets is much more challenging and is not studied as extensively. One the most challenging aspects, from the perspective of this work, is the uncertainty in availability of resources which would add a technically challenging dimension to the problem.

Caramanis and Foster [26] and [23] take an aggregation based approach and hypothesize that only the total purchases of energy and sales of AS for each group of users with the same deadline needs to be tracked and scheduled and an optimal algorithm to distribute the optimal totals among the flexible resources can be found. Using this assumption and focusing on PEVs, they model the multi-settlement market consisting of a day-ahead and an hour-ahead market and consider the interaction between various entities in the market. They particularly aim at modeling the decision problem faced by the Load Aggregator, which is obtaining optimal bids for energy and reserves in both markets. They propose a stochastic dynamic programming formulation for this problem and discuss its extension to other classes of flexible loads like HVAC systems. They, however, do not discuss tractability of their model

and have not shown any numerical results as to how their model performs should approximate techniques be used to tractably solve the problem. In their follow up work [24], the authors suggest modifications to the market structure to enable better integration of flexible loads in the multi-settlement market by opening the possibility of complex bids.

Jin *et al.* [53] propose a scheduling model for co-optimizing PEV load and energy storage in a multi-settlement market as well as a communication infrastructure model to support their scheduling algorithm. They show that their model admits a mixed integer linear program and propose a heuristic method to tackle its tractability which is essentially rounding a continuous relaxation of the original problem. They study the performance of their model through simulation and show major reduction in total cost by optimal scheduling compared to uncontrolled charging. Moreover, they show that the loss of performance due to their heuristic solution to the mixed integer program is acceptable. The major shortcoming of their work, however, is adopting a deterministic model and resorting to the flexibility of the energy storage asset to tackle the uncertainties faced by the system.

Subramanian *et al.* [95] consider the problem of a "Cluster Manager (CM)" (i.e. Load Aggregator) which participates in a two stage market. The CM has to satisfy the demand of a group of flexible and non-flexible loads by purchasing energy on their behalf in the market and has access to an intermittent cheap generation asset (e.g. a wind farm). Unlike typical models, they also assume that the CM has to *buy* reserve capacity to cover its de-

viations from its base points cleared in the market. They aim at obtaining cost minimizing decisions for bulk energy and reserve purchases in the day-ahead market. They present their results for the case of fully flexible loads and non-flexible loads. They obtain the optimal energy purchase policies for the two cases by solving the dynamic programming problem resulting from their model. Besides the fact that their model does not match the established market rules in terms of reserve provision, their theoretical results apply only to extreme cases they consider, i.e. the fully flexible loads and non-flexible loads. While providing some insight into the nature of the problem, the simplifying assumptions in studying the two extreme cases limit the applicability of the model by relaxing essential constraints in the model. Consequently, it is hard to generalize the result or numerically evaluate the performance of the full model using the presented results.

Al-Awami and Sortomme [5], similar to the work presented here, approach the problem of optimal decisions in DAM and RTM using stochastic programming. However, they differ from our work in that they assume availability of multiple generation resources, both intermittent and firm, to the load aggregator and do not consider the possibility of AS provision by the flexible loads, nor the distribution network constraints that the load aggregator might be subject to. They also factor in the trading risk between DAM and RTM by adding a conditional value at risk term to their objective. Their model results in a stochastic mixed integer linear program which they solve using CPLEX. Their model, however, captures uncertainty only in wind production scenar-

ios and assumes PEV demand is known. Therefore, their scenario generation technique is completely different from what is presented here. Their results only show modest gains from coordination, about 3% improvement in total cost. Unsurprisingly, their results show that including risk in their objective improves the Conditional Value at Risk (CVaR) measure substantially.

In this chapter, we extend the work in Chapter 6 and [58] and propose a model focused on the challenges in capturing the uncertainties in flexible loads, particularly PEV loads, in a systematic way. The first contribution of this work is to propose a stochastic programming approach that fits well with the multi-settlement structure of the market and provides a realistic scheduling mechanism for implementation by the load aggregators. The proposed scenario generation technique which can handle heterogeneous scenarios is the second main contribution of this work.

The rest of this chapter is organized as follows: In Section 7.2 we introduce our system model. In Section 7.3 we present our formulation for the planning method for DAM scheduling and our proposed scenario generation technique. In Section 7.4 we analyze the performance of the proposed stochastic programming approach through numerical simulation. Finally, in Section 7.5 we conclude and discuss our future directions.

7.2 System Model

To fully utilize the demand response potential of flexible loads, a systematic approach should be adopted for market participation and load schedul-

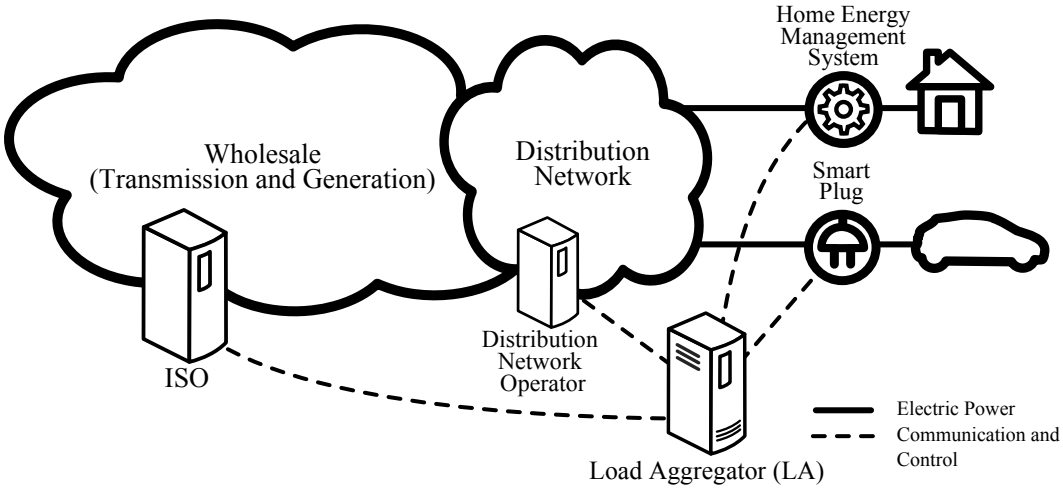

Figure 7.1: Interactions of the Load Aggregator (LA) with other entities.

ing by the LA. This is the problem we tackle in this chapter by proposing a model for the decision problem faced by the LA in the context of a multi-settlement electricity market. To this end, similar to Chapter 6, we assume a general information and power flow architecture which can be implemented on smart grids or even independently. As illustrated in Figure 7.1, we assume the LA communicating with the ISO for wholesale related operations, namely bidding in the DAM and RTM for purchasing energy and offering AS as well as other wholesale level information. The LA also communicates with the distribution network operator to ensure feasibility of energy transfers and AS services scheduled without overloading the network. Finally, the LA communicates with the flexible loads to gather their energy requests and preferences and implement the energy delivery schedule and AS deployment commands. The LA is assumed to participate in both DAM and RTM as a price taker,

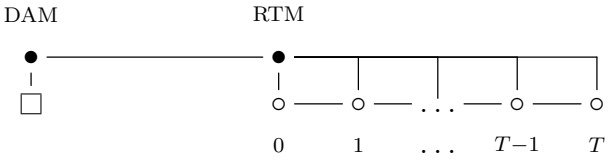

Figure 7.2: Decision time-line and stages.

i.e. its decisions will not affect the prices.

The multi-settlement structure of the market calls for two main stages for decision making, namely day-ahead and real-time. Day-ahead decisions consist of bids for total energy purchased and offers for reserves for every interval, usually an hour, in the following day. The decision problem faced in real-time, however, has a multi-stage structure itself, i.e. at every interval, which is usually five to fifteen minutes long, the LA should decide its bids for energy, and reserves, should there be a real-time market for reserves.[1] Moreover, the LA should decide the amount of energy transferred to each flexible load as well as the portion of reserves provided by it at every real-time stage. These decisions are subject to distribution network constraints and individual load capacity constraints. Figure 7.2 depicts the decision time-line where the square corresponds to the day-ahead decisions and the circles denote the decisions made at each real-time stage and T denotes the number of real-time stages considered by the LA.

Let us first introduce our notation. We denote the arrival time, depar-

[1]In RTM, the bids might be only allowed to change once every couple of intervals, e.g. once every hour, although the market is run for every interval, e.g. 5 minutes.

ture time/deadline and electric demand of each flexible load, e.g. a plug-in electric vehicle (PEV), by t_i^a, t_i^d and d_i respectively where $i \in I$ is the set of flexible loads. We assume that the ESCo has to supply the flexible load its desired demand, d_i, up to the given deadline at some pre-negotiated rate and any shortfall in the energy delivery is penalized at s^{EV} \$/kWh, which can be seen as a proxy for price of gasoline in case of plug-in hybrid electric vehicles (PHEV) like Chevy Volt. We further assume that the instantaneous rate of energy delivered to each load can be varied continuously between zero and $\bar{x}_i$. In other words, each load is assumed to have an individual capacity of $\bar{x}_i$ kW. In case of a PEV, t_i^d denotes the desired departure time, d_i can be the depleted capacity of the EV battery and $\bar{x}_i$ represents the Electric Vehicle Supply Equipment (EVSE) capacity.

For simplicity, we assume a single feeder which we model to a single capacity limited element. We denote *excess capacity* of this element by C_t. As will be discussed later, our method can be extended for handling more sophisticated radial distribution networks as well as multi-feeder setups, where feeders are all in the same load hub.

Participation in DAM and RTM has a very different nature in the sense that DAM is a forward market whose corresponding decisions are made without the exact knowledge of the flexible loads availability and demand. Moreover, only the aggregate amount of power needed for serving flexible load is to be decided. Finally, the time resolution in DAM is usually different from RTM (e.g. 1 hour vs. 5 minutes in ERCOT). This implies that the decisions

made for DAM should be good for multiple market intervals in RTM. We denote the DAM and RTM interval lengths by Δt^{DA} and Δt^{RT}, respectively. For simplicity, we assume $m = \frac{\Delta t^{\mathrm{DA}}}{\Delta t^{\mathrm{RT}}}$ to be an integer. Since we are assuming all the loads under the same bus, from the bulk power system perspective, we only have to consider a single set of energy and reserves, in particular regulation, prices. Since our focus here is to address the coupling between DAM and RTM, we assume that the ESCo participates in the market as a price taker and does not focus on optimal bidding. That is, unlike our previous work in Chapter 6 and [58], the ESCo estimates prices for DAM and forms its offers based on its marginal penalty (s^{EV}). We denote the DAM predicted prices for energy and reserves by $p_t^{e,\mathrm{DA}}$ and $p_t^{r,\mathrm{DA}}$ respectively. In RTM, we assume that the ESCo is only allowed to purchase or sell energy, whose price is denoted by $p_t^{e,\mathrm{RT}}$. We assume only statistical information of the real-time prices are available to the ESCo.

The multi-settlement setup of the market implies two main set of decisions to be made by the ESCo. In DAM, the ESCo should decide amounts of total energy to purchase and reserves to sell for each time interval, which we denote by $x_t^{e,\mathrm{DA}}$ and $x_t^{r,\mathrm{DA}}$ respectively. In real-time operation, in contrast, amount of energy to be delivered to each load as well the share of the committed AS is to be decided besides the amount of purchases/sales of energy to achieve a balanced schedule.

7.3 Scheduling in Multi-settlement Electricity Markets

7.3.1 Participation in the Day-Ahead Market (DAM)

To address the day-ahead decisions, we adopt a stochastic optimization model in accordance with the two stage structure of the problem. Our first stage planning decisions consist of the quantities of energy purchased and reserves offered in the day-ahead market. These decisions are used as nominal values for total energy consumption and reserves offered in the recourse stage, i.e. real-time. Constructing the recourse expected cost, as a function of the planning stage decisions, however, is a challenging problem since the recourse is a multi-stage problem itself. Moreover, in practice, only historical sample information is available about load availability and demand amount, rather than their distribution and patterns.

We formulate the DAM planning problem as follows:

$$\begin{aligned} \min_{\boldsymbol{x}^{e,\mathrm{DA}},\boldsymbol{x}^{r,\mathrm{DA}}} \quad & (\boldsymbol{p}^{e,\mathrm{DA}}\boldsymbol{x}^{e,\mathrm{DA}} - \boldsymbol{p}_t^{r,\mathrm{DA}}\boldsymbol{x}^{e,\mathrm{DA}})\Delta t^{\mathrm{DA}} + \mathbb{E}_\xi[h(\boldsymbol{x}^{\mathrm{DA}},\xi)] \\ \text{st.} \quad & \boldsymbol{x}^{e,\mathrm{DA}}, \boldsymbol{x}^{r,\mathrm{DA}} \geq 0, \\ & \mathbf{1}_{|T^{\mathrm{DA}}|}^{\top}\boldsymbol{x}^{e,\mathrm{DA}} \leq \overline{x}^{e,\mathrm{DA}}, \end{aligned} \tag{7.1}$$

where:

- Vectorization is done with respect to the DAM time index, $t \in T^{\mathrm{DA}}$;
- T^{DA} is the set of DAM time indices;
- $\boldsymbol{p}^{e,\mathrm{DA}}$, $\boldsymbol{p}^{r,\mathrm{DA}}$ represent the expected day-ahead prices for energy and regulation in a row vector format;
- $\mathbf{1}_n$ denotes the column vector of all ones with length n;

- $|A|$ denotes the number of elements of set A;
- $\boldsymbol{x}^{\mathrm{DA}} = (\boldsymbol{x}^{e,\mathrm{DA}}, \boldsymbol{x}^{r,\mathrm{DA}})$;
- $\xi \in \Xi$ is the random variable indexing different potential scenarios;
- Ξ is the scenario set;
- $\overline{\boldsymbol{x}}^{e,\mathrm{DA}}$, the upper bound on the total DAM energy purchases;
- Δt^{DA} is the time interval length for the DA market;
- $h(\boldsymbol{x}^{\mathrm{DA}}, \xi)$ is the optimal objective of the real-time (RT) problem.

The upper bound on the total energy purchases in DAM, $\overline{\boldsymbol{x}}^{e,\mathrm{DA}}$, is added as a regulatory constraint to decrease the scheduler's tendency towards DAM-RTM trading and arbitrage, particularly because risk is not directly modeled in this formulation. In this work we have set $\overline{\boldsymbol{x}}^{e,\mathrm{DA}}$ to $\min_{\xi} \sum_{i \in I_\xi} d_{i,\xi}$, that is, the ESCo is required not to buy more energy in DAM than it almost surely is going to consume. We will comment on this constraint later in this chapter.

In the recourse stage, the LA actually serves the PEVs and responds to the regulation signal dispatched by the ISO. The impact of the planning stage decision on this stage is the total amount of energy purchased in DAM (at DA price) and the regulation commitments. Hence, we have the following

problem in recourse (not considering the bidding process):

$$
\begin{aligned}
h(\boldsymbol{x}^{\mathrm{DA}}, \xi) = \min_{\boldsymbol{x}^{e,\mathrm{RT}}_{i,\xi}, \boldsymbol{x}^{r,\mathrm{RT}}_{i,\xi}} & \boldsymbol{p}^{e,RT}_{\xi}(\boldsymbol{x}^{e,\mathrm{RT}}_{\xi} - M\boldsymbol{x}^{e,\mathrm{DA}})\Delta t^{\mathrm{RT}} \\
& + s^{\mathrm{AS}}\Delta t^{\mathrm{RT}}\mathbf{1}^{\top}_{|T^{\mathrm{RT}}|}(M\boldsymbol{x}^{r,\mathrm{DA}} - \boldsymbol{x}^{r,\mathrm{RT}}_{\xi})^{+} \\
& + s^{\mathrm{EV}}\sum_{i\in I_{\xi}}(d_{i,\xi} - \Delta t^{\mathrm{RT}}\mathbf{1}^{\top}_{|T^{\mathrm{RT,EV}}|}\boldsymbol{x}^{e,\mathrm{RT}}_{i,\xi}) && (7.2) \\
\text{st.} \quad & \boldsymbol{x}^{e,\mathrm{RT}}_{\xi} = W_{\xi}\sum_{i\in I_{\xi}}\boldsymbol{x}^{e,\mathrm{RT}}_{i,\xi}, && (7.3) \\
& \boldsymbol{x}^{r,\mathrm{RT}}_{\xi} = W_{\xi}\sum_{i}\boldsymbol{x}^{r,\mathrm{RT}}_{i,\xi}, && (7.4) \\
& \boldsymbol{x}^{e,\mathrm{RT}}_{\xi} + \boldsymbol{x}^{r,\mathrm{RT}}_{\xi} \leq \boldsymbol{C}_{\xi} && (7.5) \\
& \boldsymbol{x}^{e,\mathrm{RT}}_{i,\xi} + \boldsymbol{x}^{r,\mathrm{RT}}_{i,\xi} \leq \overline{\boldsymbol{x}}_{i,\xi}, \qquad \forall i \in I_{\xi}, && (7.6) \\
& \boldsymbol{x}^{r,\mathrm{RT}}_{i,\xi} \leq \boldsymbol{x}^{e,\mathrm{RT}}_{i,\xi}, \qquad \forall i \in I_{\xi}, && (7.7) \\
& \Delta t^{\mathrm{RT}}\mathbf{1}^{\top}_{|T^{\mathrm{RT}}|}\boldsymbol{x}^{e,\mathrm{RT}}_{i,\xi} \leq d_{i,\xi}, \qquad \forall i \in I_{\xi}, && (7.8) \\
& x^{e,\mathrm{RT}}_{\tau,i,\xi} = 0, \qquad \forall \tau \notin [t^{a}_{i,\xi}, t^{d}_{i,\xi}), i \in I_{\xi}, && (7.9) \\
& \boldsymbol{x}^{e}_{i,\xi}, \boldsymbol{x}^{r}_{i,\xi} \geq 0, \qquad \forall i \in I_{\xi}, && (7.10)
\end{aligned}
$$

where:

- Vectorization is done with respect to the RTM time index, τ, $\tau \in T^{\mathrm{RT}}$;
- T^{RT} denotes the set of RTM time indices (as seen in the planning stage) for all variables except the ones that are indexed by i, the PEV index, for which, $\tau \in T^{\mathrm{RT,EV}}_{\xi} = [\min\{T^{\mathrm{RT}}\}, \max_i t^{d}_{i,\xi} - \min\{T^{\mathrm{RT}}\}]$;
- I_{ξ} is the PEV index set for scenario ξ;

- M is the time synchronization matrix between markets which is defined as:

$$M = \boldsymbol{I}_{|T^{\mathrm{DA}}|} \otimes \mathbf{1}_m; \tag{7.11}$$

- $m = {}^{\Delta t^{\mathrm{DA}}}/_{\Delta t^{\mathrm{RT}}}$ as defined previously;
- $\boldsymbol{I}_n$ denotes the $n \times n$ identity matrix;
- $\otimes$ denotes Kronecker product;
- $\boldsymbol{p}_{\xi}^{e,RT}$ is the real-time price of electricity in row format;
- s^{AS} captures the penalty for unsatisfied regulation commitment;
- s^{EV} captures the penalty for the unserved EV demand;
- Δt^{RT} is the period of the real-time market;
- $\boldsymbol{C}_{\xi}$ represents the excess capacity of the distribution network available for charging;
- $t^a_{i,\xi}, t^d_{i,\xi}, d_{i,\xi}, \overline{\boldsymbol{x}}_{i,\xi}$ represent arrival time, departure time, energy demand and EVSE capacity for each vehicle;
- W_{ξ} is the time wrapping matrix, defined as:

$$W_{\xi} = \mathrm{cols}(\mathbf{1}^{\top}_{\lceil \frac{|T^{\mathrm{RT,EV}}_{\xi}|}{|T^{\mathrm{RT}}|} \rceil} \otimes \boldsymbol{I}_{|T^{\mathrm{RT}}|}, [1, |T^{\mathrm{RT,EV}}_{\xi}|]); \tag{7.12}$$

- $\mathrm{cols}(M, A)$ denoted the columns of M whose indices appear in set A;

W_{ξ} is essentially a horizontal repetition of the identity matrix with width truncated to $|T^{\mathrm{RT,EV}}_{\xi}|$. The main purpose of using this time wrapping

matrix is to give the optimization problem a consistent rolling view of time. Time wrapping basically wraps the time line of each of the PEVs back in T^{RT} range. Let us elaborate on time wrapping by going through an example. Consider a PEV that arrives at 5pm and leaves at 8am next day. Assuming $\Delta t^{\mathrm{DA}} = 1\mathrm{hr}$ and $\Delta t^{\mathrm{RT}} = 15\mathrm{min}$ with a 24 hour planning horizon, the time span of the PEV stay goes beyond the planning horizon for a particular day. However, when time wrapped, the period between 12am to 8am is mapped back to the same period in the problem's time span, as if some other PEV has previously started at 5pm yesterday and is finishing today at 8am. In other words, time wrapping folds individual PEV time lines and aligns them to the DAM and RTM time windows.

As discussed, constraints (7.3) and (7.4) define the time wrapped total energy and AS variables, $\boldsymbol{x}_{\xi}^{e,\mathrm{RT}}$, $\boldsymbol{x}_{\xi}^{r,\mathrm{RT}}$. Constraint (7.5) ensures that total PEV energy consumption and head room reserved for REG down remain below distribution network capacity. Constraint (7.6) ensures individual PEV capacity limits of EVSE are similarly observed. Constraint (7.7) guarantees feasibility of down REG. Constraint (7.8) prevents over-satisfaction of individual PEVs. Constraint (7.9) ensures that energy can be consumed only over the availability window of the PEV. Finally, constraint (7.10) ensures unidirectional flow of power, i.e. no-V2G.

There are a couple of parameters that are potentially different in each scenario. We overload ξ to represent the particular realization of these param-

eters as:

$$\xi = (\boldsymbol{p}_{\xi}^{e,RT}, \boldsymbol{C}_{\xi}, \{(t_{i,\xi}^{a}, t_{i,\xi}^{d}, d_{i,\xi}, \overline{\boldsymbol{x}}_{i,\xi}) | i \in I_{\xi}\}). \tag{7.13}$$

That is, we can have uncertainty in real-time prices, (excess) distribution network capacity, and the PEV parameter set which includes demand arrivals, departures, amount of energy requested by each EV and its EVSE capacity. Consequently, each scenario has a realization of all of the above parameters. Note that the parameters in the above triplet is a set, whose size, namely the number of PEVs, is scenario dependent and hence imposes a challenge in forming the distribution needed for scenario generation.

7.3.2 Participation in the Real-Time Market (RTM)

The stochastic program proposed above results in DAM market positions, $\boldsymbol{x}^{\mathrm{DA}}$. In real-time however, the ESCo faces another multi stage problem as the PEVs show up and prices change. The problem in real-time, however, is very similar to the problem we studied in Chapter 6 and [58]. Therefore, we skip further treatment of the real time decision problem for the sake of brevity and to keep our focus on the effect of DAM planning on the overall cost faced by the ESCo.

7.3.3 Scenario Generation

In this subsection we introduce how we obtain the expected value in (7.1) by discussing our scenario generation approach. The major challenge in obtaining scenarios, which are essentially realizations of (7.13) is the third

element of it, which is the set of PEVs and their demands. Generating scenarios for time series data, i.e. prices and distributions network capacity, has been studied in the past, e.g. [81], [80] and the references within. So the main challenge is generating good scenarios for the group of PEVs.

Generating PEV scenarios has a couple of challenging aspects: First, the number of PEVs in each group can be different and hence, the size of each scenario is different. This makes finding a proper probability distribution function rather challenging. Second, the arrival, departure and demand process of the PEVs may have hidden correlations that might be hard to capture by tractable probability distributions. As discussed in earlier chapters, user preferences can be very diverse and capturing the non-stationary and time and location dependent behavior of the users is a challenging problem.

To address these issues, we propose data driven method based on subsetting and sampling for scenario generation. The main motivation here is that the ESCo has access to all the realized charging sessions for PEVs subscribing to its programs at different locations. Using this dataset, similar to what we used in the previous chapters, the ESCo first subsets the dataset to obtain the *relevant* data subset, e.g. by time and/or location. Then based on the probability distribution of the number of users in each scenario, it decides the number of users in each scenario. Note that forming a distribution function for the number of users expected to arrive over each day is relatively straightforward. Then, for each scenario ξ, given the $|I_\xi|$, the ESCo picks $|I_\xi|$ samples from the relevant dataset with uniform probability. Alternatively, this

method uniformly picks a subset of the relevant set with size $|I_\xi|$. Finally, the probability assigned to each of the scenarios is set to $\frac{1}{|\Xi|}$.

The main advantage of the proposed scenario generation method is simplicity and the fact that it does not need to form the distribution functions (empirical or parametric) from the data and then sample them for scenario generation. This would be particularly challenging since the correlation between various aspects of the loads and their potential correlation with each other would be hard to capture. Moreover the dimensionality of the joint distributions does not pose an issue in the proposed method.

The major downside of the proposed scenario generation method, however, is inability in capturing low probability tail scenarios. We do not believe that this would pose an issue in our case since rare behavior patterns can only minimally affect the bulk transactions in DAM and the ESCo usually has an adequate amount of flexibility in recourse.

7.4 Performance Analysis

To establish the effectiveness of our proposed method, we measure the cost reductions compared to various localized charging policies through simulation. We also measure the amount of reserves offered by the LA and their reliability in terms of deviations of reserves offered in real-time from day-ahead offers. Finally, we study the aggregate load to measure the distribution level impacts of our proposed method.

To generate the simulation model and furnish it with data, we use the transportation induced PEV dataset we introduced in Chapter 2, similar to Chapter 6, where we use ERCOT prices for Houston load zone as our reference prices, ERCOT's diurnal load pattern as the pattern from which we drive out excess distribution network capacity and the PEV dataset resulting from everywhere charging with minimum dwell time of three hours. More specifically, the prices are generated by perturbing the historical prices with Gaussian samples with roughly 5%-10% standard deviation. The distribution network is first obtained by subtracting the ERCOT minutely average diurnal pattern from 120% of its maximum (as the feeder capacity) and then scaling the total energy capacity in the pattern appropriately so that 50% excess capacity loading is achieved.

We implemented the stochastic program in its deterministic expansion form. The entire simulation process is implemented in MATLAB$^{\text{TM}}$ [67], including scenario generation, and YALMIP [65] is used as the optimization modeling interface to the solvers. We have experimented with various solvers including CPLEX 12.6 [51], Gurobi 5.6 [2], MOSEK 7 [3] and GLPK [1], where the first three are commercial and were available on an academic license and the latter is an open source solver. Our computational experience with these solvers in our application was mixed, and sometimes contrary to established benchmarks [71]. All the commercial solvers performed much better than GLPK as expected. CPLEX performed worst among the commercial solvers, ranging between 2-3 times slower than Gurobi. To our surprise, however,

MOSEK performed better in most cases, our performing Gurobi between 10% to 20% in terms of run time.

We assume roughly 50 charging sessions per day scenario (since the exact number depends on the scenario and day of week). To achieve a consistent result from the DAM stochastic program we experimented with the number of scenarios. Based on our dataset and sampling, we found out that the total cost of the DAM planning problem does not change more than 10^{-3} for number of scenarios greater than 250 scenarios; therefore, we ran each day of planning with 250 scenarios.

We have performed the simulations for the complete year of 2012 to minimize the effect of fluctuations in prices. Figure 7.3 summarizes the results in terms of the average normalized cost over 2012. In comparison with uncoordinated charging, as expected from the results in the previous chapter, there is substantial amount of saving even when the coordinated users are subject to capacity constraints while uncoordinated users are not. We have also demonstrated the effect of savings on the total cost as the stacked block. That is, if the savings from AS offering, which can only happen if the ESCo participates in the market, are taken off the ESCo's balance sheet, the cost will go up by the block on top of the cost for the scheduled users. Note that this is a rough estimate of the contribution of AS provision in total costs since if the ESCo forgoes the AS provision option, its schedule would most likely change. In other words, the AS savings block shown here is an upper bound on the contribution of AS in total cost reduction.

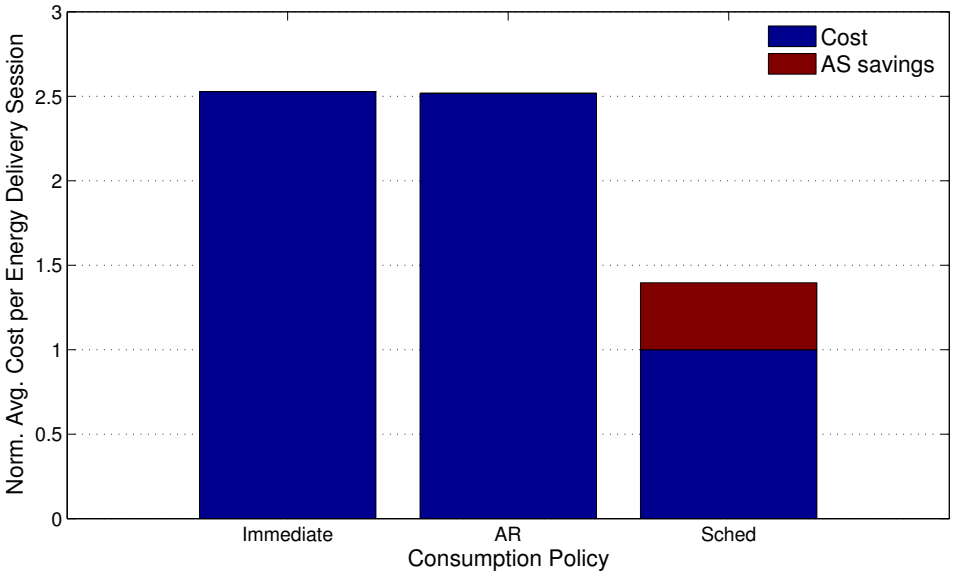

Figure 7.3: Average cost comparison between immediate charging, AR charging and multi-settlement scheduling.

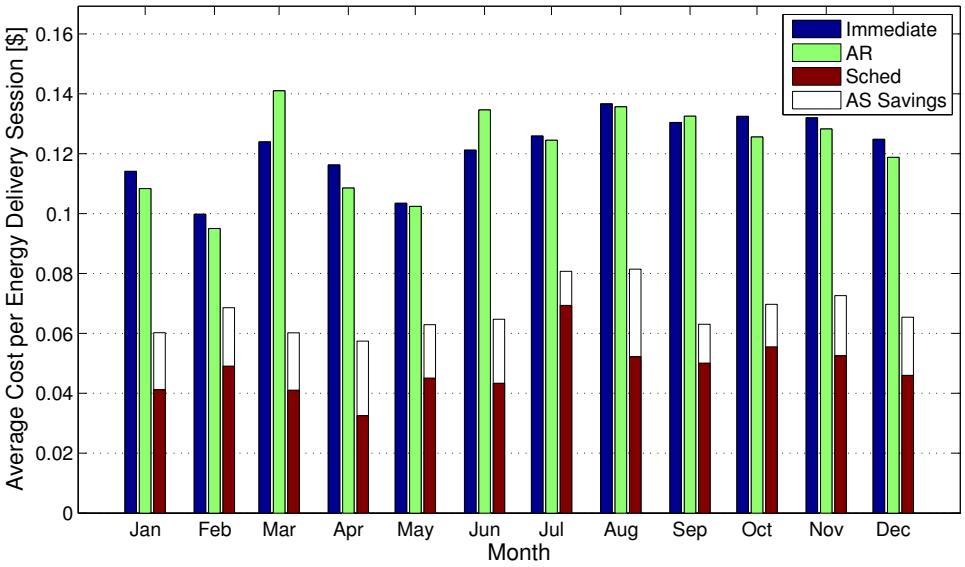

Figure 7.4: Average cost of multi-settlement scheduling per month over the year.

As demonstrated by Figure 7.3, scheduling in DAM reduces the energy cost to approximately half that of price insensitive methods. Also, roughly one fourth of the savings comes from the AS provision. In order to get a more detailed view and observe the seasonalities in costs, we have also plotted the monthly averages of cost per PEV charging session in Figure 7.4. This figure shows that the main monthly trend of the costs remain the same and are mostly influenced by the trend of electricity and AS prices.

Finally, we study the ratio of AS capacity offered to energy served in Figure 7.5, where we have plotted this ratio for year 2012 on a monthly basis. Based on this figure, the ratio of AS capacity offered to energy served remains

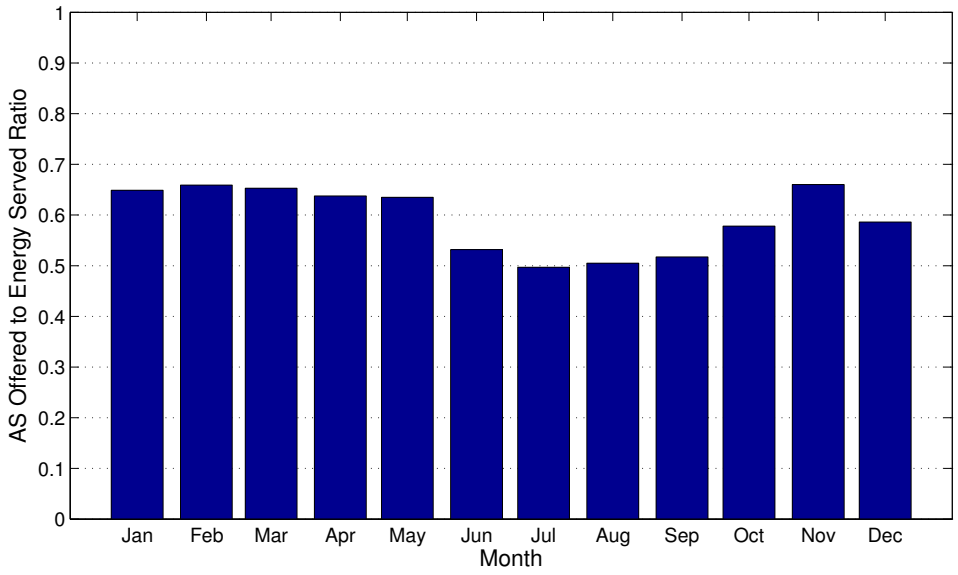

Figure 7.5: Monthly AS offered to energy served ratio.

above 50% for all months and relatively steady. This is good news since it suggests that overall, the PEV load can be seen as a substantial and reliable source of AS in terms of capacity.

Careful investigation of the source of cost savings, which is better than what expected from the previous chapter, revealed that some of the savings, in some cases a major portion of it, came from the ESCo ceasing the DAM-RTM trading opportunities. Since we have assumed that unused DAM purchases can be sold back to the market, when prices are expected to be better in DAM, the ESCo purchases considerable amounts in those times, almost regardless of its schedule and sells it in RTM. Since we expect these arbitrage opportunities to be short lived, we tried to set in place measures to prevent extensive oc-

currence of such situations. In this work, as discussed in the formulation, we have bound the total amount energy purchase volume in DAM to be the minimum amount of total energy demand over the scenarios. We believe, however, that systematic modeling of risk in DAM-RTM decisions, through including a systematic measure of risk into the objective function, e.g. CVaR, would help with such situations. Finally, we believe there is nothing systematically wrong in ESCo seeking profit maximization in any possible way, if the risks of such decision making is modeled properly. We have left investigation of this path for future work.

7.5 Conclusion

In this chapter we proposed a systematic method for an Energy Services Company, particularly one that serves PEV load, to participate in a multi-settlement market structure. We focused on the DAM planning problem and formulated it as a stochastic program. We then discussed the challenges in scenario generation in case of PEV load and proposed a data driven approach for generating scenarios. We finally presented our performance analysis on the proposed method and showed that adopting the proposed method can result in cost reductions of about 50%, roughly half of which is due to AS sales by the ESCo. Moreover, we observed that the ESCo would offer roughly 50% of its served load back in the market as AS.

We plan to add a measure of risk to our future implementation of our proposed method to have a more realistic view of the decision making process

by the ESCo. Moreover, we are working on more efficient implementation of the proposed stochastic program though L-shaped method [16] and similar techniques.

Chapter 8

Conclusion

8.1 Conclusion

Utilizing demand flexibility is key for increasing efficiency of asset utilization in the current grid and effective integration of intermittent renewables. In this dissertation, we investigated various methods for harnessing demand flexibility and its extension to other assets.

First, we investigated the potential of PEV load and proposed simple, yet effective charging policies that could have substantial impact on the demand patterns of the grid without much overhead for communication and control. We demonstrated that PEV load is substantially flexible under different charging behavior models and proposed easy to implement charging algorithms that can substantially impact the demand patterns induced by PEV charging. We also discussed methods for improving these charging algorithms to be more robust with respect to uncertainties in departure times. We demonstrated that the proposed charging algorithms can be modified to improve grid stability by automatically responding to frequency deviations. We quantified the capacity of frequency responsive PEV load and showed substantial potential in that capacity.

Then we investigated the optimal response of flexible loads under real-time pricing and proved that the optimal policy can be calculated recursively and in a computationally efficient manner. We also studied the impact of widespread adoption of such optimal algorithms and concluded that while they would substantially reduce energy costs to the users, the load patterns they induce at network level can cause high peak-to-average ratios and adversely impact the grid. We further extended the theoretical foundation we laid in this part of the work to the case where flexible loads can provide ancillary services while consuming energy and obtained the optimal response under such scenarios. We also showed that the model for flexible loads can be extended to storage assets. We used this connection to obtain optimal operation policy of an ideal storage asset under real-time prices.

Next, we proposed a new model for pricing energy for flexible loads that would encourage them to reveal their flexibility under a centralized load aggregation model. We demonstrated that this method not only encourages loads to reveal their flexibility but also provides most loads with a better total energy cost because the ESCo can aggregate loads for provision of ancillary services.

Finally, we considered the decision problem faced by a load aggregator when the market is organized in a multi-settlement fashion, namely deciding the levels of energy purchase and ancillary service sales in the day-ahead market. We formulated this problem as a two stage stochastic program and proposed a data driven scenario generation method capable of dealing with the

uncertainties in availability and demand from flexible loads at the day-ahead stage.

8.2 Future Directions

The work presented in this dissertation can be extended in multiple directions. Using more data from PEV users, we can build more realistic PEV charging models which would help us to study the current and proposed charging algorithms more accurately. Also, using a dynamic model for the grid, such as one proposed by Peydayesh [83] or Chavez [28], we plan to study the impact of frequency responsive flexible loads, particularly under high penetration of renewables, on the frequency performance of the grid and quantify its economic value by measuring potential reductions in ancillary service utilization, and hence purchases.

The theoretical framework we used in Chapter 3, Chapter 4 and Chapter 5 can be further used to obtain optimal energy consumption and ancillary service provision by the flexible loads when capacity reservation should be made for offering ancillary services. This is a problem we are already working on as one immediate directions for extending this thesis. The results of this extension can then be used at the load aggregator level to approximate the optimal decision making problem faced by the Energy Services Company, the same problem we discussed in Chapter 6. The main promise of this approach, which bridges from single load price based coordination to more sophisticated and cooperative energy delivery mechanisms is that it would result in a com-

putationally efficient dynamic approximation for the ESCo's decision problem.

We believe that the Transaction Pricing concept we introduced in this dissertation can be studied further, particularly from a game theoretic perspective. Finally, we are planning to extend our work in multi-settlement markets to capture risk in inter-stage trading and model the real-time operation more carefully.

Finally, we would like to mention that, in cooperation with ERCOT, we have implemented a testbed for implementing and evaluating PEV charging algorithms. Our current testbed, implemented by the author and Dr. Mike Legatt from ERCOT, includes servers at UT-Austin and ERCOT which would play as the ESCo, PEV communication and control server and grid information server. The current testbed includes eight EVSEs at ERCOT offices in Taylor, three EVSEs at ERCOT Met Center. Due to API issues, our current testbed can only control PEVs though EVSE control using the ChargePoint network [27]. All the EVSEs are also measured through eGauge system [37] at a secondly resolution besides every 30sec measurements by the ChargePoint network. The communication over the testbed is implemented through a Web API between the entities: ESCo (a.k.a. scheduling server), Grid Information Server and PEV Control Server. Since December 2011, the EVSEs have delivered more than 13.7MWh of energy to six employee PEVs as well as visitor EVs.

We have already implemented AR charging and coordinated energy delivery algorithm discussed in Chapter 6 on the testbed. The latter is imple-

mented in C♯, leveraging Microsoft Solver Foundation [68] as the middleware for modeling and coding the optimization problem and using Gurobi solver. Implementing more advanced charging algorithms discussed in this dissertation and perfecting the testbed is another direction we are pursuing.

Appendices

Appendix A

Proof of Theorem 3.1

The proof is by establishing that the proposed optimal value function satisfies the Bellman equation. We assume the cdfs, expected values, and integrals exist throughout and the correlation structure is well behaved, which holds for all cases of interest.

The convexity of the optimal value function can be deduced from stage and final costs convexity and linearity of dynamics, so we skip its explicit treatment for brevity. A similar argument can be found in the proof of Proposition 1 in [79].

First, we claim that the optimal value function has the following form:

$$J_t^*(x,\theta) = \sum_{j=1}^{\infty} m_t^j(\theta)[(x - j\bar{u})^+ \wedge \bar{u}] + C(t). \tag{A.1}$$

where we define $m_t^j(\theta) = m_t^T$ for $j \geq T$. We establish this claim by showing that it satisfies the Bellman equation and establish the optimal policy along the way. The proof is then completed by backward induction on t using the assumption $m_T^i = m_T$. From the Bellman equation and using (3.2) we have:

$$J_t^*(x_t,\theta_t) = \mathbb{E}_{\epsilon_t}[\min_u \left\{\gamma_t u + \eta_t(x_t - u) + \eta_t' + \alpha_t J_{t+1}^*(x_t - u, \gamma_t)\right\}], \tag{A.2}$$

since $\theta_{t+1} = \gamma_t$ by definition. Without loss of generality, let i satisfy $i\bar{u} \leq x_t \leq (i+1)\bar{u}$. By the induction hypothesis, assuming that (A.1) holds for $t+1$, we prove it for t. This is equivalent to obtaining $m_t^i(\theta)$ and the desired optimal value function in the following form:

$$J_t^*(x_t, \theta) = \sum_{j=1}^{i-1} m_t^j(\theta)\bar{u} + m_t^i(\theta)[x_t - i\bar{u}] + C(t). \tag{A.3}$$

Since $0 \leq u \leq \bar{u}$, $(i-1)\bar{u} \leq x_t - u \leq (i+1)\bar{u}$, using (A.1) for $t+1$ and similar to (A.3), we have:

$$\begin{aligned} J_{t+1}^*(x_t - u, \gamma_t) = & \sum_{j=1}^{i-2} m_{t+1}^j(\gamma_t)\bar{u} \\ & + m_{t+1}^{i-1}(\gamma_t)[(x_t - u - (i-1)\bar{u})^+ \wedge \bar{u}] \\ & + m_{t+1}^i(\gamma_t)(x_t - u - i\bar{u})^+ + C(t+1), \\ = & \sum_{j=1}^{i-1} m_{t+1}^j(\gamma_t)\bar{u} + m_{t+1}^i(\gamma_t)[x_t - i\bar{u}] \\ & - m_{t+1}^{i-1}(\gamma_t)[(u - (x_t - i\bar{u}))^+] \\ & - m_{t+1}^i(\gamma_t)[u \wedge (x_t - i\bar{u})] + C(t+1), \end{aligned} \tag{A.4}$$

Now, let us substitute (A.4) in (A.2) as depicted in (A.5):

$$\begin{aligned} J_t^*(x_t, \theta_t) = \mathbb{E}_{\epsilon_t} \Bigg[\min_u \Bigg\{ & (\gamma_t - \eta_t)u + \eta_t x_t + \eta_t' \\ & + \alpha_t \Bigg(\sum_{j=1}^{i-1} m_{t+1}^j(\gamma_t)\bar{u} + m_{t+1}^i(\gamma_t)[x_t - i\bar{u}] + C(t+1) \\ & - m_{t+1}^{i-1}(\gamma_t)[(u - (x_t - i\bar{u}))^+] - m_{t+1}^i(\gamma_t)[u \wedge (x_t - i\bar{u})] \Bigg) \Bigg\} \Bigg] \end{aligned} \tag{A.5}$$

$$\stackrel{(a)}{=} \mathbb{E}_{\epsilon_t}\Big[\min_u \big\{(\gamma_t-\eta_t)u-\alpha_t m_{t+1}^{i-1}(\gamma_t)[(u-(x_t-i\bar{u}))^+] \\ -\alpha_t m_{t+1}^{i}(\gamma_t)[u\wedge(x_t-i\bar{u})]\big\}\Big] \\ +\eta_t x_t+\alpha_t\left(\sum_{j=1}^{i-1} m_{t+1}^{j}(\gamma_t)\bar{u}+m_{t+1}^{i}(\gamma_t)[x_t-i\bar{u}]\right)+C(t)$$

$$\stackrel{(b)}{=} \mathbb{E}_{\epsilon_t}\Bigg[\min_u \big\{(\gamma_t-\tilde{m}_{t+1}^{i-1}(\gamma_t))(u-(x_t-i\bar{u}))^+ \\ +(\gamma_t-\tilde{m}_{t+1}^{i}(\gamma_t))[u\wedge(x_t-i\bar{u})]\big\} \\ +\sum_{j=1}^{i-1}\tilde{m}_{t+1}^{j}(\gamma_t)\bar{u}+\tilde{m}_{t+1}^{i}(\gamma_t)[x_t-i\bar{u}]\Bigg]+C(t)$$

where, (a) is obtained by rearranging terms and the fact that $C(t) = \alpha_t C(t+1) + \eta_t'$ and (b) is obtained by rewriting x_t as $i\bar{u} + (x_t - i\bar{u})$, rewriting u as $(u-b)^+ + [u \wedge b]$ where $b = x_t - i\bar{u}$ and then factoring terms. Since $\tilde{m}_{t+1}^{j-1}(\gamma_t) \leq \tilde{m}_{t+1}^{j}(\gamma_t), \forall j$ due to convexity of the optimal value function, we need to consider only three cases for obtaining the optimal u. Considering the two terms inside the minimization, either both coefficients are negative, denoted by event (e_3), in that case we want u as large as possible (namely $\bar{u}$), or just the second term's coefficient is negative, denoted by event (e_2), which makes the optimal $u = x_t - i\bar{u}$ or none of the coefficients are negative, denoted by event (e_1), and the optimal u will be zero. Hence the optimal policy, $u^*(x, \gamma_t)$, is given by:

$$u^*(x,\gamma_t)=\begin{cases}0 & \text{if } (e_1): \quad \tilde{m}^i_{t+1}(\gamma_t)\leq\gamma_t,\\ x-i\bar{u} & \text{if } (e_2): \quad \tilde{m}^{i-1}_{t+1}(\gamma_t)<\gamma_t\leq\tilde{m}^i_{t+1}(\gamma_t),\\ \bar{u} & \text{if } (e_3): \quad \gamma_t\leq\tilde{m}^{i-1}_{t+1}(\gamma_t).\end{cases}$$

Note that in order to find the actual thresholds on γ_t for each event we need to solve $\tilde{m}^j_{t+1}(\mu)=\mu$. Calling this fixed point $\hat{m}^j_{t+1}$ gives (3.9). Aggregating this policy over i results in (3.10).

Now, let us obtain the optimal value function encoded by $\tilde{m}^i_t(\theta_t)$ by plugging-in the optimal policy and correspondingly conditioning the expected value on each event e_k, which after simplifications yields:

$$J^*_t(x_t,\theta_t)=J^*_t(x_t,\theta_t|e_1)\mathbb{P}\{e_1\}+J^*_t(x_t,\theta_t|e_2)\mathbb{P}\{e_2\}+J^*_t(x_t,\theta_t|e_3)\mathbb{P}\{e_3\}, \quad \text{(A.6)}$$

where,

$$J^*_t(x,\theta_t|e_1)=C(t)+\sum_{j=1}^{i-1}\mathbb{E}_{\epsilon_t}[\tilde{m}^j_{t+1}(\gamma_t)|e_1]\bar{u}+\mathbb{E}_{\epsilon_t}[\tilde{m}^i_{t+1}(\gamma_t)|e_1][x-i\bar{u}],$$

$$J^*_t(x,\theta_t|e_2)=C(t)+\sum_{j=1}^{i-1}\mathbb{E}_{\epsilon_t}[\tilde{m}^j_{t+1}(\gamma_t)|e_2]\bar{u}+\mathbb{E}_{\epsilon_t}[\gamma_t|e_2](x-i\bar{u}),$$

$$J^*_t(x,\theta_t|e_3)=C(t)+(\sum_{j=1}^{i-2}\mathbb{E}_{\epsilon_t}[\tilde{m}^j_{t+1}(\gamma_t)|e_3]+\mathbb{E}_{\epsilon_t}[\gamma_t|e_3])\bar{u}+\mathbb{E}_{\epsilon_t}[\tilde{m}^{i-1}_{t+1}(\gamma_t)|e_3][x-i\bar{u}].$$

Note the evolution of prices given by (3.1) and $\theta_t=\gamma_{t-1}$. It can be seen now that the optimal value function has the same structure as claimed in (A.3) and equivalently (A.1). Now, it remains to establish the recursion in (3.7) by

obtaining $m_t^i(\theta_t)$ from (A.6) using $M(\theta, \epsilon)$ as defined in (3.8):

$$\begin{aligned} m_t^i(\theta_t) =& \mathbb{E}_{\epsilon_t}[\tilde{m}_{t+1}^i(\lambda_t(\theta_t) + \epsilon_t)|e_1]\mathbb{P}\{e_1\} + \mathbb{E}_{\epsilon_t}[\gamma_t|e_2]\mathbb{P}\{e_2\} + \mathbb{E}_{\epsilon_t}[\tilde{m}_{t+1}^{i-1}(\lambda_t(\theta_t) + \epsilon_t)|e_3]\mathbb{P}\{e_3\} \\ =& \mathbb{E}_{\epsilon_t}[M(\theta_t, \epsilon_t)]. \end{aligned} \tag{A.7}$$

The proof is completed by induction over t backward and the desired value function as given in (3.15) is obtained at $t = 0$. ■

Appendix B

Proof of Theorem 3.2

In case of independent prices, the state space is automatically reduced to the remaining commitment. Nevertheless, more can be done to simplify the recursions and ease the computation burden. We establish the result by starting from state independent m_t^i (and consequently $\tilde{m}_t^i$) and show that it remains state independent and obtain the simplified update equation as shown in (3.9) along the way.

Starting with state independent m_t^i, which holds for $t = T$ by assumption, we can simplify $M(\theta, \epsilon)$ to $M(\epsilon)$ as:

$$M(\epsilon) = \begin{cases} \tilde{m}_{t+1}^i & (e_1): \quad \tilde{m}_{t+1}^i \leq \epsilon \\ \epsilon & (e_2): \quad \tilde{m}_{t+1}^{i-1} \leq \epsilon < \tilde{m}_{t+1}^i \\ \tilde{m}_{t+1}^{i-1} & (e_3): \quad \epsilon < \tilde{m}_{t+1}^{i-1} \end{cases},$$

Hence, since $\gamma_t = \epsilon_t$, similar to (A.7) we have:

$$m_t^i = \tilde{m}_{t+1}^i \mathbb{P}\{e_1\} + \underbrace{\mathbb{E}_{\epsilon_t}[\epsilon_t | e_2] \mathbb{P}\{e_2\}}_{A} + \tilde{m}_{t+1}^{i-1} \mathbb{P}\{e_3\}. \tag{B.1}$$

Using integration by parts:

$$\begin{aligned} A &= \int_{\tilde{m}_{t+1}^{i-1}}^{\tilde{m}_{t+1}^{i}} \zeta \, dF_t(\zeta) \\ &= \tilde{m}_{t+1}^{i} F_t(\tilde{m}_{t+1}^{i}) - \tilde{m}_{t+1}^{i-1} F_t(\tilde{m}_{t+1}^{i-1}) - \int_{\tilde{m}_{t+1}^{i-1}}^{\tilde{m}_{t+1}^{i}} F_t(\zeta) \, d\zeta \\ &= \tilde{m}_{t+1}^{i} \mathbb{P}\{\bar{e}_1\} - \tilde{m}_{t+1}^{i-1} \mathbb{P}\{e_3\} - G_t(\tilde{m}_{t+1}^{i-1}, \tilde{m}_{t+1}^{i}), \end{aligned}$$

where $\bar{e}_1$ is the complement of e_1. Plugging for A in (B.1) we get:

$$m_t^i = \tilde{m}_{t+1}^{i} - G_t(\tilde{m}_{t+1}^{i-1}, \tilde{m}_{t+1}^{i}).$$

■

Appendix C

Proof of Theorem 4.1

We establish that the proposed optimal value function satisfies the Bellman equation. As in Appendix A, we assume the cdfs and expected values exist throughout and the correlation structure is well behaved, which holds for most practical cases. Before going through the details, let us first establish some lemmas that help us streamline the proof.

Lemma C.1. *For any d, e, $\overline{e}$ such that $0 \leq d$, $0 \leq \overline{e}$, $0 \leq e \leq \overline{e}$, and letting $i = \lfloor {}^{d}/_{\overline{e}} \rfloor$, and $\tilde{d} = d - i\overline{e}$, we have:*

1. $[(d - e - (i-1)\overline{e})^+ \wedge \overline{e}] = \overline{e} - (e - \tilde{d})^+$,
2. $(\tilde{d} - e)^+ = \tilde{d} - (e \wedge \tilde{d})$.

Proof. 1. First observe that the left hand side (LHS) can be simplified as:

$$[(d - e - (i-1)\overline{e})^+ \wedge \overline{e}] = [(\tilde{d} - e + \overline{e})^+ \wedge \overline{e}].$$

Considering the left hand side, only three cases are possible:

(a) $\tilde{d} - e + \overline{e} \leq 0$: In this case, LHS=0. This condition can be rearranged as $\overline{e} \leq e - \tilde{d}$. But given the conditions in the assumption, this can

only happen if $\overline{e} = e - \tilde{d}$. Consequently, the right hand side (RHS) results in:

$$\overline{e} - (e - \tilde{d})^+ = \overline{e} - \overline{e} = 0.$$

(b) $0 \leq \tilde{d} - e + \overline{e} \leq \overline{e}$: In this case, LHS=$\tilde{d} - e + \overline{e}$. Rearranging this condition results in $0 \leq e - \tilde{d} \leq \overline{e}$, which results in:

$$\overline{e} - (e - \tilde{d})^+ = \overline{e} - e + \tilde{d} = \text{LHS}.$$

(c) $\overline{e} \leq \tilde{d} - e + \overline{e}$: In this case, LHS=$\overline{e}$. This case can be also rearranged to $e - \tilde{d} \leq 0$, and hence:

$$\overline{e} - (e - \tilde{d})^+ = \overline{e} - 0 = \text{LHS}.$$

2. For this part, only two cases can happen, if $\tilde{d} - e \geq 0$, then:

$$(\tilde{d} - e)^+ = \tilde{d} - e = \tilde{d} - (e \wedge \tilde{d}),$$

otherwise,

$$(\tilde{d} - e)^+ = 0 = \tilde{d} - \tilde{d} = \tilde{d} - (e \wedge \tilde{d}).$$

■

Lemma C.2. *For any $\tilde{d}$, e such that $0 \leq e$, $0 \leq \tilde{d}$, we have $e = (e - \tilde{d})^+ + (e \wedge \tilde{d})$.*

Proof. If $e \leq \tilde{d}$:

$$(e - \tilde{d})^+ + (e \wedge \tilde{d}) = 0 + e = e,$$

otherwise:

$$(e - \tilde{d})^+ + (e \wedge \tilde{d}) = e - \tilde{d} + \tilde{d} = e.$$

■

We skip establishing the convexity of the optimal value function for brevity. As in the proof of Theorem 3.1 in Appendix A, a proof similar to Proposition 1 in [79] can be applied using convexity of the stage and final costs and linearity of dynamics.

The main proof is based on backward induction on t; to this end, let us assume that the proposed following form of the value function in Theorem 4.1 holds:

$$J_t^*(d_t, \boldsymbol{\theta}_t) = \sum_{j=1}^{\infty} m_t^j(\boldsymbol{\theta}_t)[(d_t - j\overline{e})^+ \wedge \overline{e}]. \tag{C.1}$$

where $m_t^j(\boldsymbol{\theta}) = m_t^T$ for $j \geq T$. We need to show that if this assumption holds for $t+1$, then it holds for t. These consecutive time slots are linked by the Bellman equation; that is:

$$J_t^*(d_t, \boldsymbol{\theta}_t) = \mathbb{E}_{\boldsymbol{\epsilon}_t}[\min_{e,r} \left\{\pi_t^e e - \pi_t^r r + J_{t+1}^*(d_t - e, \boldsymbol{\pi}_t)\right\}], \tag{C.2}$$

using system dynamics equations and $\boldsymbol{\theta}_{t+1} = \boldsymbol{\pi}_t$ as assumed previously. Define $i = \lfloor {}^{d_t}/_{\overline{e}} \rfloor$, $i\overline{e} \leq d_t < (i+1)\overline{e}$. Our objective is to obtain $m_t^i(\boldsymbol{\theta})$ in the desired optimal value function; which in this case can be rewritten as:

$$J_t^*(d_t, \boldsymbol{\theta}_t) = \sum_{j=1}^{i-1} m_t^j(\boldsymbol{\theta}_t)\overline{e} + m_t^i(\boldsymbol{\theta}_t)\tilde{d}_t, \tag{C.3}$$

where $\tilde{d}_t \triangleq d_t - i\overline{e}$. Let us first rearrange the $J_{t+1}^*(d_t - e, \boldsymbol{\pi}_t)$ term in (C.2). Since $0 \leq e \leq \overline{e}$, $(i-1)\overline{e} \leq d_t - e \leq (i+1)\overline{e}$. Using (C.1) for $t+1$, by the

induction hypothesis and similar to (C.3), we have:

$$\begin{aligned} J^*_{t+1}(d_t - e, \boldsymbol{\pi}_t) &= \sum_{j=1}^{i-2} m^j_{t+1}(\boldsymbol{\pi}_t)\overline{e} \\ &\quad + m^{i-1}_{t+1}(\boldsymbol{\pi}_t)[(d_t - e - (i-1)\overline{e})^+ \wedge \overline{e}] \\ &\quad + m^i_{t+1}(\boldsymbol{\pi}_t)(d_t - e - i\overline{e})^+, \\ &= \sum_{j=1}^{i-1} m^j_{t+1}(\boldsymbol{\pi}_t)\overline{e} + m^i_{t+1}(\boldsymbol{\pi}_t)\tilde{d}_t \\ &\quad - m^{i-1}_{t+1}(\boldsymbol{\pi}_t)(e - \tilde{d}_t)^+ - m^i_{t+1}(\boldsymbol{\pi}_t)(e \wedge \tilde{d}_t), \end{aligned} \tag{C.4}$$

where we have used Lemma C.1 to obtain the second equality. Now, let us substitute (C.4) in (C.2) as depicted in (C.5):

$$\begin{aligned} J^*_t(d_t, \boldsymbol{\theta}_t) &= \mathbb{E}_{\boldsymbol{\epsilon}_t}\left[\min_{e,r}\left\{\pi^e_t e - \pi^r_t r + \sum_{j=1}^{i-1} m^j_{t+1}(\boldsymbol{\pi}_t)\overline{e} + m^i_{t+1}(\boldsymbol{\pi}_t)\tilde{d}_t \right.\right. \\ &\qquad \left.\left. - m^{i-1}_{t+1}(\boldsymbol{\pi}_t)(e - \tilde{d}_t)^+ - m^i_{t+1}(\boldsymbol{\pi}_t)[e \wedge \tilde{d}_t]\right\}\right] \\ &\overset{(a)}{=} \mathbb{E}_{\boldsymbol{\epsilon}_t}\left[\min_{e,r}\left\{\pi^e_t e - \pi^r_t r \right.\right. \\ &\qquad \left. - m^{i-1}_{t+1}(\boldsymbol{\pi}_t)(e - \tilde{d}_t)^+ - m^i_{t+1}(\boldsymbol{\pi}_t)(e \wedge \tilde{d}_t)\right\} \\ &\qquad \left. + \sum_{j=1}^{i-1} m^j_{t+1}(\boldsymbol{\pi}_t)\overline{e} + m^i_{t+1}(\boldsymbol{\pi}_t)\tilde{d}_t\right] \\ &\overset{(b)}{=} \mathbb{E}_{\boldsymbol{\epsilon}_t}\left[\min_{e,r}\left\{(\pi^e_t - m^{i-1}_{t+1}(\boldsymbol{\pi}_t))(e - \tilde{d}_t)^+ \right.\right. \\ &\qquad \left. + (\pi^e_t - m^i_{t+1}(\boldsymbol{\pi}_t))(e \wedge \tilde{d}_t) - \pi^r_t r\right\} \\ &\qquad \left. + \sum_{j=1}^{i-1} m^j_{t+1}(\boldsymbol{\pi}_t)\overline{e} + m^i_{t+1}(\boldsymbol{\pi}_t)\tilde{d}_t\right] \end{aligned} \tag{C.5}$$

$$\overset{(c)}{=} \mathbb{E}_{\boldsymbol{\epsilon}_t}\Bigg[\min_{e}\Bigg\{(\pi_t^e-(\pi_t^r)^+-m_{t+1}^{i-1}(\boldsymbol{\pi}_t))(e-\tilde{d}_t)^+ \\ +(\pi_t^e-(\pi_t^r)^+-m_{t+1}^{i}(\boldsymbol{\pi}_t))(e\wedge\tilde{d}_t)\Bigg\} \\ +\sum_{j=1}^{i-1}m_{t+1}^{j}(\boldsymbol{\pi}_t)\overline{e}+m_{t+1}^{i}(\boldsymbol{\pi}_t)\tilde{d}_t\Bigg]$$

where, (a) is obtained by rearranging terms, (b) is obtained by using Lemma C.2 and factoring common terms. To obtain (c), notice that the minimization problem in r can be tackled directly, that is, if its coefficient, (π_t^r) is positive, then we want to maximize r and minimize it otherwise. But we already know the $0 \leq r \leq e$, hence, we can obtain the optimal reserve offering policy as:

$$r_t^*(d,\boldsymbol{\pi}_t) = e_t^*(d,\boldsymbol{\pi}_t) * \mathbb{1}\{\pi_t^r \geq 0\}. \tag{C.6}$$

Now (c) is obtained by using (C.6), essentially substituting r with e with proper conditionals on π_t^r, namely its positivity. The result of (C.5) leaves us with a much simpler optimization problem since it is all in terms of e, which is essentially cut into two pieces: $(e-\tilde{d}_t)^+$ and $(e\wedge\tilde{d}_t)$ using Lemma (C.2). The problem at hand is essentially a linear programing problem, however, using the convexity of the value function, we can parametrically solve it, basically by inspection. Since the value function is piecewise linear, its convexity is equivalent to $m_{t+1}^{j-1}(\boldsymbol{\pi}_t) \leq m_{t+1}^{j}(\boldsymbol{\pi}_t), \forall j$; noting that $m_{t+1}^{j}(\boldsymbol{\pi}_t)$ is the slope of the jth piece of the value function. This leaves us with essentially three cases to consider for the minimization problem at hand, which we denote them by

events $\mathcal{E}_1$, $\mathcal{E}_2$ and $\mathcal{E}_3$:

$$\mathcal{E}_1: \quad m^i_{t+1}(\boldsymbol{\pi}_t) \leq \quad \pi^e_t - (\pi^r_t)^+, \tag{C.7}$$

$$\mathcal{E}_2: \quad m^{i-1}_{t+1}(\boldsymbol{\pi}_t) \leq \quad \pi^e_t - (\pi^r_t)^+ \leq m^i_{t+1}(\boldsymbol{\pi}_t), \tag{C.8}$$

$$\mathcal{E}_3: \qquad\qquad\qquad\quad \pi^e_t - (\pi^r_t)^+ \leq m^{i-1}_{t+1}(\boldsymbol{\pi}_t). \tag{C.9}$$

Note that in each of these conditions, $\boldsymbol{\pi}_t$ appears on both sides and hence the above conditions are implicitly defined. Moreover, notice that each of these events consist of two simple events corresponding to positivity of π^r_t. Conditioned on each of these events, it is straightforward to solve the final minimization problem in (C.5), understanding that the only constraint we are facing is $0 \leq e \leq \overline{e}$: Under $\mathcal{E}_1$, none of the coefficients in are positive and hence, the optimal decision is to minimize e. Under $\mathcal{E}_2$, only the second coefficient is negative and hence the optimal decision is to maximize the second term, i.e. $e^* = \tilde{d}_t$. Finally, under $\mathcal{E}_3$, both coefficients are negative and hence the optimal decision is to maximize e, i.e. $e^* = \overline{e}$. This basically gives us the optimal policy as:

$$e^*(d_t, \boldsymbol{\pi}_t) = \begin{cases} 0 & \text{if } (\mathcal{E}_1): \quad m^i_{t+1}(\boldsymbol{\pi}_t) \leq \pi^e_t - (\pi^r_t)^+, \\ d - i\overline{e} & \text{if } (\mathcal{E}_2): \quad m^{i-1}_{t+1}(\boldsymbol{\pi}_t) \leq \pi^e_t - (\pi^r_t)^+ \leq m^i_{t+1}(\boldsymbol{\pi}_t), \\ \overline{e} & \text{if } (\mathcal{E}_3): \qquad\qquad\qquad\quad \pi^e_t - (\pi^r_t)^+ \leq m^{i-1}_{t+1}(\boldsymbol{\pi}_t). \end{cases} \tag{C.10}$$

As mentioned before, the conditions defining these events are implicit. Therefore, we need to solve the following equation to obtain the explicit conditions:

$$m^j_{t+1}(\pi^e_t, \pi^r_t) = \pi^e_t - (\pi^r_t)^+ \tag{C.11}$$

Defining $\hat{m}^j_{t+1}$ as:

$$\hat{m}^j_{t+1} = \{m^j_{t+1}(\pi^e_t, \pi^r_t) | m^j_{t+1}(\pi^e_t, \pi^r_t) = \pi^e_t - (\pi^r_t)^+\}, \tag{C.12}$$

similar to (4.9), we can make these conditions explicit. The desired form in (4.10), is then obtained by paying attention to the fact that $\hat{m}^j_{t+1}$ is increasing in j by convexity and hence there exists i^* such that $\pi^e_t - (\pi^r_t)^+ < \hat{m}^{i^*}_{t+1}, \forall j > i^*$ and therefore, we can formulate the optimal policy as stated in the theorem.

Plugging in the optimal policy in (C.5), we can continue the proof. Conditioning based on the $\mathcal{E}_k$ events, we have:

$$J^*_t(d_t, \boldsymbol{\theta}_t) = J^*_t(d_t, \boldsymbol{\theta}_t|\mathcal{E}_1)\mathbb{P}\{\mathcal{E}_1\} + J^*_t(d_t, \boldsymbol{\theta}_t|\mathcal{E}_2)\mathbb{P}\{\mathcal{E}_2\} + J^*_t(d_t, \boldsymbol{\theta}_t|\mathcal{E}_3)\mathbb{P}\{\mathcal{E}_3\}, \tag{C.13}$$

where,

$$J^*_t(d_t, \boldsymbol{\theta}_t|\mathcal{E}_1) = \sum_{j=1}^{i-1} \mathbb{E}_{\boldsymbol{\epsilon}_t}[m^j_{t+1}(\boldsymbol{\pi}_t)|\mathcal{E}_1]\overline{e} + \mathbb{E}_{\boldsymbol{\epsilon}_t}[m^i_{t+1}(\boldsymbol{\pi}_t)|\mathcal{E}_1]\tilde{d}_t,$$

$$J^*_t(d_t, \boldsymbol{\theta}_t|\mathcal{E}_2) = \sum_{j=1}^{i-1} \mathbb{E}_{\boldsymbol{\epsilon}_t}[m^j_{t+1}(\boldsymbol{\pi}_t)|\mathcal{E}_2]\overline{e} + \mathbb{E}_{\boldsymbol{\epsilon}_t}[\pi^e_t - (\pi^r_t)^+|\mathcal{E}_2]\tilde{d}_t,$$

$$J^*_t(d_t, \boldsymbol{\theta}_t|\mathcal{E}_3) = \sum_{j=1}^{i-2} \mathbb{E}_{\boldsymbol{\epsilon}_t}[m^j_{t+1}(\boldsymbol{\pi}_t)|\mathcal{E}_3]\overline{e} + \mathbb{E}_{\boldsymbol{\epsilon}_t}[\pi^e_t - (\pi^r_t)^+|\mathcal{E}_3]\overline{e} + \mathbb{E}_{\boldsymbol{\epsilon}_t}[m^{i-1}_{t+1}(\boldsymbol{\pi}_t)|\mathcal{E}_3]\tilde{d}_t.$$

It is now clear that the optimal value function has the desired form and what remains is to calculate the coefficient of $\tilde{d}_t$, i.e. $m^i_t(\boldsymbol{\theta}_t)$, to obtain the full recursion and conclude the proof. To this end, we use (C.13) and combine the

three cases we introduced previously:

$$
\begin{aligned}
m_t^i(\boldsymbol{\theta}_t) =& \mathbb{E}_{\boldsymbol{\epsilon}_t}[m_{t+1}^i(\boldsymbol{\pi}_t)|\mathcal{E}_1]\mathbb{P}\{\mathcal{E}_1\} + \mathbb{E}_{\boldsymbol{\epsilon}_t}[\pi_t^e - (\pi_t^r)^+|\mathcal{E}_2]\mathbb{P}\{\mathcal{E}_2\} + \mathbb{E}_{\boldsymbol{\epsilon}_t}[m_{t+1}^{i-1}(\boldsymbol{\pi}_t)|\mathcal{E}_3]\mathbb{P}\{\mathcal{E}_3\} \\
=& \mathbb{E}_{\boldsymbol{\epsilon}_t}[m_{t+1}^i(\boldsymbol{\lambda}_t(\boldsymbol{\theta}_t) + \boldsymbol{\epsilon}_t)|\mathcal{E}_1]\mathbb{P}\{\mathcal{E}_1\} \\
& + \mathbb{E}_{\boldsymbol{\epsilon}_t}[\lambda_t^e(\boldsymbol{\theta}_t) + \epsilon_t^e - (\lambda_t^e(\boldsymbol{\theta}_t) + \epsilon_t^r)^+|\mathcal{E}_2]\mathbb{P}\{\mathcal{E}_2\} \\
& + \mathbb{E}_{\boldsymbol{\epsilon}_t}[m_{t+1}^{i-1}(\boldsymbol{\lambda}_t(\boldsymbol{\theta}_t) + \boldsymbol{\epsilon}_t)|\mathcal{E}_3]\mathbb{P}\{\mathcal{E}_3\} \\
=& \mathbb{E}_{\boldsymbol{\epsilon}_t}[M_i(\boldsymbol{\theta}_t, \boldsymbol{\epsilon}_t)],
\end{aligned}
\tag{C.14}
$$

where we have used the price evolution equation we defined in (4.1) and the definition of $M(\boldsymbol{\theta}_t, \boldsymbol{\epsilon}_t)$ from (4.8). The proof is completed by backward induction over t where (4.6) is obtained at $t = 0$. ■

Appendix D

Proof of Theorem 4.2

With independent prices, we have $\boldsymbol{\pi}_t = \boldsymbol{\epsilon}_t$. Moreover, remaining demand, d_t, is the only element of state space. Therefore, the proposed form of the value function is automatically obtained since $m_t^i(\boldsymbol{\theta}_t)$ is no longer a function of $\boldsymbol{\theta}_t$ and hence $m_t^i(\boldsymbol{\theta}_t) = \hat{m}_t^i$. This is because $M_i(\boldsymbol{\theta}_t, \boldsymbol{\epsilon}_t)$ is no longer a function of $\boldsymbol{\theta}_t$, i.e. $M_i(\boldsymbol{\theta}_t, \boldsymbol{\epsilon}_t) = M_i(\boldsymbol{\epsilon}_t)$ and hence there would be no need to solve (4.9). Consequently, equations (4.7), (4.8) and (4.9) can be consolidated into a single recursion and conditional expected values can be approached directly. This is essentially what we establish in this proof.

First let us define $\epsilon_t^a = \pi_t^a \triangleq \pi_t^e - (\pi_t^r)^+$ as the effective price variable. Now, let us revisit the definition of $M_i(\boldsymbol{\epsilon}_t)$, in this case:

$$M_i(\boldsymbol{\epsilon}_t) = \begin{cases} \hat{m}_{t+1}^i & \hat{m}_{t+1}^i \leq \epsilon_t^a, \\ \epsilon_t^a & \hat{m}_{t+1}^{i-1} \leq \epsilon_t^a < \hat{m}_{t+1}^i, \\ \hat{m}_{t+1}^{i-1} & \epsilon_t^a < \hat{m}_{t+1}^{i-1}. \end{cases} \tag{D.1}$$

Note that the three cases in the above definition corresponds to the three events $\mathcal{E}_1$, $\mathcal{E}_2$ and $\mathcal{E}_3$ defined in (C.7), (C.8) and (C.9) respectively. Now, we can use this notation to obtain a closed form for (4.9), which would essentially be (4.14). Starting with (4.9):

$$
\begin{aligned}
\hat{m}_t^i &= \mathbb{E}_{\boldsymbol{\epsilon}_t}[M_i(\boldsymbol{\epsilon})] \\
&= \mathbb{E}_{\boldsymbol{\epsilon}_t}[\hat{m}_{t+1}^i|\mathcal{E}_1]\mathbb{P}\{\mathcal{E}_1\} + \mathbb{E}_{\boldsymbol{\epsilon}_t}[\epsilon_t^a|\mathcal{E}_2]\mathbb{P}\{\mathcal{E}_2\} + \mathbb{E}_{\boldsymbol{\epsilon}_t}[\hat{m}_{t+1}^{i-1}|\mathcal{E}_3]\mathbb{P}\{\mathcal{E}_3\} \\
&= \hat{m}_{t+1}^i\mathbb{P}\{\mathcal{E}_1\} + \underbrace{\mathbb{E}_{\boldsymbol{\epsilon}_t}[\epsilon_t^a|\mathcal{E}_2]\mathbb{P}\{\mathcal{E}_2\}}_{A} + \hat{m}_{t+1}^{i-1}\mathbb{P}\{\mathcal{E}_3\}
\end{aligned}
\tag{D.2}
$$

Now, using integration by parts:

$$
\begin{aligned}
A &= \int_{\hat{m}_{t+1}^{i-1}}^{\hat{m}_{t+1}^i} \zeta \, dF_t^a(\zeta) \\
&= \hat{m}_{t+1}^i F_t^a(\hat{m}_{t+1}^i) - \hat{m}_{t+1}^{i-1}F_t^a(\hat{m}_{t+1}^{i-1}) - \int_{\hat{m}_{t+1}^{i-1}}^{\hat{m}_{t+1}^i} F_t^a(\zeta)\, d\zeta \\
&= \hat{m}_{t+1}^i\mathbb{P}\{\overline{\mathcal{E}}_1\} - \hat{m}_{t+1}^{i-1}\mathbb{P}\{\mathcal{E}_3\} - G_t(\hat{m}_{t+1}^{i-1}, \hat{m}_{t+1}^i),
\end{aligned}
$$

where $\overline{\mathcal{E}}_1$ is the complement of event $\mathcal{E}_1$ and we have used definition (4.15). Plugging back for A in (D.2), we get:

$$
\begin{aligned}
\hat{m}_t^i &= \hat{m}_{t+1}^i\mathbb{P}\{\mathcal{E}_1\} + \hat{m}_{t+1}^i\mathbb{P}\{\overline{\mathcal{E}}_1\} - \hat{m}_{t+1}^{i-1}\mathbb{P}\{\mathcal{E}_3\} - G_t(\hat{m}_{t+1}^{i-1}, \hat{m}_{t+1}^i) + \hat{m}_{t+1}^{i-1}\mathbb{P}\{\mathcal{E}_3\} \\
&= \hat{m}_{t+1}^i - G_t(\hat{m}_{t+1}^{i-1}, \hat{m}_{t+1}^i),
\end{aligned}
$$

which is the desired result. ■

Appendix E

Proof of Theorem 5.1

We prove the result by establishing that the proposed optimal value function satisfies the Bellman equation and deriving the optimal policy on the way. As in Appendix A, we assume that the correlation function is well behaved and to avoid technicalities, assume existence of expected values, cdfs and integrals throughout.

Since the stage and final cost functions are assumed concave, linear in fact, and the dynamics is linear establishing concavity of the optimal value function is straightforward, hence we skip it here for brevity. As in the proof of 3.1 in Appendix A, a similar argument can be found in the proof of Proposition 1 in [79].

To establish part (a), we basically use backward induction on t, that is, we assume that the optimal value function has the desired form as in (5.12) for $t+1$:

$$J^*_{t+1}(x,\theta)=\sum_{j=0}^{n_P} m^j_{t+1}(\theta)[(x-j\bar{u})^+\wedge\bar{u}]+c_{t+1}(\theta)\bar{u}, \tag{E.1}$$

and then plug it into the Bellman equation to show its validity for t. Note that this form is valid for $t=T$ by simply setting $m^j_T(\theta)=m_T$, $\forall j$.

Using the Bellman equation, we need to show:

$$J_t^*(x_t,\theta_t)=\mathbb{E}_{\epsilon_t}[\max_u\{g_t(x_t,u)+\alpha_t J_{t+1}^*(x_{t+1},\theta_{t+1})\}], \tag{E.2}$$

Using the dynamics equations, (5.1) and (5.2), (E.2) is transformed to:

$$J_t^*(x_t,\theta_t)=\mathbb{E}_{\epsilon_t}[\max_u\left\{\pi_t u+\alpha_t J_{t+1}^*(x_t-u,\pi_t)\right\}], \tag{E.3}$$

noting that $\theta_{t+1}=\pi_t$ by definition.

Since $\underline{x}\le x_t\le\overline{x}$, there exists some $i\le n_P$ such that $i\bar{u}\le x_t\le(i+1)\bar{u}$. Hence, we can rewrite (E.1) as:

$$J_t^*(x_t,\theta)=\sum_{j=1}^{i-1}m_t^j(\theta)\bar{u}+m_t^i(\theta)[x_t-i\bar{u}]+c_t(\theta)\bar{u}. \tag{E.4}$$

Since $-\bar{u}\le u\le\bar{u}$, $(i-1)\bar{u}\le x_t-u\le(i+2)\bar{u}$, hence invoking a similar expansion on $J_{t+1}^*(x_t-u,\pi_t)$ and some rearrangement, we have:

$$\begin{aligned}
J_{t+1}^*(x_t-u,\pi_t)=&\sum_{j=1}^{i-2}m_{t+1}^j(\pi_t)\bar{u}+c_{t+1}(\pi_t)\bar{u} \\
&+m_{t+1}^{i-1}(\pi_t)[(x_t-u-(i-1)\bar{u})^+\wedge\bar{u}] \\
&+m_{t+1}^{i}(\pi_t)[(x_t-u-i\bar{u})^+\wedge\bar{u}] \\
&+m_{t+1}^{i+1}(\pi_t)(x_t-u-(i+1)\bar{u})^+, \\
\overset{(a)}{=}&\sum_{j=1}^{i-1}m_{t+1}^j(\pi_t)\bar{u}+m_{t+1}^i(\pi_t)\tilde{x}_t \\
&+c_{t+1}(\pi_t)\bar{u} \\
&-m_{t+1}^{i-1}(\pi_t)[(u-\tilde{x}_t)^+] \\
&+m_{t+1}^{i}(\pi_t)[((\tilde{x}_t-u)^+\wedge\bar{u})-\tilde{x}_t] \\
&+m_{t+1}^{i+1}(\pi_t)(\tilde{x}_t-u-\bar{u})^+
\end{aligned} \tag{E.5}$$

$$
\begin{aligned}
&= \sum_{j=1}^{i-1} m_{t+1}^{j}(\pi_t)\bar{u} + m_{t+1}^{i}(\pi_t)\tilde{x}_t \\
&\quad + c_{t+1}(\pi_t)\bar{u} \\
&\quad - m_{t+1}^{i-1}(\pi_t)(u - \tilde{x}_t)^+ \\
&\quad + m_{t+1}^{i}(\pi_t)[((\tilde{x}_t - u)^+ \wedge \bar{u}) - \tilde{x}_t] \\
&\quad + m_{t+1}^{i+1}(\pi_t)(\tilde{x}_t - u - \bar{u})^+
\end{aligned}
$$

where $\tilde{x}_t \triangleq x_t - i\bar{u}$. Now, substituting (E.5) in (E.3), we proceed as depicted in (E.7) where, (a) is obtained by using the fact that $-(\bullet)^+ = (-\bullet)^-$ and substitution and (b) is obtained by using the equality:

$$
-u \equiv [(\tilde{x}_t - u)^-] + [((\tilde{x}_t - u)^+ \wedge \bar{u}) - \tilde{x}_t] + (\tilde{x}_t - u - \bar{u})^+, \tag{E.6}
$$

and refactoring. Equality (E.6) can be verified to be valid for $-\bar{u} \leq u \leq \bar{u}$ and $0 \leq \tilde{x}_t \leq \bar{u}$ by simple conditioning and inspection.

$$
\begin{aligned}
J_t^*(x_t, \theta_t) &= \mathbb{E}_{\epsilon_t}\Big[\max_u \left\{\pi_t u + \alpha_t J_{t+1}^*(x_t - u, \pi_t)\right\}\Big] \qquad \text{(E.7)} \\
&\overset{(a)}{=} \mathbb{E}_{\epsilon_t}\Bigg[\max_u \Bigg\{\pi_t u + \alpha_t \Bigg(\sum_{j=1}^{i-1} m_{t+1}^{j}(\pi_t)\bar{u} + m_{t+1}^{i}(\pi_t)\tilde{x}_t + c_{t+1}(\pi_t)\bar{u} \\
&\qquad\qquad m_{t+1}^{i-1}(\pi_t)(\tilde{x}_t - u)^- + m_{t+1}^{i}(\pi_t)[((\tilde{x}_t - u)^+ \wedge \bar{u}) - \tilde{x}_t] \\
&\qquad\qquad + m_{t+1}^{i+1}(\pi_t)(\tilde{x}_t - u - \bar{u})^+\Bigg)\Bigg\}\Bigg]
\end{aligned}
$$

$$\stackrel{(b)}{=} \mathbb{E}_{\epsilon_t}\Bigg[\max_u \Bigg\{(\tilde{m}_{t+1}^{i-1}(\pi_t)-\pi_t)(\tilde{x}_t-u)^- + (\tilde{m}_{t+1}^{i}(\pi_t)-\pi_t)(((\tilde{x}_t-u)^+\wedge\bar{u})-\tilde{x}_t) + (\tilde{m}_{t+1}^{i+1}(\pi_t)-\pi_t)(\tilde{x}_t-u-\bar{u})^+\Bigg\} + \left(\sum_{j=1}^{i-1}\tilde{m}_{t+1}^{j}(\pi_t)\bar{u}+\tilde{m}_{t+1}^{i}(\pi_t)\tilde{x}_t+\alpha_t c_{t+1}(\pi_t)\bar{u}\right)\Bigg]$$

Now, note that the optimization is only on the first three terms in (E.7) since the sum is independent of u. Moreover, concavity of the value function, implies that m_τ^j is increasing in j; i.e. $m_\tau^j \leq m_\tau^{j'}$, $\forall j \geq j'$. This implies that the price dependent coefficients of the form $(\pi_t - \alpha_t m_{t+1}^j)$ are ordered as:

$$\pi_t-\alpha_t m_{t+1}^{i-1}(\pi_t)\leq\pi_t-\alpha_t m_{t+1}^{i}(\pi_t)\leq\pi_t-\alpha_t m_{t+1}^{i+1}(\pi_t). \tag{E.8}$$

Since the optimization problem at hand is piecewise linear in u, and the ordering of the coefficients as in (E.8), only four cases can happen depending on π_t, resulting in different signs of the coefficients. Let us label the events corresponding to each of these cases as:

$$e_1 \quad : \quad \pi_t\leq\alpha_t m_{t+1}^{i+1}(\pi_t) \tag{E.9}$$

$$e_2 \quad : \quad \alpha_t m_{t+1}^{i+1}(\pi_t)\leq\pi_t\leq\alpha_t m_{t+1}^{i}(\pi_t) \tag{E.10}$$

$$e_3 \quad : \quad \alpha_t m_{t+1}^{i}(\pi_t)\leq\pi_t\leq\alpha_t m_{t-1}^{i-1}(\pi_t) \tag{E.11}$$

$$e_4 \quad : \quad \alpha_t m_{t+1}^{i-1}(\pi_t)\leq\pi_t \tag{E.12}$$

In each case, the optimal u can be easily obtained by inspecting the corresponding term in the optimization problem in (E.7):

- Under e_1, all the coefficients are positive and hence all the terms involving u need to be maximized. This is achieved by minimizing u and setting $u^* = \underline{u} = -\bar{u}$.
- Under e_2, only the first two coefficients are positive and hence $u^* = \tilde{x}_t - \bar{u}$.
- Under e_3, only the first coefficient is positive and hence $u^* = \bar{u} - \tilde{x}_t$.
- Under e_4, all the coefficient are negative and hence all terms should be minimized. This is achieved by setting $u^* = \bar{u}$.

Therefore, using the definition of $\tilde{x}_t$, the optimal policy can be summarized as:

$$u^*(x_t, \pi_t) = \begin{cases} -\bar{u} & \text{if} \quad e_1, \\ x_t - (i+1)\bar{u} & \text{if} \quad e_2, \\ x_t - i\bar{u} & \text{if} \quad e_3, \\ \bar{u} & \text{if} \quad e_4. \end{cases}$$

The conditions defining e_k are not explicit. Therefore, to achieve the desired form in (5.18), we need to make the conditions explicit. Given the assumptions on $\lambda_t(\bullet)$, this is achieved by simply calculating the extended fixed point of the corresponding $\hat{m}^j_{t+1}$, as defined in (5.15).

Now we can plug the optimal policy and find the desired optimal value function, $J^*_t(x_t, \theta_t)$. To this end, we decompose the optimal value function to its conditionals over the partition formed by $\{e_k\}$:

$$J_t^*(x_t,\theta_t)=J_t^*(x_t,\theta_t|e_1)\mathbb{P}\{e_1\}+J_t^*(x_t,\theta_t|e_2)\mathbb{P}\{e_2\} \\ +J_t^*(x_t,\theta_t|e_3)\mathbb{P}\{e_3\}+J_t^*(x_t,\theta_t|e_4)\mathbb{P}\{e_4\}, \quad \text{(E.13)}$$

where,

$$\begin{aligned}
J_t^*(x,\theta_t|e_1)=&\sum_{j=1}^{i-1}\mathbb{E}_{\epsilon_t}[\tilde{m}_{t+1}^j(\pi_t)|e_1]\bar{u}\\
&+\alpha_t\mathbb{E}_{\epsilon_t}[c_{t+1}(\pi_t)|e_1]\bar{u}\\
&+\mathbb{E}_{\epsilon_t}[\tilde{m}_{t+1}^i(\pi_t)-\pi_t|e_1]\bar{u}\\
&+\mathbb{E}_{\epsilon_t}[\tilde{m}_{t+1}^{i+1}(\pi_t)|e_1][x-i\bar{u}],\\
J_t^*(x,\theta_t|e_2)=&\sum_{j=1}^{i-1}\mathbb{E}_{\epsilon_t}[\tilde{m}_{t+1}^j(\pi_t)|e_2]\bar{u}\\
&+\alpha_t\mathbb{E}_{\epsilon_t}[c_{t+1}(\pi_t)|e_2]\bar{u}\\
&+\mathbb{E}_{\epsilon_t}[\tilde{m}_{t+1}^i(\pi_t)-\pi_t|e_2]\bar{u}\\
&+\mathbb{E}_{\epsilon_t}[\pi_t|e_2][x-i\bar{u}],\\
J_t^*(x,\theta_t|e_3)=&\sum_{j=1}^{i-1}\mathbb{E}_{\epsilon_t}[\tilde{m}_{t+1}^j(\pi_t)|e_2]\bar{u}\\
&+\alpha_t\mathbb{E}_{\epsilon_t}[c_{t+1}(\pi_t)|e_3]\bar{u}\\
&+\mathbb{E}_{\epsilon_t}[\pi_t|e_3][x-i\bar{u}],\\
J_t^*(x,\theta_t|e_4)=&\sum_{j=1}^{i-1}\mathbb{E}_{\epsilon_t}[\tilde{m}_{t+1}^j(\pi_t)|e_4]\bar{u}\\
&+\alpha_t\mathbb{E}_{\epsilon_t}[c_{t+1}(\pi_t)|e_4]\bar{u}\\
&+\mathbb{E}_{\epsilon_t}[\pi_t-\tilde{m}_{t+1}^{i-1}(\pi_t)|e_4]\bar{u}\\
&+\mathbb{E}_{\epsilon_t}[\tilde{m}_{t+1}^{i-1}(\pi_t)|e_4][x-i\bar{u}].
\end{aligned} \quad \text{(E.14)}$$

Combining these results with (E.13) we conclude the desired form as claimed in (E.4) and equivalently (5.12). Now, what remains is to obtain recursions for $m_t^i(\theta_t)$ and $c_t(\theta_t)$, which are basically coefficients of $x - i\bar{u}$ and $\bar{u}$. To this end, we use the definitions of $M(\theta, \epsilon)$ and $C(\theta, \epsilon)$ as given in (5.14) and (5.17) respectively. Using (E.13) and (E.14):

$$\begin{aligned} m_t^i(\theta_t) =& \mathbb{E}_{\epsilon_t}[\tilde{m}_{t+1}^{i+1}(\lambda_t(\theta_t) + \epsilon_t)|e_1]\mathbb{P}\{e_1\} \\ &+ \mathbb{E}_{\epsilon_t}[\lambda_t(\theta_t) + \epsilon_t|e_2 \cup e_3]\mathbb{P}\{e_2 \cup e_3\} \\ &+ \mathbb{E}_{\epsilon_t}[\tilde{m}_{t+1}^{i-1}(\lambda_t(\theta_t) + \epsilon_t)|e_4]\mathbb{P}\{e_4\} \\ =& \mathbb{E}_{\epsilon_t}[M(\theta_t, \epsilon_t)]. \end{aligned} \tag{E.15}$$

Similarly:

$$\begin{aligned} c_t(\theta_t) =& \mathbb{E}_{\epsilon_t}[\alpha_t c_{t+1}(\pi_t)] \\ &+ \mathbb{E}_{\epsilon_t}[\tilde{m}_{t+1}^{i}(\pi_t) - \pi_t|e_1 \cup e_2]\mathbb{P}\{e_1 \cup e_2\} \\ &+ \mathbb{E}_{\epsilon_t}[\pi_t - \tilde{m}_{t+1}^{i-1}(\pi_t)|e_4]\mathbb{P}\{e_4\} \\ =& \mathbb{E}_{\epsilon_t}[C(\theta_t, \epsilon_t)]. \end{aligned} \tag{E.16}$$

■

Appendix F

Proof of Theorem 5.2

Under price independence assumption, i.e. $\lambda_t(\bullet) = 0, \forall t$, the state space only consists of SoC. Moreover, there is no need for calculation of fixed points since the conditions defining events e_k automatically become explicit. More simplification in the corresponding recursions can be made as well, which is mainly what is claimed by this theorem.

To this end, we treat the corresponding recursions for m_t^i and c_t directly by expanding the corresponding expectations noting that the price independence assumption results in $\pi_t = \epsilon_t$. Using (E.15), we have:

$$m_t^i = \tilde{m}_{t+1}^{i+1}\mathbb{P}\{e_1\} + \underbrace{\mathbb{E}_{\epsilon_t}[\epsilon_t | e_2 \cup e_3]\mathbb{P}\{e_2 \cup e_3\}}_{A} + \tilde{m}_{t+1}^{i-1}\mathbb{P}\{e_4\}. \tag{F.1}$$

Now, by definition of the conditional expected value and using integration by parts:

$$\begin{aligned} A &= \int_{\tilde{m}_{t+1}^{i+1}}^{\tilde{m}_{t+1}^{i-1}} \zeta \, dF_t(\zeta) \\ &= \tilde{m}_{t+1}^{i-1} F_t(\tilde{m}_{t+1}^{i-1}) - \tilde{m}_{t+1}^{i+1} F_t(\tilde{m}_{t+1}^{i+1}) - \int_{\tilde{m}_{t+1}^{i+1}}^{\tilde{m}_{t+1}^{i-1}} F_t(\zeta)\, d\zeta \\ &= \tilde{m}_{t+1}^{i-1}\mathbb{P}\{\bar{e}_4\} - \tilde{m}_{t+1}^{i+1}\mathbb{P}\{e_1\} - G_t(\tilde{m}_{t+1}^{i+1}, \tilde{m}_{t+1}^{i-1}), \end{aligned}$$

where $\bar{e}_k$ is the complement of e_k. Plugging for A in (F.1):

$$m_t^i = \tilde{m}_{t+1}^{i-1} - G_t(\tilde{m}_{t+1}^{i+1}, \tilde{m}_{t+1}^{i-1}).$$

Similarly, using (E.16), we have:

$$\begin{aligned} c_t=&\alpha_t c_{t+1}+\mathbb{E}_{\epsilon_t}[\tilde{m}^i_{t+1}-\epsilon_t|e_1\cup e_2]\mathbb{P}\{e_1\cup e_2\}\\ &+\mathbb{E}_{\epsilon_t}[\epsilon_t-\tilde{m}^{i-1}_{t+1}|e_4]\mathbb{P}\{e_4\}\\ =&\alpha_t c_{t+1}+\tilde{m}^i_{t+1}\mathbb{P}\{e_1\cup e_2\}-\tilde{m}^{i-1}_{t+1}\mathbb{P}\{e_4\}\\ &-\underbrace{\mathbb{E}_{\epsilon_t}[\epsilon_t|e_1\cup e_2]\mathbb{P}\{e_1\cup e_2\}}_{A'}+\underbrace{\mathbb{E}_{\epsilon_t}[\epsilon_t|e_4]\mathbb{P}\{e_4\}}_{B'} \end{aligned} \tag{F.2}$$

Similar to A:

$$\begin{aligned} A' &= \int_{-\infty}^{\tilde{m}^i_{t+1}} \zeta\, dF_t(\zeta)\\ &= \tilde{m}^i_{t+1}F_t(\tilde{m}^i_{t+1}) + \int_{-\infty}^{\tilde{m}^i_{t+1}} F_t(\zeta)\, d\zeta\\ &= \tilde{m}^i_{t+1}\mathbb{P}\{e_1\cup e_2\}-G_t(-\infty,\tilde{m}^i_{t+1}), \end{aligned}$$

$$\begin{aligned} B' &= \int_{\tilde{m}^{i-1}_{t+1}}^{\infty} \zeta\, dF_t(\zeta)\\ &= \tilde{m}^{i-1}_{t+1}(1-F_t(\tilde{m}^{i-1}_{t+1})) + \int_{\tilde{m}^{i-1}_{t+1}}^{\infty} (1-F_t(\zeta))\, d\zeta\\ &= \tilde{m}^{i-1}_{t+1}\mathbb{P}\{e_4\}+\bar{G}_t(\tilde{m}^{i-1}_{t+1},\infty), \end{aligned}$$

Now using A' and B':

$$c_t=\alpha_t c_{t+1}+G_t(-\infty,\tilde{m}^i_{t+1})+\bar{G}_t(\tilde{m}^{i-1}_{t+1},\infty),$$

which is the desired result. ■

Bibliography

[1] GNU linear programming kit. http://www.gnu.org/software/glpk/.

[2] Gurobi optimizer. http://www.gurobi.com/.

[3] MOSEK optimization software. http://www.mosek.com/.

[4] D. Aigner. The residential electricity time-of-use pricing experiments: What have we learned? http://www.nber.org/chapters/c8372.pdf, 1985.

[5] A.T. Al-Awami and E. Sortomme. Coordinating vehicle-to-grid services with energy trading. *Smart Grid, IEEE Transactions on*, 3(1):453–462, March 2012. ISSN 1949-3053. doi:10.1109/TSG.2011.2167992.

[6] M. Alizadeh, A. Scaglione, J. Davies, and K.S. Kurani. A scalable stochastic model for the electricity demand of electric and plug-in hybrid vehicles. *Smart Grid, IEEE Transactions on*, 5(2):848–860, March 2014. ISSN 1949-3053. doi:10.1109/TSG.2013.2275988.

[7] Mahnoosh Alizadeh, Tsung-hui Chang, and Anna Scaglione. Grid integration of distributed renewables through coordinated demand response. In *Decision and Control (CDC), 2012 IEEE 51st Annual Conference on*, pages 3666–3671. IEEE, 2012.

[8] Mahnoosh Alizadeh, Anna Scaglione, and George Kesidis. Scalable model predictive control of demand for ancillary services. In *Smart Grid Communications (SmartGridComm), IEEE International Conference on*, pages 684–689. IEEE, 2013.

[9] Mahnoosh Alizadeh, Yuanzhang Xiao, Anna Scaglione, and Mihaela van der Schaar. Dynamic incentive design for participation in direct load scheduling programs. 2013.

[10] Steven Craig Anderson. *Analyzing strategic interaction in multi-settlement electricity markets: A closed-loop supply function equilibrium model*. PhD thesis, Harvard University Cambridge, Massachusetts, 2004.

[11] Fernando Banez-Chicharro, Jesus M. Latorre, and Andres Ramos. Smart charging profiles for electric vehicles. *Computational Management Science*, 11(1-2):87–110, 2014. ISSN 1619-697X. doi:10.1007/s10287-013-0180-8. URL `http://dx.doi.org/10.1007/s10287-013-0180-8`.

[12] Arthur R. Bergen and Vijay Vittal. *Power Systems Analysis, 2nd Edition*. Prentice Hall, Inc., 2000.

[13] D.P. Bertsekas. *Dynamic Programming and Optimal Control: Volume I*. Athena Scientific, 2005. ISBN 9781886529267. URL `http://books.google.com/books?id=-E5qQgAACAAJ`.

[14] E. Bilgin and M.C. Caramanis. Decision support for offering load-side regulation service reserves in competitive power markets. In *Decision and*

Control (CDC), 2013 IEEE 52nd Annual Conference on, pages 5628–5635, Dec 2013. doi:10.1109/CDC.2013.6760776.

[15] E. Bilgin, M.C. Caramanis, and I.C. Paschalidis. Smart building real time pricing for offering load-side regulation service reserves. In *Decision and Control (CDC), 2013 IEEE 52nd Annual Conference on*, pages 4341–4348, Dec 2013. doi:10.1109/CDC.2013.6760557.

[16] John R Birge and Francois Louveaux. *Introduction to stochastic programming*. Springer, 2011.

[17] E. Bitar and S. Low. Deadline differentiated pricing of deferrable electric power service. In *Decision and Control (CDC), 2012 IEEE 51st Annual Conference on*, pages 4991–4997, Dec 2012. doi:10.1109/CDC.2012.6425944.

[18] E. Bitar and X. Xu. On incentive compatibility of deadline differentiated pricing for deferrable demand. In *Decision and Control (CDC), 2013 IEEE 52st Annual Conference on*, pages 4991–4997, Dec 2013. doi:10.1109/CDC.2013.6425944.

[19] E. Bitar, R. Rajagopal, P. Khargonekar, and K. Poolla. The role of co-located storage for wind power producers in conventional electricity markets. In *American Control Conference (ACC), 2011*, pages 3886–3891, June 2011.

[20] California ISO. Demand Response in California ISO. http://www.caiso.com/participate/Pages/Load/DemandResponse/Default.aspx, .

[21] California ISO. Market processes. http://www.caiso.com/market/Pages/MarketProcesses.aspx, .

[22] M. Caramanis, I.C. Paschalidis, C. Cassandras, E. Bilgin, and E. Ntakou. Provision of regulation service reserves by flexible distributed loads. In *Decision and Control (CDC), 2012 IEEE 51st Annual Conference on*, pages 3694–3700, Dec 2012. doi:10.1109/CDC.2012.6426025.

[23] M.C. Caramanis and J.M. Foster. Coupling of day ahead and real-time power markets for energy and reserves incorporating local distribution network costs and congestion. In *Communication, Control, and Computing (Allerton), 2010 48th Annual Allerton Conference on*, pages 42–49, Sept 2010. doi:10.1109/ALLERTON.2010.5706886.

[24] M.C. Caramanis, E. Goldis, P.A. Ruiz, and A. Rudkevich. Power market reform in the presence of flexible schedulable distributed loads. new bid rules, equilibrium and tractability issues. In *Communication, Control, and Computing (Allerton), 2012 50th Annual Allerton Conference on*, pages 1089–1096, Oct 2012. doi:10.1109/Allerton.2012.6483339.

[25] Michael C. Caramanis and Justin M. Foster. Management of electric vehicle charging to mitigate renewable generation intermittency and distri-

bution network congestion. In *IEEE CDC*, pages 4717–4722, Shanghai, China, 2009. doi:10.1109/CDC.2009.5399955.

[26] Michael C. Caramanis, Justin M. Foster, and Evegeniy A. Goldis. Load participation in electricity markets: Day-Ahead and Hour-Ahead market coupling with Wholesale/Transmission and Retail/Distribution cost and congestion modeling. In *IEEE SmartGridComm.*, pages 513–518, Gaithersburg, MD, 2010. doi:10.1109/SMARTGRID.2010.5622096.

[27] ChargePoint. `http://www.chargepoint.com/`.

[28] H. Chavez, R. Baldick, and S. Sharma. Regulation adequacy analysis under high wind penetration scenarios in ERCOT nodal. *IEEE Transactions on Sustainable Energy*, 3(4):743 –750, October 2012. ISSN 1949-3029. doi:10.1109/TSTE.2012.2200050.

[29] K.W. Cheung, P. Shamsollahi, David Sun, J. Milligan, and M. Potishnak. Energy and ancillary service dispatch for the interim iso new england electricity market. In *Power Industry Computer Applications, 1999. PICA '99. Proceedings of the 21st 1999 IEEE International Conference*, pages 47–53, Jul 1999. doi:10.1109/PICA.1999.779384.

[30] K. Clement, E. Haesen, and J. Driesen. Coordinated charging of multiple plug-in hybrid electric vehicles in residential distribution grids. In *Power Systems Conference and Exposition, 2009. PSCE '09. IEEE/PES*, pages 1–7, March 2009. doi:10.1109/PSCE.2009.4839973.

[31] K. Clement-Nyns, E. Haesen, and J. Driesen. The impact of charging plug-in hybrid electric vehicles on a residential distribution grid. *Power Systems, IEEE Transactions on*, 25(1):371–380, Feb 2010. ISSN 0885-8950. doi:10.1109/TPWRS.2009.2036481.

[32] Michael A. Crew, Chitru S. Fernando, and Paul R. Kleindorfer. The theory of peak-load pricing: A survey. *Journal of Regulatory Economics*, 8(3):215–248, 1995. ISSN 0922-680X. doi:10.1007/BF01070807.

[33] D. Dallinger, D. Krampe, and M. Wietschel. Vehicle-to-grid regulation reserves based on a dynamic simulation of mobility behavior. *Smart Grid, IEEE Transactions on*, 2(2):302–313, June 2011. ISSN 1949-3053. doi:10.1109/TSG.2011.2131692.

[34] Stacy C. Davis, Susan W. Diegel, and Robert G. Boundy. *Transportation Energy Data Book, Edition 31.* U.S. Department of Energy, Office of Energy Efficiency and Renewable Energy, July 2012.

[35] Paul Denholm and Ramteen Sioshansi. The value of compressed air energy storage with wind in transmission-constrained electric power systems. *Energy Policy*, 37(8):3149–3158, August 2009. ISSN 0301-4215. doi:10.1016/j.enpol.2009.04.002.

[36] K.C. Divya and Jacob Østergaard. Battery energy storage technology for power systems?An overview. *Electric Power Systems Research*, 79(4): 511–520, April 2009. ISSN 0378-7796. doi:10.1016/j.epsr.2008.09.017.

[37] eGauge Systems. http://www.egauge.net/.

[38] Environmental Protection Agency (EPA). Electric vehicles: Compare side-by-side. http://fueleconomy.gov/feg/evsbs.shtml, 2011.

[39] Jim Eyer and Garth Corey. Energy storage for the electricity grid: Benefits and market potential assessment guide. *Sandia National Laboratories*, 2010.

[40] Ali Faghih, Mardavij Roozbehani, and Munther A. Dahleh. On the economic value and price-responsiveness of ramp-constrained storage. *arXiv:1211.1696 [math]*, nov 2012.

[41] Federal Energy Regulatory Commission (FERC). Demand response compensation in organized wholesale energy markets (final rule). Mar. 2011.

[42] Federal Energy Regulatory Commission (FERC). Frequency regulation compensation in organized wholesale power markets (final rule). Oct. 2011.

[43] Federal Highwy Administration (FHWA). State motor-vehicle registrations. http://www.fhwa.dot.gov/policyinformation/statistics/2010/xls/mv1.xls, 2010.

[44] J.M. Foster and M.C. Caramanis. Optimal power market participation of plug-in electric vehicles pooled by distribution feeder. *Power Systems, IEEE Transactions on*, 28(3):2065–2076, Aug 2013. ISSN 0885-8950. doi:10.1109/TPWRS.2012.2232682.

[45] Justin M. Foster and Michael Caramanis. Energy reserves and clearing in stochastic power markets: The case of plug-in-hybrid electric vehicle battery charging. In *IEEE CDC*, Atlanta, GA, USA, 2010.

[46] Matthias D. Galus and G. Andersson. Demand management of grid connected plug-in hybrid electric vehicles (phev). In *Energy 2030 Conference, 2008. ENERGY 2008. IEEE*, pages 1–8, Nov 2008. doi:10.1109/ENERGY.2008.4781014.

[47] Matthias D. Galus and G. Andersson. Integration of plug-in hybrid electric vehicles into energy networks. In *PowerTech, 2009 IEEE Bucharest*, pages 1–8, June 2009. doi:10.1109/PTC.2009.5282135.

[48] Matthias D. Galus, R. La Fauci, and G. Andersson. Investigating phev wind balancing capabilities using heuristics and model predictive control. In *Power and Energy Society General Meeting, 2010 IEEE*, pages 1–8, July 2010. doi:10.1109/PES.2010.5589267.

[49] Matthias D. Galus, S. Koch, and G. Andersson. Provision of load frequency control by phevs, controllable loads, and a cogeneration unit. *Industrial Electronics, IEEE Transactions on*, 58(10):4568–4582, Oct 2011. ISSN 0278-0046. doi:10.1109/TIE.2011.2107715.

[50] Stephen P Holland and Erin T Mansur. Is Real-Time pricing green? the environmental impacts of electricity demand variance. *Review of Economics and Statistics*, 90(3):550–561, 2008. doi:10.1162/rest.90.3.550.

[51] IBM ILOG. CPLEX optimizer. http://www.ibm.com/software/commerce/optimization/cplex-optimizer/.

[52] ISO New England. Rules and procedures. http://www.iso-ne.com/rules_proceds/index.html.

[53] Chenrui Jin, Jian Tang, and P. Ghosh. Optimizing electric vehicle charging with energy storage in the electricity market. *Smart Grid, IEEE Transactions on*, 4(1):311–320, March 2013. ISSN 1949-3053. doi:10.1109/TSG.2012.2218834.

[54] R. Kamat and S.S. Oren. Multi-settlement systems for electricity markets: zonal aggregation under network uncertainty and market power. In *Proceedings of the 35th Annual Hawaii International Conference onSystem Sciences (HICSS)*, pages 739–748, Jan 2002. doi:10.1109/HICSS.2002.993956.

[55] Mahdi Kefayati and Ross Baldick. Energy delivery transaction pricing for flexible electrical loads. In *2011 IEEE International Conference on Smart Grid Communications (SmartGridComm)*, pages 363–368, Brussels, Belgium, October 2011. ISBN 978-1-4577-1704-8. doi:10.1109/SmartGridComm.2011.6102348.

[56] Mahdi Kefayati and Ross Baldick. Harnessing demand flexibility to match renewable production using localized policies. In *50th Annual Allerton Conference on Communication, Control and Computing*, Allerton, IL, October 2012.

[57] Mahdi Kefayati and Ross Baldick. On energy delivery to delay averse flexible loads: Optimal algorithm, consumer value and network level impacts. In *Proceedings of the 51st IEEE Conference on Decision and Control (CDC)*, Maui, HI, December 2012.

[58] Mahdi Kefayati and Constantine Caramanis. Efficient energy delivery management for PHEVs. In *2010 IEEE International Conference on Smart Grid Communications (SmartGridComm)*, pages 525–530, Gaithersburg, MD, October 2010. doi:10.1109/SMARTGRID.2010.5621990.

[59] Willett Kempton and Jasna Tomić. Vehicle-to-grid power fundamentals: Calculating capacity and net revenue. *Journal of Power Sources*, 144(1): 268 – 279, 2005. ISSN 0378-7753. doi:10.1016/j.jpowsour.2004.12.025.

[60] Willett Kempton and Jasna Tomić. Vehicle-to-grid power implementation: From stabilizing the grid to supporting large-scale renewable energy. *Journal of Power Sources*, 144(1):280 – 294, 2005. ISSN 0378–7753. doi:10.1016/j.jpowsour.2004.12.022.

[61] Mobashwir Khan and Kara M. Kockelman. Predicting the market potential of plug-in electric vehicles using multiday GPS data. *Energy Policy*, 46:225–233, July 2012. ISSN 0301-4215. doi:10.1016/j.enpol.2012.03.055.

[62] M. Kintner-Meyer, K. Schneider, and R. Pratt. Impacts assessment of plug-in hybrid vehicles on electric utilities and regional US power grids,

part 1: Technical analysis. *Pacific Northwest National Laboratory (a)*, 2007.

[63] Magnus Korpaas, Arne T. Holen, and Ragne Hildrum. Operation and sizing of energy storage for wind power plants in a market system. *International Journal of Electrical Power & Energy Systems*, 25(8):599–606, October 2003. ISSN 0142-0615. doi:10.1016/S0142-0615(03)00016-4.

[64] Lawrence Livermore National Laboratory. Estimated U.S. energy use in 2011. `https://flowcharts.llnl.gov/content/energy/energy_archive/energy_flow_2011/LLNLUSEnergy2011.png`, 2011.

[65] J. Löfberg. YALMIP : A toolbox for modeling and optimization in MATLAB. In *Proceedings of the CACSD Conference*, Taipei, Taiwan, 2004.

[66] Zhongjing Ma, D.S. Callaway, and I.A. Hiskens. Decentralized charging control of large populations of plug-in electric vehicles. *Control Systems Technology, IEEE Transactions on*, 21(1):67–78, Jan 2013. ISSN 1063-6536. doi:10.1109/TCST.2011.2174059.

[67] MathWorks. MATLAB. `http://www.mathworks.com/products/matlab/`.

[68] Microsoft Solver Foundation. `http://msdn.microsoft.com/en-us/library/ff524509%28v=vs.93%29.aspx`.

[69] Midcontinent Independent System Operator, Inc. Demand Response in the Midcontinent ISO. https://www.misoenergy.org/WHATWEDO/STRATEGICINITIATIVES/Pages/DemandResponse.aspx, .

[70] Midcontinent Independent System Operator, Inc. Business practices manuals. https://www.misoenergy.org/Library/BusinessPracticesManuals/Pages/BusinessPracticesManuals.aspx, .

[71] Hans Mittelmann. Benchmarks for optimization software. http://plato.la.asu.edu/bench.html.

[72] Amir-Hamed Mohsenian-Rad and Alberto Leon-Garcia. Optimal residential load control with price prediction in Real-Time electricity pricing environments. *Smart Grid, IEEE Transactions on*, 1(2):120–133, 2010. ISSN 1949-3053. doi:10.1109/TSG.2010.2055903.

[73] Amir-Hamed Mohsenian-Rad, Vincent W. S. Wong, Juri Jatskevich, Robert Schober, and Alberto Leon-Garcia. Autonomous Demand-Side management based on Game-Theoretic energy consumption scheduling for the future smart grid. *IEEE Transactions on Smart Grid*, 1(3):320–331, 2010. ISSN 1949-3053. doi:10.1109/TSG.2010.2089069.

[74] I. Momber, G. Morales-Espana, A. Ramos, and T. Gomez. Pev storage in multi-bus scheduling problems. *Smart Grid, IEEE Transactions on*, 5(2):1079–1087, March 2014. ISSN 1949-3053. doi:10.1109/TSG.2013.2290594.

[75] National Renewable Energy Lab. (NREL). NREL Secure Transportation Data Project. http://www.nrel.gov/vehiclesandfuels/secure_transportation_data.html, 2010.

[76] M.J. Neely, A.S. Tehrani, and A.G. Dimakis. Efficient algorithms for renewable energy allocation to delay tolerant consumers. In *IEEE SmartGridComm*, pages 549–554, Gaithersburg, MD, 2010. doi:10.1109/SMARTGRID.2010.5621993.

[77] New York ISO. Market manuals. http://www.nyiso.com/public/markets_operations/documents/manuals_guides/index.jsp.

[78] Hui Niu, R. Baldick, and Guidong Zhu. Supply function equilibrium bidding strategies with fixed forward contracts. *Power Systems, IEEE Transactions on*, 20(4):1859–1867, Nov 2005. ISSN 0885-8950. doi:10.1109/TPWRS.2005.857272.

[79] Anthony Papavasiliou and Shmuel S. Oren. Supplying renewable energy to deferrable loads: Algorithms and economic analysis. In *IEEE PES General Meeting*, pages 1–8, Minneapolis, MN, 2010. doi:10.1109/PES.2010.5589405.

[80] Heejung Park. *Electric transmission system expansion planning for the system with uncertain intermittent renewable resources*. PhD thesis, The University of Texas at Austin, Austin, TX, 2013.

[81] Heejung Park and Ross Baldick. Transmission planning under uncertainties of wind and load: Sequential approximation approach. *Power Systems, IEEE Transactions on*, 28(3):2395–2402, Aug 2013. ISSN 0885-8950. doi:10.1109/TPWRS.2013.2251481.

[82] RobertH. Patrick and FrankA. Wolak. Real-time pricing and demand side participation in restructured electricity markets. In Ahmad Faruqui and B.Kelly Eakin, editors, *Electricity Pricing in Transition*, volume 42 of *Topics in Regulatory Economics and Policy Series*, pages 345–360. Springer US, 2002. ISBN 978-1-4613-5261-7. doi:10.1007/978-1-4615-0833-5_23. URL `http://dx.doi.org/10.1007/978-1-4615-0833-5_23`.

[83] M. Peydayesh and R. Baldick. Modeling power system to study frequency control. *submitted to IEEE Transactions on Power Systems*, May 2014.

[84] PJM. Market manuals. `http://www.pjm.com/documents/manuals.aspx`.

[85] Junjie Qin, R. Sevlian, D. Varodayan, and R. Rajagopal. Optimal electric energy storage operation. pages 1–6. IEEE, July 2012. ISBN 978-1-4673-2729-9, 978-1-4673-2727-5, 978-1-4673-2728-2. doi:10.1109/PESGM.2012.6345242. URL `http://ieeexplore.ieee.org/lpdocs/epic03/wrapper.htm?arnumber=6345242`.

[86] Andres Ramos, Kristin Dietrich, Fernando Banez-Chicharro, Luis Olmos, and Jesus M. Latorre. Analysis of the impact of increasing shares of electric vehicles on the integration of res generation. In Miguel A. Sanz-Bobi, editor, *Use, Operation and Maintenance of Renewable Energy Systems*, Green Energy and Technology, pages 371–385. Springer International Publishing, 2014. ISBN 978-3-319-03223-8. doi:10.1007/978-3-319-03224-5_11. URL `http://dx.doi.org/10.1007/978-3-319-03224-5_11`.

[87] Nicola Secomandi. Optimal commodity trading with a capacitated storage asset. *Management Science*, 56(3):449–467, March 2010. ISSN 0025-1909, 1526-5501. doi:10.1287/mnsc.1090.1049. URL `http://pubsonline.informs.org/doi/abs/10.1287/mnsc.1090.1049`.

[88] R. Sioshansi. OR FORUM–Modeling the impacts of electricity tariffs on Plug-In hybrid electric vehicle charging, costs, and emissions. *Operations Research*, February 2012. ISSN 0030-364X, 1526-5463. doi:10.1287/opre.1120.1038.

[89] Kandler Smith, Matthew Earleywine, Eric Wood, and Ahmad Pesaran. Battery wear from disparate duty-cycles: Opportunities for electric-drive vehicle battery health management. In *2012 American Control Conference (ACC)*, Montreal, Canada, June 2012.

[90] E. Sortomme and M.A. El-Sharkawi. Optimal power flow for a system of microgrids with controllable loads and battery storage. In *Power*

Systems Conference and Exposition, 2009. PSCE '09. IEEE/PES, pages 1–5, March 2009. doi:10.1109/PSCE.2009.4840050.

[91] E. Sortomme and M.A. El-Sharkawi. Optimal charging strategies for unidirectional vehicle-to-grid. *Smart Grid, IEEE Transactions on*, 2(1): 131–138, March 2011. ISSN 1949-3053. doi:10.1109/TSG.2010.2090910.

[92] E. Sortomme and M.A. El-Sharkawi. Optimal combined bidding of vehicle-to-grid ancillary services. *Smart Grid, IEEE Transactions on*, 3 (1):70–79, March 2012. ISSN 1949-3053. doi:10.1109/TSG.2011.2170099.

[93] E. Sortomme and M.A. El-Sharkawi. Optimal scheduling of vehicle-to-grid energy and ancillary services. *Smart Grid, IEEE Transactions on*, 3(1):351–359, March 2012. ISSN 1949-3053.

[94] E. Sortomme, M.M. Hindi, S.D.J. MacPherson, and S.S. Venkata. Coordinated charging of plug-in hybrid electric vehicles to minimize distribution system losses. *Smart Grid, IEEE Transactions on*, 2(1):198–205, March 2011. ISSN 1949-3053. doi:10.1109/TSG.2010.2090913.

[95] A. Subramanian, J.A. Taylor, E. Bitar, D. Callaway, K. Poolla, and P. Varaiya. Optimal power and reserve capacity procurement policies with deferrable loads. In *Decision and Control (CDC), 2012 IEEE 51st Annual Conference on*, pages 450–456, Dec 2012. doi:10.1109/CDC.2012.6426102.

[96] S. Teleke, M.E. Baran, A.Q. Huang, S. Bhattacharya, and L. Anderson. Control strategies for battery energy storage for wind farm dispatching. *IEEE Transactions on Energy Conversion*, 24(3):725–732, September 2009. ISSN 0885-8969. doi:10.1109/TEC.2009.2016000.

[97] The Electric Reliability Council of Texas (ERCOT). `http://www.ercot.com/`, .

[98] The Electric Reliability Council of Texas (ERCOT). Demand Response in ERCOT. `http://www.ercot.com/services/programs/load/`, .

[99] The Electric Reliability Council of Texas (ERCOT). Market rules. `http://www.ercot.com/mktrules`.

[100] The Electric Reliability Council of Texas (ERCOT). Draft FRRS governing document 10.16.12. `http://www.ercot.com/mktrules/pilots/frrs/index`, Oct. 2012.

[101] The OpenADR Allicance. OpenADR 2.0 specifications. `http://www.openadr.org/specification`.

[102] Jasna Tomić and Willett Kempton. Using fleets of electric-drive vehicles for grid support. *Journal of Power Sources*, 168(2):459 – 468, 2007. ISSN 0378-7753. doi:10.1016/j.jpowsour.2007.03.010.

[103] Konstantin Turitsyn, Nikolai Sinitsyn, Scott Backhaus, and Misha Chertkov. Robust Broadcast-Communication control of electric vehicle charging. *1006.0165*, June 2010.

[104] Konstantin Turitsyn, Scott Backhaus, Maxim Ananyev, and Michael Chertkov. Smart finite state devices: A modeling framework for demand response technologies. In *2011 50th IEEE Conference on Decision and Control and European Control Conference (CDC-ECC)*, pages 7–14, December 2011. doi:10.1109/CDC.2011.6160649.

[105] W. Tushar, W. Saad, H.V. Poor, and D.B. Smith. Economics of electric vehicle charging: A game theoretic approach. *Smart Grid, IEEE Transactions on*, 3(4):1767–1778, Dec 2012. ISSN 1949-3053. doi:10.1109/TSG.2012.2211901.

[106] U.S. Department of Transportation (DoT). NHTS Data Center. `http://nhts.ornl.gov/download.shtml`, 2011.

[107] U.S. Energy Information Administration (EIA). How is electricity used in U.S. homes? `http://www.eia.doe.gov/tools/faqs/faq.cfm?id=96&t=3`, 2009.

[108] U.S. Energy Information Administration (EIA). Estimated U.S. residential electricity consumption by end-use. `http://www.eia.gov/tools/faqs/faq.cfm?id=96&t=3`, 2010.

[109] Daniel J. Veit, Anke Weidlich, Jian Yao, and Shmuel S. Oren. Simulating the dynamics in two-settlement electricity markets via an agent-based approach. *International Journal of Management Science and Engineering Management*, 1(2):83–97, 2006. doi:10.1080/17509653.2006.10671000.

[110] Frank A. Wolak. An experimental comparison of critical peak and hourly pricing: The PowerCentsDC program. `http://bit.ly/hF0OV0`, 2010.

[111] J. Yao, S.S. Oren, and I. Adler. Computing cournot equilibria in two settlement electricity markets with transmission constraint. In *Proceedings of the 37th Annual Hawaii International Conference on System Sciences (HICSS)*, pages 1–9, Jan 2004. doi:10.1109/HICSS.2004.1265176.

[112] Taiyou Yong, C.R. Philbrick, R. Entriken, and A. Tuohy. Multi-settlement simulation of reserve procurement using stochastic optimal power flow. In *Power and Energy Society General Meeting, 2012 IEEE*, pages 1–7, July 2012. doi:10.1109/PESGM.2012.6345665.

[113] C. Zhao, U. Topcu, N. Li, and S. Low. Design and stability of load-side primary frequency control in power systems. *Automatic Control, IEEE Transactions on*, 59(5):1177–1189, May 2014. ISSN 0018-9286. doi:10.1109/TAC.2014.2298140.

[114] Changhong Zhao, U. Topcu, and S. Low. Swing dynamics as primal-dual algorithm for optimal load control. In *Smart Grid Communications (SmartGridComm), 2012 IEEE Third International Conference on*, pages 570–575, Nov 2012. doi:10.1109/SmartGridComm.2012.6486046.

[115] Changhong Zhao, U. Topcu, and S.H. Low. Fast load control with stochastic frequency measurement. In *Power and Energy Society General Meeting, 2012 IEEE*, pages 1–8, July 2012. doi:10.1109/PESGM.2012.6344781.

[116] Changhong Zhao, Ufuk Topcu, and S.H. Low. Frequency-based load control in power systems. In *American Control Conference (ACC), 2012*, pages 4423–4430, June 2012.

Vita

Mahdi Kefayati received his BSc Degree in Electrical Engineering from University of Tehran, Iran in 2004. In the same year, he joined the graduate program of Sharif University of Technology and earned his MSc in Information Technology in 2007. He pursued his studies joining the graduate program at the University of Texas at Austin, in the same year. From 2007 to 2011, he was a member of the Wireless Communication and Networking Group (WNCG) where he focused on problems in wireless communication, estimation over lossy networks and smart energy systems. He moved to Energy Systems Lab to pursue his interests in smart energy systems and finished his PhD in 2014 under supervision of Professor Ross Baldick. He served as a research intern at Fujitsu Labs of America form June 2012 to January 2013. From June 2013 to September 2013, he worked at Electric Power Engineering (EPE) Consultants as a software engineering intern. He has chaired multiple sessions in conferences and delivered multiple invited talks beyond publishing more than ten peer-reviewed papers.

Email address: kefayati@utexas.edu, kefayati@gmail.com

This dissertation was typeset with LaTeX[†] by the author.

[†]LaTeX is a document preparation system developed by Leslie Lamport as a special version of Donald Knuth's TeX Program.